

Scientific Report No. 40-2011

NHCM-1: Non-hydrostatic climate modelling

Part II

Current state of selected cloud resolving regional climate models and their error characteristics

Martin Suklitsch
Heimo Truhetz
Andreas F. Prein
Andreas Gobiet

February 2011



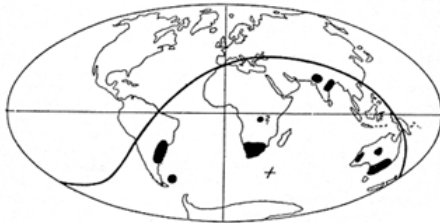
kindly supported by:



Der Wissenschaftsfonds.

The **Wegener Center for Climate and Global Change** combines as an interdisciplinary, internationally oriented research center the competences of the University of Graz in the research area „Climate, Environmental and Global Change“. It brings together, in a dedicated building close to the University central campus, research teams and scientists from fields such as geo- and climate physics, meteorology, economics, geography, and regional sciences. At the same time close links exist and are further developed with many cooperation partners, both nationally and internationally. The research interests extend from monitoring, analysis, modeling and prediction of climate and environmental change via climate impact research to the analysis of the human dimensions of these changes, i.e., the role of humans in causing and being effected by climate and environmental change as well as in adaptation and mitigation. (more information at www.wegcenter.at)

The research documented in this report was supported by the Austrian Science Fund.



Alfred Wegener (1880-1930), after whom the Wegener Center is named, was founding holder of the University of Graz Geophysics Chair (1924-1930) and was in his work in the fields of geophysics, meteorology, and climatology a brilliant, interdisciplinary thinking and acting scientist and scholar, far ahead of his time with this style. The way of his ground-breaking research on continental drift is a shining role model — his sketch on the relationship of the continents based on traces of an ice age about 300 million years ago (left) as basis for the Wegener Center Logo is thus a continuous encouragement to explore equally innovative scientific ways: *paths emerge in that we walk them* (Motto of the Wegener Center).

Wegener Center Verlag • Graz, Austria

© 2011 All Rights Reserved.

Selected use of individual figures, tables or parts of text is permitted for non-commercial purposes, provided this report is correctly and clearly cited as the source. Publisher contact for any interests beyond such use: wegcenter@uni-graz.at.

ISBN 978-3-9502940-7-1

February 2011

Contact: *Martin Suklitsch*
martin.suklitsch@uni-graz.at

Wegener Center for Climate and Global Change
University of Graz
Leechgasse 25
A-8010 Graz, Austria
www.wegcenter.at

NHCM-1: Non-hydrostatic climate modelling

Part II

**Current state of selected cloud-resolving regional climate models
and their error characteristics**

Martin Suklitsch, Heimo Truhetz, Andreas Prein, Andreas Gobiet

Wegener Center for Climate and Global Change
and
Institute for Geophysics, Astrophysics and Meteorology, Institute of Physics
University of Graz, Graz, Austria

Februar 2011

Contents

Preface	iii
Abstract	v
Acknowledgments	vii
1 Introduction	9
2 Models and Data	12
2.1 Model components	12
2.1.1 Dynamics and numerics	12
2.1.2 Physics	13
2.2 The models	15
2.3 Experimental design	16
2.3.1 Initial and boundary conditions	16
2.3.2 Model domains	18
2.3.3 Model settings	18
2.4 Correlative datasets	22
2.4.1 The Integrated Nowcasting through Comprehensive Analysis (INCA)	24
2.4.2 The station network WegenerNet	25
2.4.3 Analysis of the reference data	26
2.4.4 Analysis of the driving data	28
2.5 Synoptic overview	31
2.5.1 General overview	31
2.5.2 July 2007	32
2.5.3 January 2008	32
2.6 Interesting weather events	32
3 Results	34
3.1 Evaluation concept	34
3.1.1 Performance in mean climate	35
3.1.2 Spatial performance	36
3.1.3 Temporal performance	37

Contents

3.2	Preliminary cloud resolving climate simulations	38
3.2.1	Evaluation in the D4a region	38
3.2.2	Evaluation in the D4b region	40
3.2.3	Concluding remarks	42
3.3	Longer term cloud resolving climate simulations	42
3.3.1	Evaluation in D3	43
3.3.2	Comparison with evaluation in the two test regions D4a and D4b .	43
3.4	Sensitivity experiments at the cloud resolving scale	44
3.4.1	D4a region	44
3.4.2	D4b region	47
4	Discussion	50
5	Conclusions	57
A	Figures of the results	60
	List of Figures	XCIX
	List of Tables	CI
	Acronyms	CII
	Bibliography	CV

Preface

This document describes progress and results of the **Austrian Science Fund (Fonds zur Förderung der wissenschaftlichen Forschung) (FWF)** funded project **Non-Hydrostatic Climate Modelling (NHCM-1)** (project ID P19619). It is part two of a three document collection. The other parts are:

- A. Prein, A. Gobiet, H. Truhetz (2011): *Defining and Detecting Added Value in Cloud Resolving Climate Simulations*. WegCenter Report, **39**, WegCenter Verlag, Graz, Austria, ISBN 978-3-9502940-6-4.
- A. Prein, H. Truhetz, M. Suklitsch, A. Gobiet (2011): *Evaluation of the Local Climate Model Intercomparison Project (LocMIP) simulations*. WegCenter Report, **41**, WegCenter Verlag, Graz, Austria, ISBN 978-3-9502940-8-8.

Further results have been or will be published in peer reviewed literature:

- Awan, N. K., A. Gobiet, M. Suklitsch, 2011: *Simulating climate extremes: Performance of high resolution regional climate models in European Alpine region*, J. Geophys. Res., submitted
- Awan, N. K., A. Gobiet, H. Truhetz, 2010: *Parameterization induced error-characteristics of MM5 and WRF operated in climate mode over the Alpine Region: An ensemble based analysis*, J. Climate, accepted
- Suklitsch, M., A. Gobiet, H. Truhetz, N. K. Awan, H. Göttel, D. Jacob, 2010: *Error Characteristics of High Resolution Regional Climate Models over the Alpine Area*, Clim. Dyn., doi: 10.1007/s00382-010-0848-5, published “online first” (<http://www.springerlink.com/content/qj813x0255712826/>)
- Suklitsch, M., A. Gobiet, A. Leuprecht, C. Frei, 2008: *High Resolution Sensitivity Studies with the Regional Climate Model CCLM in the Alpine Region*, Meteorol. Z., **17**, 4, 467 – 476

Additionally, three peer reviewed articles covering the topics in the three reports are currently prepared.

Abstract

Regional Climate Models (RCMs) are widely used for case studies as well as regional climate projections. The horizontal grid spacing at which they are applied is usually 10 km or larger. This is at the edge of the so-called ‘cloud-resolving’ or ‘convection-resolving’ scale. Below that scale processes like deep convection start to get explicitly resolved, and hence it is believed that **RCMs** operated at horizontal resolutions of 3 km and below produce more accurate results than coarser resolved models.

The project **NHCM-1**, funded by the **FWF** under project ID P19619, was (amongst other objectives) dedicated to find out whether or not this belief is justified, whether or not there is an added value in **Convection-Resolving Climate Simulations (CRCS)**, and how climate models should be improved to be successfully operated at convection-resolving scales. Three different **RCMs** have been applied in various configurations in two regions and two periods. The two regions and periods differ strongly in their climatological characteristics in order to allow to draw general conclusions from the results.

The results demonstrate that **CRCS** have comparable quality as conventional climate simulations and that they feature added value in some aspects, particularly regarding spatial patterns, biases related to specific temperatures or precipitation intensities, and partially also regarding overall biases. Model improvement options have been identified that could further enhance the quality of **CRCS**.

This demonstrates that the realisation of long-term **CRCS** is already in reach, but currently still at extremely high computational costs. Technical advances in the field of high performance computing are expected to allow long-term **CRCS** with about 3 km grid spacing at reasonable costs within the next few years.

Acknowledgments

The authors acknowledge the data providers at **Central Institute for Meteorology and Geodynamics (ZAMG)** for data of the **Integrated Nowcasting through Comprehensive Analysis (INCA)** dataset and the data providers at **Wegener Center for Climate and Global Change (WEGC)** for data of the WegenerNet, which made this detailed evaluation possible in the first place.

The authors are also thankful to all persons who helped to put this study into practice, either through advice or technical support or by contributing simulations. In this respect many thanks go to Axel Seifert and Matthias Baldauf and Jochen Förstner at **German Weather Service (DWD)** who gave advice regarding the **COSMO-CLM** setup at the cloud resolving scale. Further thanks go to Hans-Jürgen Panitz (**Karlsruhe Institute of Technology (KIT)**), Ulrich Schättler (**DWD**) and Burkhardt Rockel (**Helmholtz-Zentrum Geesthacht (HZG)**) who gave a helping hand every time when technical problems tried to bring down the **COSMO model in CLimate Mode (COSMO-CLM)** experiments. For the contribution of the **Weather Research and Forecasting model (WRF)** simulation thanks go to Nauman Khurshid Awan (**WEGC**).

This study heavily relied on computing resources. The authors are therefore grateful to the **Center for IT services of the University of Graz (ZID, Uni Graz)**, the **European Centre for Medium-Range Weather Forecasts (ECMWF)** and the **Jülich Supercomputing Centre (JSC)** for providing these resources. The **ECMWF** also receive thanks for providing operational **Integrated Forecasting System (IFS)** analysis and short term forecasts which served as **lateral boundary conditions (LBCs)** for the simulations.

Last but not least many thanks go the **FWF** who funded this research under project ID P19619.

1 Introduction

RCMs have become more sophisticated over the last decade. Nowadays they are highly complex representations of the true nature. The error characteristics and error ranges of RCMs at scales between 10 km and 50 km have been thoroughly investigated in long term climate projections (e.g., Christensen et al. 2007; Hewitt 2005, <http://www.narccap.ucar.edu>) as well as in short term sensitivity studies (e.g., Jaeger et al. 2008; Suklitsch et al. 2010; Awan et al. 2010). Most RCMs stem from models originally built for Numerical Weather Prediction (NWP), where the horizontal (and vertical) resolution has steadily increased. For example, the global NWP model IFS of the ECMWF had a resolution of roughly 40 km horizontally and 60 levels vertically in the year 2000. This was increased to about 25 km/91 levels in 2006 and reached a resolution of roughly 15 km/91 levels in 2010. Many limited area NWP models operationally run at horizontal resolutions of less than 3 km already. This gives opportunity also for the climate modelling community to simulate on those highly resolved grids, i.e., grids with a horizontal resolution of less than 10 km, often also referred to as the lower meso- γ -scale or cloud-resolving scale.

In “NWP mode” the limit of predictability of such highly resolved models lies at 48 hours to 72 hours, depending on the horizontal resolution and domain size. Longer runs eventually will crash due to numerical instabilities caused by the chaotic nature of the environmental flows. In “RCM mode” however these models have to simulate the climate of decades or centuries. This is achieved by constantly prescribing the state of the atmosphere along the lateral boundaries of the model domain with information from a coarser resolved model. Such model can be a Atmosphere-Ocean General Circulation Model (AOGCM) (or some other incarnation of a GCM) or other sources like re-analysis data. The most prominent re-analysis datasets, depending on the region of the world where simulations are carried out, are the American NCEP/NCAR re-analysis dataset (Kalnay et al. 1996), the European ERA-40 re-analysis dataset (Uppala et al. 2005) and the Japanese 25-year re-analysis dataset (JRA-25, Onogi et al. 2007). Although re-analysis are referred to as “perfect boundary conditions” they contain errors (after all, they are models themselves), which get transferred into the RCM domain. The RCMs then take these faulty conditions and react to them, either by amplifying or by reducing them. This is also known as the “garbage in, garbage out” issue in regional climate modelling. This and other issues with RCMs are thoroughly discussed in literature, e.g., Giorgi and Mearns (1999), Laprise et al. (2008), Laprise (2008).

One of the most restrictive issues in terms of cloud-resolving climate modelling is the availability of sufficient computational resources — mainly regarding the bare computing

power of **High Performance Computings (HPCs)**, but at such resolution also input/output, and disk space in general, is becoming an issue. Further, parameterizations as well as the numerical methods have to be adapted for the high resolution: existing parameterizations were originally developed for coarse resolutions, new ones have been added in the course of time. As a consequence the existing ones have to be reconsidered, since they partly may interact with additional model components. The numerical methods have to be adapted since, for example, steep terrain causes numerical instabilities.

These are the main reasons why **RCMs** operated at cloud-resolving scales are at the very beginning of their application. Luckily, in recent years the computing power has risen to a level where climate simulations on cloud-resolving scales became feasible. Additionally, also the horizontal resolution of the **General Circulation Models (GCMs)** and re-analysis datasets is constantly increasing. For example, the latest re-analysis dataset by the **ECMWF**, ERA-Interim, has a horizontal resolution of $0.75^\circ \times 0.75^\circ$, which at mid latitudes roughly corresponds to $65 \text{ km} \times 90 \text{ km}$. This enables regional climate modelers to leave out nesting steps or shift them towards higher resolution to reach the desired fine grid mesh, and thus helps to save some computational resources. As a result, in the near future even long term climate simulations at grid spacings of less than 5 km might become standard.

A screening of the current literature pool shows that there has not been published much on climate simulation on cloud-resolving scales. Most simulations were done for process studies, both on the regional (e.g., Meissner et al. 2009) as well as on the global scale (e.g., Sato et al. 2009; Noda et al. 2010). Meissner et al. (2009) investigated the dependence of model results on horizontal resolution and different driving data. They found in simulations using the **COSMO-CLM** with a 7 km grid spacing that the choice of the model domain has more effects on the results than the horizontal resolution. A horizontal resolution of 7 km also features the study of Noda et al. (2010). They focused on the spatial reproducibility of cloud characteristics in their global cloud-resolving model. They found that turbulent transport caused by subgrid-scale clouds is a key factor controlling cloud behavior — at least in their model. They state that large-eddy simulations with resolutions of some 10 m are necessary to explicitly resolve small-scale convections. Sato et al. (2009) found in their global convection resolving simulations a remarkable resolution dependence in the phase and amplitude of the diurnal cycle of precipitation over land.

Besides these process studies efforts arise to perform also long(er) term simulations at cloud-resolving scales. Hohenegger et al. (2008) performed a slightly longer simulation (one year, to be exact) at 2.2 km horizontal resolution. They showed that the use of cloud resolving resolution yields a better localization of precipitation maxima as wells as a more accurate triggering of convective precipitation. Knote et al. (2010) did a climate change analysis focusing on return values of climate extremes using two 10-year time slices over a small region in Germany at 1.3 km horizontal resolution. They found, for example, that mountainous regions will experience the strongest change in daily

minimum temperature.

Current research emphasizes on the correct simulation of precipitation. But there is still much to learn also about the performance at the meso-gamma scale with respect to other parameters like global radiation. However, the basic question arises whether or not current state-of-the-art RCMs are suitable for that horizontal resolution at all. After all, existing parameterizations within RCMs have been built for much coarser grid meshes. They were programmed at a time when the models used a horizontal resolution which made it unaware of important physical processes such as deep convection and turbulence. Reducing the mesh size helps in a way that these processes become “explicitly resolved” by the model. But no matter how fine the resolution gets, there will always be “subgrid-scale” processes which in that case become increasingly important for a correct simulation of weather and climate. According to Pielke, Sr. (2002), for example, a grid spacing of about 1 m is necessary to resolve turbulence. And even so, only weak turbulence can be resolved since the numerical solver can only handle turbulent flows with Reynolds numbers of $< 10^4$ while in meteorology we deal with Reynolds numbers up to $< 10^{15}$.

In this study the authors give an overview on the error ranges and error characteristics related to current state-of-the-art RCMs operated at grid spacings down to about 1 km. The overall aim is to point out ‘crucial’ model components which have to be improved in order to get more realistic and ultimately more reliable model results. A general overview on the main components of an RCM and their potential related to cloud resolving climate simulations is given in Chapter 2. Also in this chapter the authors describe the actual models used in this study and which setups had been chosen for the sensitivity experiments. The evaluation concept along with a short description of the evaluation methods used and the results obtained in the process of the simulations are shown in Chapter 3. A final comparative evaluation of all sensitivity experiments and an in-depth discussion of these results is given in Chapter 4. Conclusions that can be drawn from the simulations performed in this study are summarized in Chapter 5.

2 Models and Data

In this chapter the authors give an overview over the **Regional Climate Models (RCMs)** employed in this study (**Section 2.2**) and the overall experimental design (**Section 2.3**). Further the correlative datasets used to evaluate the simulations are introduced in **Section 2.4**, and an overview on the synoptic conditions during the simulation periods is given in **Section 2.5**. They start, however, with a brief overview on the main model components and their relevance to cloud resolving climate simulations.

2.1 Model components

RCMs have evolved over the past decades. With each increase in understanding theoretical aspects of **RCMs** the ‘dynamical core’, i.e., the part which does the actual forward integration in time, as well as parameterizations have been adopted applying the newly acquired knowledge. This made some parameterizations more complex, and new model parts were added in order to get a more realistic simulation of the modelled system. Today the development of **RCMs** is, similar to their global counterparts, headed towards Earth system models, which include urban parameterization as well as air chemistry and the carbon cycle. In this section the authors want to give an overview on the current state of the main model components and what has to be expected in terms of their further development. The authors further want to point out crucial components in terms of the evolving matter of cloud resolving climate simulations.

2.1.1 Dynamics and numerics

The ‘dynamical core’ (often also called the ‘numerical solver’) is needed to solve the prognostic equations of any **RCM**. It has to be accurate in terms of the resolved processes, it has to be robust with respect to the range of parameters and spatial scales it is applied at, it should exhibit conservation properties, and while doing that it should be efficient with respect to computational resources. These requirements give much freedom in terms of what processes to include and what is the appropriate set of prognostic equations to include these processes. Also the type of discretizations (both spatial and temporal) as well as the kind of boundary conditions are arguable. Today there are many versions of time integration schemes: Leapfrog and Runge-Kutta, for example, use finite difference formulations. In future, however, finite volume methods might be preferably applied

since their equations are strictly conservative. This means that both mass fluxes and energy fluxes across the boundaries of the **RCM** equal to zero over the integration time.

The question about the choice of the numerical solver becomes more pressing with the ongoing increase of the horizontal resolution towards cloud resolving scales, i.e., grid distances of less than 3 km. One issue that becomes apparent is the occurrence of more complex orographical structures, e.g., steeper slopes and more pronounced valleys. This induces problems related to advection processes. Essentially, there are two groups of such advection schemes: Semi-Lagrange schemes and Eulerian methods. While the first group lacks conservations properties but through their theoretical background can be easily formulated in a 3D environment, the other group (mainly finite volume schemes) conserve the quantity they are advecting but are hard to formulate in 3D and usually have Courant number restrictions. Traditionally, the advection is treated outside the dynamical core. When advection is computed separately for specific so-called tracer gases, as currently widely applied, it may occur that in strongly deformational flow situations a grid cell becomes emptied in one advection step, and that the following compensating advection step lets the specific tracer mass ‘explode’. This is tied to the mass conservation and mass consistency issue touched above. Further, the explicit simulation of deep moist convection which is achieved at such resolutions requires a closer coupling between the dynamical core and the parameterizations, and more processes have to be handled by the dynamical core itself.

2.1.2 Physics

In **RCMs** the term ‘physics’ basically summarizes all physical parameterization schemes available. The term means the parameterization of turbulence and the **planetary boundary layer (PBL)** as well as the parameterization of cloud microphysical processes, moist convection, radiation, soil processes and sea ice. In recent years, and with increasing horizontal resolution, also the parameterization of lakes and urban areas — to name only a few — became increasingly important. The state of knowledge differs from one topic to another.

Turbulence and the PBL are often mentioned in one sentence, since turbulence largely occurs within the **PBL**. Its parameterization is one of the major challenges in atmospheric modelling, and most existing schemes show serious shortcomings. There is often a poor interaction with other parameterization schemes such as moist convection and cloud microphysics as well as with the thermodynamics at the resolved scale. Down to a horizontal resolution of 10 km current **RCMs** use a separate scheme for deep moist convection. At such resolutions the interaction between the turbulence scheme and the convection scheme is unclear, e.g., energetically relevant modes could be counted twice. At even higher horizontal resolutions (i.e., less than 10 km) it is thought — and widely done — that this deep convection scheme can be simply switched off. Yet it is unclear at which resolution exactly that can or should occur. Currently, much effort is put

into the unification of several parameterization schemes, such as subgrid scale motions, shallow convection (i.e., the formation of non-precipitating clouds) and turbulence. Such a unification should further be scale independent, so that it can be applied at cloud resolving scales as well as at the current ‘standard’ resolution of about 25 km.

Moist convection schemes, a.k.a. cumulus convection schemes, have to be applied in **RCMs** with horizontal resolutions in the order of tens of kilometers. Such parameterization schemes have to include turbulent mixing, the organization of updrafts and downdrafts within a convective system, cloud microphysical processes and the coupling to the **PBL** and the underlying surface. Today there are mainly two types of convection schemes: mass-flux schemes (the mass flow through the cumulus cloud is used to predict all associated tendencies) and moist convective adjustment schemes (moist convective instability is diagnosed and adjusted towards specified temperature and humidity profiles). They both have in common the assumption of an established equilibrium between the local downdrafts and updrafts with the large scale subsidence. With increasing horizontal resolution this assumption is most likely not true anymore. Current developments go towards hybrid schemes in which only the downdraft and updraft part is parameterized while the large scale subsidence is left to grid scale equations. These developments were recently bundled within the COST action ES0905 (<http://convection.zmaw.de>). For the time being it is believed that, as mentioned above, simply switching off the moist convection scheme at horizontal resolutions below about 5 km is a valid and appropriate step. In **NHCM-1** this has been done, too, for the simulations at 3 km and 1 km horizontal resolution.

Cloud microphysics is the research area with the largest gaps in knowledge, most importantly due to the lack of adequate observations. Current state-of-the-art **RCMs** still use so-called one-moment schemes in fully prognostic form. Besides water droplets they employ two or three ice species. In research much more sophisticated (and complex) schemes are already available, but they are far too costly in terms of computational resources in order to be applied in long-term simulations. Such schemes either are two- or three-moment bulk schemes (where the number of prognostic equations lies between 8 and 20) or spectral bin models with several hundred prognostic equations. Another possibility is the application of several dozens or hundreds of ice species in bulk schemes. Cloud microphysics schemes themselves are rather independent from the horizontal resolution of a **RCM** since these processes are always of ‘subgrid’ scale. But through their interaction with other parameterization schemes, most importantly convection, their relevance for high resolution simulations is undeniable.

The term **SVAT scheme** means ‘soil vegetation atmosphere transfer scheme’. Such schemes are the link between turbulence/**PBL** schemes and the model soil. **SVAT** schemes decide, for example, how much of the incoming radiation is absorbed and reflected, how much water evaporates from the soil or dissipates into the soil, and how much water remains in the vegetation which has an impact on the near surface temperature. To sum it up, they provide the lower boundary conditions for the atmospheric part of the

RCM. As such they have a large impact on the evolution of near surface parameters as well as atmospheric processes. The heterogeneity of the land surface at subgrid scale may be important for both the energy budget of the **PBL** and the atmospheric part of the hydrological cycle. This heterogeneity is taken into account in more complex SVAT schemes through the so-called ‘tile approach’. In this approach more than one surface type may be specified for one grid cell, and the surface prognostic variables (e.g., heat fluxes) are solved for each of the different types. The atmospheric part of the model is then supplied with a weighted average of the fluxes over all types. Such an approach might indeed be necessary at cloud resolving scales since the heterogeneity of the surface does not stop at, e.g., a grid distance of 1 km. The question then arises where to get the necessary information for the model. Satellite data might be one answer, but from a climatological point of view the annual cycle of the land surface has to be accounted, too. A continuous satellite coverage of the Earth’s surface at very high resolution, on the other hand, is currently not available.

Radiation is the ultimate source and sink of energy for the Earth system. In reality radiation interacts with all parts of the atmosphere (e.g., clouds, aerosols) and the soil surface. In a **RCM** the interactions of the parameterization scheme for radiation are also manifold, but limited to the numerical solver and certain other parts of the model such as those related to cloud formation. One parameter that is particularly dependent on a successful simulation of the radiation transfer and its associated budget is the near surface temperature. **RCMs** with a pronounced temperature bias most likely fail to appropriately reproduce the radiative transfer. Radiation schemes have a strong impact on the runtime of a simulation. Even in their current implementation with many simplifications (only vertical incoming/outgoing radiation is regarded, only a handful of spectral bands instead of the continuous spectrum are included) they are the most resource intensive part of a **RCM**. With increasing horizontal resolution a three-dimensional implementation becomes more and more necessary, e.g., the ‘bouncing’ of radiation between the slopes of a valley, or the casting of shadows of high mountain ranges. This in return affects the local winds, turbulence and the **PBL** and by that closes the circle of parameterization schemes.

2.2 The models

This study employs three **RCMs**: the **COSMO** model in **CLimate Mode (COSMO-CLM)**, the **Fifth-Generation Mesoscale Model (MM5)** and the **Weather Research and Forecasting model (WRF)**.

CCLM: The **COSMO** model in **CLimate Mode** is the German community climate model. It is based on the primitive hydro-thermodynamical equations describing a compressible non-hydrostatic flow in a moist atmosphere without any scale approximations. Much information about **CCLM** and its applications in the **CLM** community

is compiled in a special issue of *Meteorologische Zeitschrift* volume 17, no. 4 (e.g., Rockel and Geyer 2008; Feldmann et al. 2008). The model version used in the present study is 4.0.

MM5: The 5th Generation Mesoscale Model has the longest running history: it evolved from a hydrostatic model in the early 1970's that was later documented by Anthes and Warner (1978). Over the years multiple-nest capability, non-hydrostatic dynamics (Dudhia 1993), and more parameterization options (including soil-vegetation-atmosphere-transfer models) were implemented along with several numerical modifications and optimizations. In 2004 further development was suspended in favor of the next generation model **WRF** (see next paragraph). In its latest version (3.7.4) **MM5** solves the governing coupled partial differential equations (capturing the atmosphere) by means of finite differencing schemes: second-order centered finite differences and first-order upstream schemes are used for spatial discretization on a staggered grid (Arakawa-B grid). Temporal discretization is achieved by a second-order leapfrog scheme with time-splitting to handle sound waves on shorter time steps. In vertical direction the governing equations are discretized in unequally distributed steps defined by a terrain-following sigma-pressure coordinate, which allows for implicit treatment of vertical sound waves and vertical diffusion. This latest model version was used in all but one experiments.

WRF: The Weather Research & Forecasting model is a community model. In this study version 2.2.1 and Advanced Research **WRF** dynamical core is used for all experiments. **WRF** is developed specifically for high resolution modelling applications and offers a broad range of choice in terms of physical options to the user community. **WRF** model solves the fully compressible non-hydrostatic Euler equations in flux form on a hybrid terrain following vertical coordinate system using the Runge-Kutta split-explicit time integration on an Arakawa-C type grid. It conserves mass, momentum, entropy and scalars using flux form prognostic equations. For details please refer to Skamarock et al. (2005).

2.3 Experimental design

2.3.1 Initial and boundary conditions

The driving data for all simulations is taken from the operational analysis and short term forecasts of **European Centre for Medium-Range Weather Forecasts (ECMWF)**'s **Integrated Forecasting System (IFS)** (Bechtold et al. 2008). This global **Numerical Weather Prediction (NWP)** model features a horizontal resolution of roughly 25 km and has 91 vertical levels. The use of both the analysis and the short term forecasts is necessary to obtain an update interval of 3 hours for the **lateral boundary conditions (LBCs)**. Anal-

ysis are available at the synoptic main hours (00, 06, 12 and 18 UTC), additionally the +3-hour and +9-hour fields of the 00 UTC and 12 UTC forecasts were taken.

The initial conditions were also taken from the *IFS*. The source for ‘time invariant fields’, e.g., orography, plant cover and soil type, varies from model to model. For example, *COSMO-CLM* uses the GTOPO30 topography dataset while *WRF* and *MM5* use USGS data. The spin-up time, i.e., the period that one regards as the time the *RCM* needs to reach a balanced state, was chosen to be one month or 16 days, depending on the set of simulations (see below). This part of the model results was disregarded in the evaluation. This approach is backed, for example, by Zhong et al. (2007) who showed that for an *RCM*’s atmosphere a spin-up time of 8 to 10 days is enough. For soil parameters, longer spin-up times are often advisable. In *NHCM-1*, longer spin-up times were not feasible due to constraints in computational resources. This problem was tackled by generating reasonably balanced soil fields on longer simulations for each model (S2, see below), which were used to initialize all subsequent sensitivity studies.

In this study the authors conducted a total of 26 simulations with the three *RCMs* mentioned above for mainly two test periods, July 2007 and January 2008. These two months were chosen on purpose: July 2007, as will be discussed in Subsection 2.5.2, saw several severe weather events. January 2008 was chosen for its stable atmospheric conditions on the one hand and because of the availability of suitable reference data on the other hand. The above mentioned number of 26 simulations is separated into three sets.

- The first set of simulations (called ‘S1’ in the following) was carried out with all three *RCMs* for two periods of 2 months each. The first month of each simulation period was regarded as spin-up and therefore not evaluated. The soil fields for initialization were taken directly from the *IFS*. Each model’s setup for the ‘reference’ run had been deduced from previous sensitivity experiments performed with a horizontal resolution of 10 km. This study is described in detail in Suklitsch et al. (2010) and Awan et al. (2010).
- The second set of simulations (‘S2’) was carried out with all *RCMs* but *WRF* and covered the period between January 2007 and February 2008. Again, the first month was regarded as spin-up and disregarded in the evaluation. The setup for these simulations had been deduced from the experiences gathered in the S1 simulations. Their main purpose was to produce the initial soil fields used in the S3 and S4 simulations described next.
- The ‘S3’ simulations were conducted in order to find out the spin-up time of the atmospheric part of the *RCMs*. Therefore, two representative simulations were made with the *COSMO-CLM* using slightly perturbed initial conditions (similar to the approach used by Giorgi and Bi (2000)). The results obtained were very similar to those described in Zhong et al. (2007).

- Finally, the fourth set of simulations (‘S4’) was also carried out with **COSMO-CLM** and **MM5** only. The two simulation periods in this set lasted 48 days each. Based on the results in the S3 experiments, only the first 16 days were regarded as spin-up period. In return, the authors took the soil parameters of the respective S2 simulations for initialization of the soil, since the soil of these simulations should have been in a rather balanced state — at least more balanced than if initiated from scratch. The individual model settings are displayed in the next section.

2.3.2 Model domains

This section describes all domain settings used in the course of this study. **Figure 2.1** shows the geographical location of each model domain and the next finer resolved nest for each **RCM**. As can be seen the 10 km domain is just large enough to fully enclose the Alpine region. The performance of the models in this domain (together with an analysis of the impact of changing this domain) is given in **Suklitsch et al. (2010)** and **Awan et al. (2010)**. **MM5** and **WRF** then used one domain setting each for the 3 km and the 1 km horizontal resolution. **COSMO-CLM** further did one test with an additional increased domain size, denoted as dotted rectangles in the upper row of **Figure 2.1**. The color shades correspond to the surface height shown in the legend.

The settings in the horizontal directions (in terms of number of grid points and the resolution) are described in **Table 2.1**. Regarding the vertical direction **COSMO-CLM** uses a pressure based hybrid vertical coordinate system. In principle the stretching in the vertical direction is customizable, yet the authors never experimented with that but used the predefined numbers of levels. Most of the experiments were done using 32 levels, one experiment used 50 levels. **MM5** and **WRF** use a terrain-following sigma pressure vertical coordinate. The default number of vertical levels in this study is 29 and was varied using 20 and 40 levels, depending on the sensitivity experiment.

2.3.3 Model settings

Since we are dealing with sensitivity experiments the process of model setups is done in a way that there is *one* reference setup (per simulation group), the setup of all other experiments differ from this reference setup by one setting. These changes include changes in the deep convection scheme, changes in the turbulence scheme, changes in the microphysics scheme and changes in the radiation scheme. Depending on the **RCM** and horizontal resolution of the simulation only some of these variations have been tackled.

The tables below give an overview of all the different settings of the experiments, where the reference setup is always given as the first one in each table. In these tables, as well as in the plots that follow in **Chapter 3** the acronyms for each sensitivity experiment consist of one letter denoting the **RCM** (C for **COSMO-CLM**, M for **MM5** and W for **WRF**) and a two-digit number denoting the experiment ID. There are two exceptions from

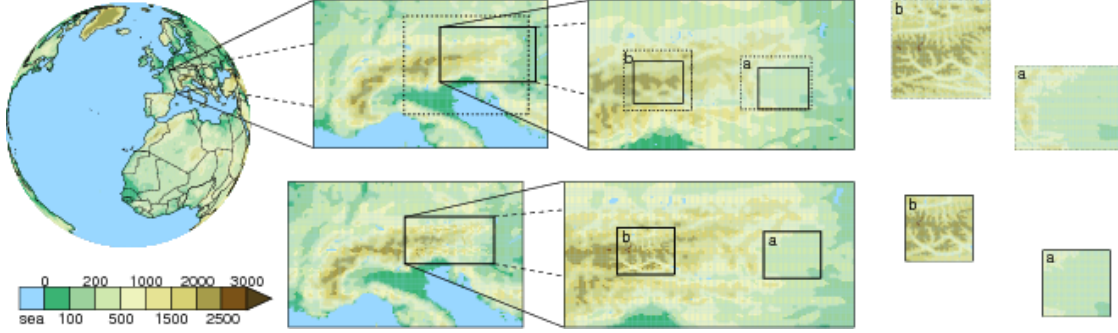


Figure 2.1: Model domains for the simulations conducted in this study. Upper row: *COSMO-CLM* domains, lower row: *MM5/WRF* model domains. Left panel shows the globe with *IFS* 25 km topography and “D2” marked, next panel to the right: 10 km horizontal resolution (“D2”) with “D3” annotated within, next: 3 km horizontal resolution (“D3”) with “D4A”/“D4B” (solid) and “D4Av2”/“D4Bv2” (dashed) annotated within, right panel: 1 km horizontal resolution with the corresponding topography. Colors show the surface height according to the legend in the lower left corner.

Table 2.1: The horizontal domain settings used in the cloud resolving climate simulations in the framework of the project *NHCM-1*. Additionally the default number of vertical layers is given.

domain acronym	model acronym	number of horizontal grid points	horizontal resolution	default number of vertical levels	in text referred to as
D2	<i>COSMO-CLM</i>	110 × 81	0.09°	32	10 km
	<i>MM5/WRF</i>	111 × 81	10 km	29	10 km
D3	<i>COSMO-CLM</i>	135 × 90	0.03°	32	3 km
	<i>MM5/WRF</i>	127 × 79	3 km	29	3 km
D3v2	<i>COSMO-CLM</i>	175 × 160	0.03°	32	3 km
D4A	<i>COSMO-CLM</i>	76 × 76	0.01°	32	1 km
	<i>MM5/WRF</i>	75 × 75	1 km	29	1 km
D4Av2	<i>COSMO-CLM</i>	108 × 96	0.01°	32	1 km
D4B	<i>COSMO-CLM</i>	76 × 76	0.01°	32	1 km
	<i>MM5/WRF</i>	75 × 75	1 km	29	1 km
D4Bv2	<i>COSMO-CLM</i>	104 × 108	0.01°	32	1 km

this rule: one simulation with **MM5** carries the suffix ‘a’ in its acronym, and the **WRF** simulation— since there is only one in the whole ensemble — is called ‘WS1’.

The three **RCMs** differ in the way their model domains are set up: **COSMO-CLM** uses a rotated coordinate system, where the north pole in the model is shifted in a way that the equator runs through the model domain, ideally through its center. This way problems resulting from the convergence of the meridians are avoided, the grid boxes are squares. The rotated pole for all **COSMO-CLM** simulations lies at 42.5°N and 170°W. **MM5** and **WRF** use a different approach, they use the Lambert conformal conic projection, where the grid points are transformed onto a plane. This ensures quadratic grid boxes which further are — in the Lambert system — equidistant. The longitude of the central meridian for the **MM5** and **WRF** simulations is 11.055°, the origin of the projection lies at 46.31499°N, the two standard parallels lie at 47°N and 49°N. Hence, the model grids are not identical and grid spacings are slightly different. On the other hand, the model domains are rather small, as was shown in [Figure 2.1](#), and therefore the Earth’s curvature has only small impact. For convenience the authors decided to use ‘km’ for the domain resolution information. The information which resolution equals to each ‘km’ reference is included in [Table 2.1](#).

The S1 experiments

- simulation period:
01/06/2007 – 01/08/2007 and 01/12/2007 – 01/02/2008 (each 00 UTC)
- evaluation period:
01/07/2007 – 31/07/2007 and 01/01/2008 – 31/01/2008

The ‘S1’ experiments feature simulations at a horizontal resolution of roughly 10 km, 3 km and 1 km (for deviations due to the coordinate system refer to [Table 2.1](#)). **MM5** and **WRF** are set up in a way that in each simulation the full resolution chain with 3 nests is computed. For **COSMO-CLM** it was agreed to do only one simulation at 10 km horizontal resolution, and to nest several sensitivity experiments with 3 km and 1 km horizontal resolution into this single experiment. This had been done mainly for resource reasons: there was a shortage of disk storage capacity as well as computational resources. The downside of this is the discussion becomes a bit more complicated due to the unbalanced number of simulations in each resolution step of the model ensemble. The setup of all experiments is summarized in [Table 2.2a](#) to [Table 2.2c](#).

The S2 experiments

- simulation period: 01/01/2007 – 01/02/2008
- evaluation period: 01/06/2007 – 31/01/2008

Table 2.2a: Key settings of the **COSMO-CLM** in the S1 experiments. ■ denotes settings for simulations with 10 km horizontal resolution, ■ denotes settings for simulations with 3 km horizontal resolution and □ denotes settings for simulations with 1 km horizontal resolution. C35 is the “reference setup”, the settings for the rest of the simulations are identical to that reference setup with the exception of the given setting.

Acronym	Key settings
C34 ■	3 rd order Runge-Kutta time integration scheme (Foerstner and Doms 2006) (time step: 80 s); Kain-Fritsch convection scheme (Kain and Fritsch 1993; Kain 2003); radiation scheme following Ritter and Geleyn (1992); cloud ice scheme with prognostic cloud water and cloud ice, prognostic rain and snow, and transport of rain/snow; turbulent kinetic energy (TKE) -based turbulence scheme including sub-grid scale effects of condensation/evaporation; hourly LBC update; domain D2
C35 ■ □	3 rd order Runge-Kutta time integration scheme (Foerstner and Doms 2006) (time step: ■ 25 s □ 10 s); no convection; radiation scheme following Ritter and Geleyn (1992); cloud ice scheme with prognostic cloud water and cloud ice, prognostic rain and snow, and transport of rain/snow; TKE -based turbulence scheme including sub-grid scale effects of condensation/evaporation; hourly LBC update; domain D2
C36 ■ □	Change of two ‘tuning parameters’: <code>clc_diag</code> (adjusting cloud cover in case of saturation in statistical cloud diagnostics) from 0.5 to 0.25 and <code>tur_len</code> (maximum turbulence length) from 500 to 150. Both changes were made after suggestions of micro-physics developers at German Weather Service (DWD)
C37 ■ □	Kain-Fritsch convection (Kain and Fritsch 1993; Kain 2003)
C38 ■ □	additional smoothing of orography at the lateral boundaries
C39 ■ □	extended domain size (■ D3v2 □ D4aV2/D4bV2)
C40 ■ □	increased vertical resolution (50 levels)
C41 ■ □	LBC update every 3 hours
C42 ■ □	cloud ice scheme including graupel
C50 ■ □	shallow convection (reduced Tiedtke (Tiedtke 1989) scheme)

‘S2’ consists of one single simulation chain per **RCM**. The setups for these simulations build on the experience gained from ‘S1’. The simulation period, however, is extended to one year (13 months, to be exact) in order to provide a balanced soil for the next set of experiments. The setups for the individual **RCMs** are summarized in **Table 2.3a** and **Table 2.3b**.

The S4 experiments

- simulation period:
15/06/2007 – 01/08/2007 and 15/12/2007 – 01/02/2008 (each 00 UTC)
- evaluation period:
01/07/2007 – 31/07/2007 and 01/01/2008 – 31/01/2008

The ‘S4’ experiments were intended as the culmination of all previous experiments. With the knowledge built up in the S1 and S2 set of experiments some fine tuning

Table 2.2b: Same as Table 2.2 for MM5. M55 is the “reference setup”.

Acronym	Key settings
M55	Second-order leap frog scheme (Grell et al. 1995) (time steps: \blacksquare 20 s, \blacksquare 6.66 s, \square 2.22 s) with time splitting scheme (Klemp and Wilhelmson 1978) for sound wave treatment; shortwave radiation scheme from Dudhia (1989) and the Rapid Radiative Transfer Model (RRTM) from Mlawer et al. (1997) for longwave radiation; microphysics scheme (REISNER 2) for phase transition of water adapted from Reisner et al. (1998); \blacksquare Kain-Fritsch cumulus scheme from Kain and Fritsch (1993) and Kain (2003); MRF boundary layer scheme from Hong and Pan (1996) together with Zilitinkevich formulation for stable stratification; atmosphere / soil interaction is treated by the NOAH land surface model (Chen and Dudhia 2001); the LBCs between finer and coarser model domains are updated with the model-internal time steps due to two-way coupling
M55a	\blacksquare \blacksquare \square shallow convection is turned on
M57	increased vertical resolution (40 model levels)
M58	reduced vertical resolution (20 model levels)

Table 2.2c: Key settings of the WRF model in the S1 experiments.

Acronym	Key settings
WS1	Third-order Runge-Kutta split-explicit time integration scheme (time steps: \blacksquare 60 s, \blacksquare 20 s, \blacksquare 6.67 s; \blacksquare Kain-Fritsch cumulus scheme from Kain (2003), \blacksquare \square no convection; shortwave radiation scheme from Dudhia (1989) and the Rapid Radiative Transfer Model (RRTM) from Mlawer et al. (1997) for longwave radiation; Eta grid-scale cloud and precipitation (2001) scheme (Rogers et al. 2001); Yonsei State University PBL scheme (Hong et al. 2006) (plus Monin-Obukhov surface layer scheme after Skamarock et al. (2007)); atmosphere / soil interaction is treated by the NOAH land surface model (Chen and Dudhia 2001); the LBCs between finer and coarser model domains are updated with the model-internal time steps due to two-way coupling

changes should be evaluated with regard to their effects on the results. The setups of these experiments are summarized in Table 2.4a and Table 2.4b.

2.4 Correlative datasets

Any model evaluation needs observational or observation-based data as a reference. The reference reflects the natural process the model tries to capture. However, in the case of RCMs the model output covers a large area (i.e., a grid cell) and the problem arises that the quantities to be evaluated are only known at given points (e.g., at the point of observation stations). In order to obtain comparable quantities, either the model data should be further ‘downscaled’ to the locations of the stations or the station data should be ‘upscaled’ to the model grid. Thereby scale discrepancies have to be taken

Table 2.3a: Key settings of the **COSMO-CLM** in the S2 experiment.

Acronym	Key settings
C71	3 rd order Runge-Kutta numerics (time step: ■ 80 s, ■ 25 s, □ 10 s); ■ Kain-Fritsch moist convection (Kain and Fritsch 1993; Kain 2003), ■ □ shallow convection; cloud ice scheme with prognostic cloud water and cloud ice, prognostic rain and snow and transport of rain/snow; TKE -based turbulence scheme including sub-grid scale effects of condensation/evaporation, LBC update ■ every 3 hours from mixed IFS T799 analysis and short-term forecasts, ■ every hour from 10 km simulation, □ every hour from 3 km simulation

Table 2.3b: Key settings of the **MM5** in the S2 experiment. ■ and ■ denotes settings for simulations with 10 km and 3 km horizontal grid spacing.

Acronym	Key settings
M55a	Second-order leap frog scheme (Grell et al. 1995) (time steps: ■ 20 s and ■ 6.66 s) with time splitting scheme (Klemp and Wilhelmson 1978) for sound wave treatment; shortwave radiation scheme from Dudhia (1989) and the RRTM from Mlawer et al. (1997) for longwave radiation; microphysics scheme (REISNER 2) for phase transition of water adapted from Reisner et al. (1998); ■ Kain-Fritsch cumulus scheme from Kain and Fritsch (1993) and Kain (2003) with shallow convection in ■ and ■ ; MRF boundary layer scheme (Hong and Pan 1996) together with Zilitinkevich formulation for stable stratification; NOAH land surface model (Chen and Dudhia 2001); two-way coupling between finer and coarser domains; 29 model levels

into account, otherwise local effects (not resolved by the model) would influence the comparability. In both cases the representativeness of the stations plays a vital role.

In this study expertise from outside the **NHCM-1** team was consulted by using two gridded (2-dimensional) observation-based datasets. This avoids additional sources of uncertainty from station upscaling/downscaling and from station selection.

The two correlative datasets are:

- the observation-integrated fields of the **Integrated Nowcasting through Comprehensive Analysis (INCA)** system (Haiden et al. 2010) provided by the **Central Institute for Meteorology and Geodynamics (ZAMG)**
- 2-dimensional data products from the **WegenerNet** (Kirchengast et al. 2008) of the **Wegener Center** for the focus region of **Feldbach**.

Since the **WegenerNet** is limited in its extension to a 20 km × 15 km area in South-Eastern Styria (see **Subsection 2.4.2**), **WegenerNet** data is only used to evaluate the representativeness of the **INCA** dataset within the **WegenerNet** region and beyond to some extent. Hence, all model evaluation is based on the **INCA** dataset.

In order to be able to compare the model performances with the performance of their driving data, i.e., the coarse resolved (roughly 25 km × 25 km grid spacing) global dataset

Table 2.4a: Key settings of the **COSMO-CLM** in the S4 experiment. ■, ■, and □ denotes settings for simulations with 10 km, 3 km, and 1 km horizontal grid spacing, respectively.

Acronym	Key settings
C71 ■	3 rd order Runge-Kutta numerics (time step: 80 s); Kain-Fritsch moist convection (Kain and Fritsch 1993; Kain 2003); cloud ice scheme with prognostic cloud water and cloud ice, prognostic rain and snow and transport of rain/snow; TKE-based turbulence scheme including sub-grid scale effects of condensation/evaporation, LBC update every 3 hours from IFS T799
C74 ■ □	time step: ■ 30 s □ 10 s; no convection; LBC update every hour; rest as in C71
C75 ■ □	Kain-Fritsch moist convection (Kain and Fritsch 1993; Kain 2003)
C76 ■ □	3D turbulence
C77 ■ □	tur_len=150, q_crit=1.6, clc_diag=0.5
C78 ■ □	microphysics scheme including graupel
C79 ■ □	diagnostic precipitation (i.e., no prognostic equations for contents of rain, snow, ice)
C80 ■ □	radiation update every 15 min (instead of every hour)

from the **IFS** of the **ECMWF**, and hence to document the effects of dynamical downscaling, **IFS/INCA** comparisons are shown in [Subsection 2.4.4](#).

2.4.1 The Integrated Nowcasting through Comprehensive Analysis (INCA)

The **INCA** system ingests numerous sources of observational data (e.g., surface stations, satellite data, and radar observations) and provides gridded data of various parameters like temperature, precipitation, global radiation, and relative humidity. These parameters are given in an area of 600 km×350 km with a resolution of 1 km. The temporal resolution of the dataset used in this study is 1 hour. The time period provided is June 2007 to January 2008. The dataset covers the area of Austria and some of its surroundings (the Eastern Alps and Alpine Forelands, cf. [Figure 2.2](#)).

The most important data sources for the **INCA** system are surface stations (cf. [Figure 2.3](#)). **ZAMG** operates a network of about 200 automated stations (**semi-automatic weather station (TAWES)**) across the country. In vertical, this network spans most of the topographic range in Austria, with the highest stations situated at altitudes above 3000 m. The meteorological observations used in **INCA** are 2 m temperature, relative humidity and dew point (measured independently), 10 m wind, precipitation amount, precipitation minutes and insolation minutes. There are other surface meteorological stations which are increasingly used by the **INCA** system. By the end of 2008 the hydro-meteorological stations of the provinces of Lower Austria, Salzburg, Tyrol, and Carinthia had already been integrated into the operational precipitation analysis system. For hourly temperature and humidity analysis also **SYNOP** stations from neighboring countries are used (Haiden et al. 2010). Another data source for **INCA** is the Austrian weather radar network which is operated by **Austro Control (Austro Control)**. Two-dimensional

Table 2.4b: Key settings of the MM5 in the S4 experiment. ■, ■, and □ denotes settings for simulations with 10 km, 3 km, and 1 km horizontal grid spacing, respectively.

Acronym	Key settings
M59	Second-order leap frog scheme (Grell et al. 1995) (time steps: ■ 20 s, ■ 6.66 s, and □ 2.22 s) with time splitting scheme (Klemp and Wilhelmson 1978) for sound wave treatment; shortwave radiation scheme from Dudhia (1989) and the RRTM from Mlawer et al. (1997) for longwave radiation; REISNER 2 microphysics scheme (Reisner et al. 1998); ■ Kain-Fritsch cumulus scheme from Kain and Fritsch (1993) and Kain (2003) with shallow convection in all domains; ETA boundary layer scheme (Janjic 1990; Janjic 1994) together with Zilitinkevich formulation for stable stratification; NOAH land surface model (Chen and Dudhia 2001); the LBCs for ■ are derived from S2 simulation (M55a) with an hourly update rate; two-way coupling; 29 model levels
M60	same as S2 simulation (M55a) but with true z-coordinates for diffusion coefficients (Zängl 2002)
M61	same as S2 simulation (M55a) but with a different microphysics scheme based on Lin et al. (1983), Tao et al. (1989), and Tao and Simpson (1993) which includes prediction of graupel
M62	same as S2 simulation (M55a) but with slope effects on shortwave radiation

radar data are synthesized from 4 radar locations, containing column maximum values in 14 intensity categories at a temporal resolution of 5 minutes. The **Meteosat 2nd Generation (MSG)** satellite products used in **INCA** are ‘cloud type’, which consists of 17 categories, and the visible wavelength image.

For quality control of input data the precipitation data of the stations run through a number of checks. A part of these automatic tests are comparisons of station data to maximum climatological values, to radar data in the same area, to data of surrounding stations and a test for temporally constant artificial values (Haiden et al. 2010). However, the focus of **INCA** lies on generating reliable data in numerical weather prediction. Its climatological error ranges (e.g., in terms of biases and frequency distributions) are currently under investigation in close collaboration with the Wegener Center. Hence the strength of **INCA** lies in capturing structures and spatial and temporal variability. Nonetheless, biases and frequency distributions are still investigated in this study. They are believed to be reliable enough to indicate obvious deficiencies of the **RCMs**.

2.4.2 The station network WegenerNet

The Wegener Center provides data of a dense small-scale station network located around the city of Feldbach called ‘WegenerNet’ (www.wegenernet.org). 151 stations are situated in an area of approximately 20 km×15 km (one station per ~2 km²; cf. Figure 2.4) and provide data (amongst others air temperature, relative humidity and liquid precipita-

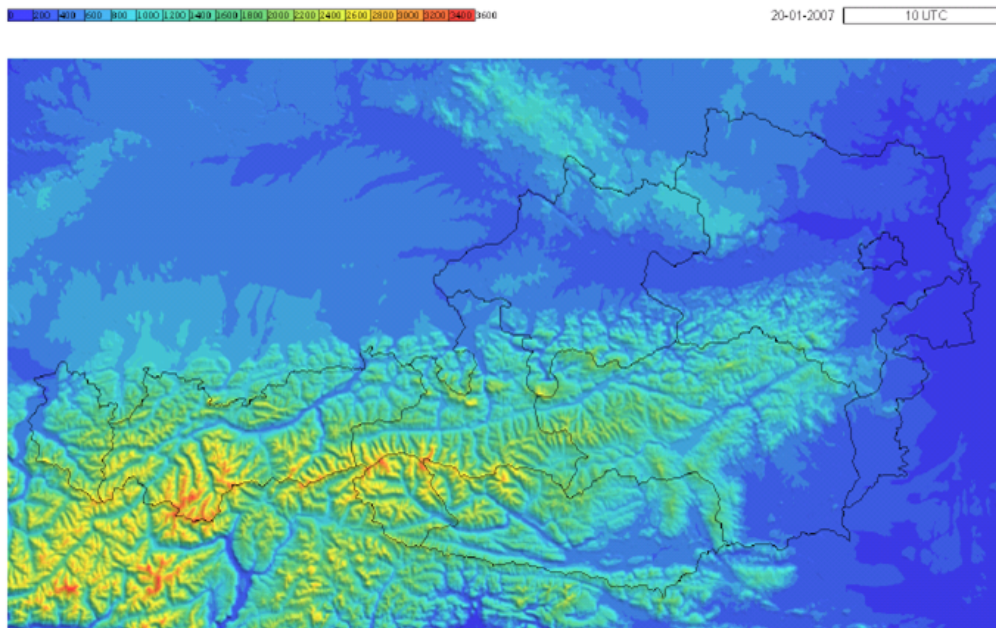


Figure 2.2: INCA’s orography given on its grid with 1 km×1 km grid spacing. Provided by ZAMG.

tion) on a 5 minute time interval (Kirchengast et al. 2008). After the application of an automated quality control system the data is interpolated and upscaled onto a regular grid with 1 km grid spacing. The gridded data cover an area of 21 km×14 km around the city of Feldbach (22 × 15 grid points). For this study the data is resampled to a temporal resolution of 60 minutes (details about the interpolation and re-sampling method can be found in Kirchengast et al. (2008)). The parameters provided are air temperature and precipitation.

2.4.3 Analysis of the reference data

In order to allow first estimates of INCA’s quality (at least in the WegenerNet region) INCA is compared to gridded data products of the WegenerNet, which has the highest station density of all observation networks accessible to the NHCM-1 project. According to the observed parameters in the WegenerNet and the INCA data, the INCA/WegenerNet comparison is based on air temperature and precipitation covering the periods July 2007 and January 2008. Influences on air temperature due to differences in surface altitude between INCA and WegenerNet are reduced by applying the average temperature lapse rate for moist air (6.5 °C/km). An extended version of this comparison with respect to longer periods can be found in the report of the NHCM-1-embedded intercomparison study Local Climate Model Intercomparison Project (LocMIP) (Prein et al. 2010b).

Figure 2.5a shows the monthly deviations (July 2007) of air temperature of INCA from

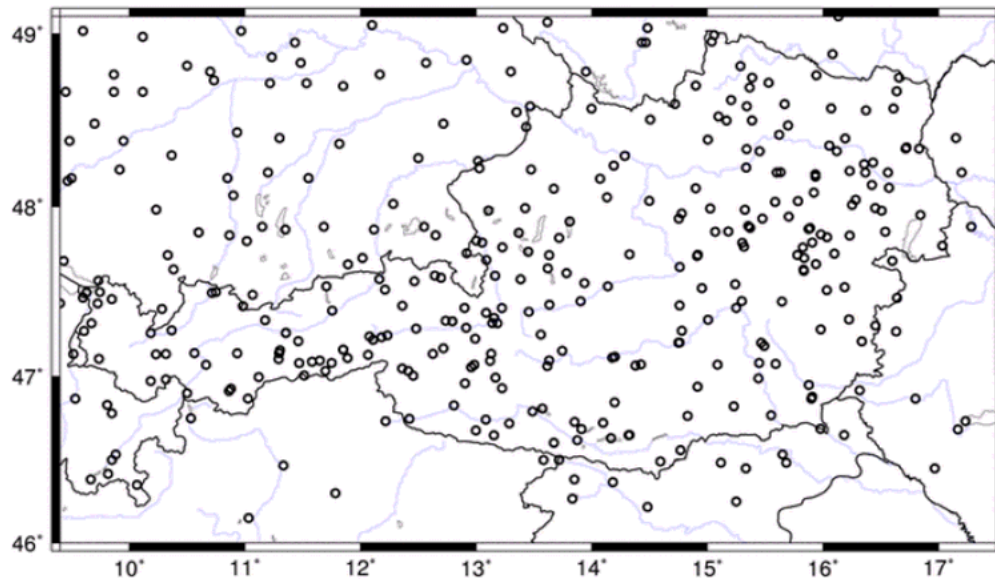


Figure 2.3: Stations operationally used in the hourly *INCA* temperature and relative humidity analysis based on *TAWES*, *SYNOP*, and hydrological stations. Source: Haiden et al. (2010).

the purely observation-based WegenerNet data. Averaged over the WegenerNet region the deviations nearly vanish, but *INCA* is warmer along the valleys (up to 1.3 K in the upper part of the Raabtal) and cooler over the ridges (up to -1.7 K at the Gleichenberger Kogel, which is a forest-covered hill with 598 m altitude). This structural behavior is also visible in winter (January 2008), but with a weaker pronounced underestimation at the Gleichenberger Kogel (up to -0.9 K, cf. Figure 2.5b). This gives reason for a systematic characteristic of over/under estimation.

Concerning precipitation *INCA* is wetter than the WegenerNet throughout the study area and in both months. In summer (July 2007) (cf. Figure 2.5c) the overestimations are stronger pronounced (up to 3.4 mm/d) and underestimations (up to -1.3 mm/d) occur. Since convective regimes are the most dominating weather patterns in summer causing heavy precipitation events, it is possible that *INCA* stronger overestimates convection-induced precipitation resulting in this observed behavior. In winter the overestimation is weaker pronounced and more homogeneously distributed with an averaged bias of 0.5 mm/d (cf. Figure 2.5d). However, since precipitation observations of the WegenerNet are not heated, the measured precipitation is lower than is actually the case at subzero temperatures.

Further comparisons with the WegenerNet data covering the complete year 2008, which have been conducted in a further research project funded by the Styrian Government (Gobiet et al. 2010), show similar results increasing the evidence for systematic errors of *INCA* with respect to the vertical gradients.

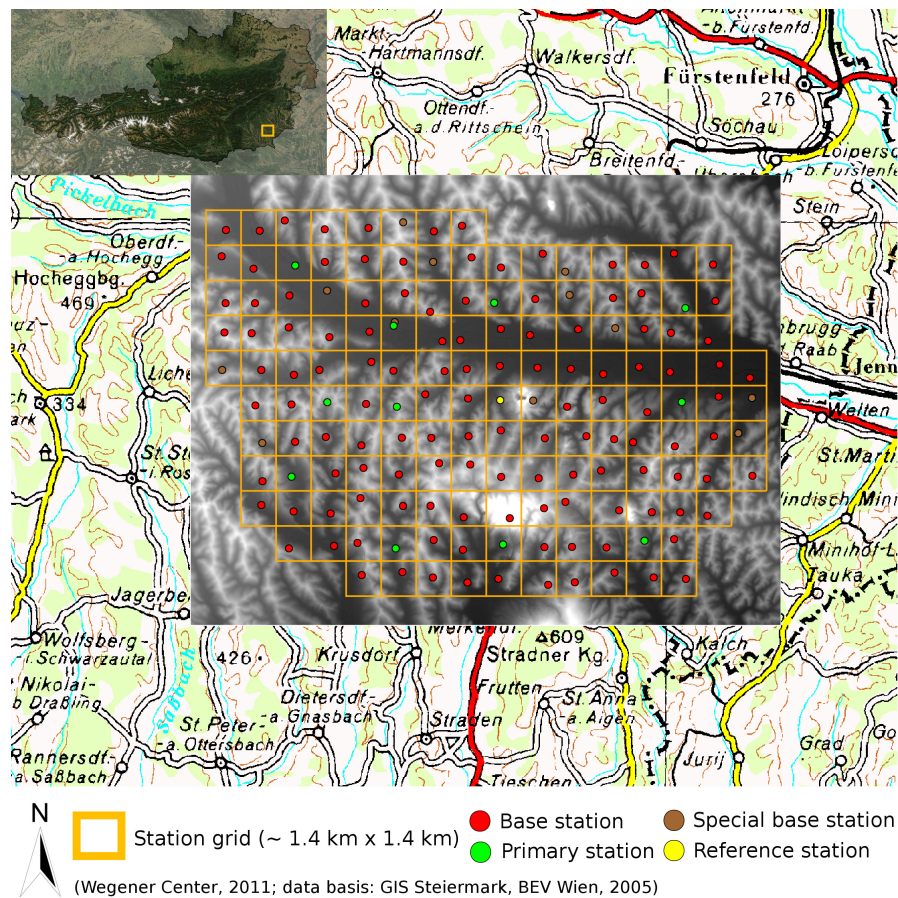


Figure 2.4: WegenerNet stations and the station grid surrounding the city of Feldbach. Mean distance between neighboring stations is ~ 1.4 km. Source: WegenerNet Team (T. Kabas)

It can be concluded, that **INCA** (a) underestimates air temperature in higher regions and overestimates temperature in valleys and (b) precipitation is overestimated in general, but underestimations with notable extent occur during July and **June–July–August (JJA)** (Gobiet et al. 2010) when convective conditions occur most frequently. A thorough evaluation of the **INCA** dataset lies outside the **NHCM-1** project and is therefore set aside. It is just pointed out that **INCA** carries certain errors and these errors have to be taken into account in any further evaluation where **INCA** is used a reference dataset.

2.4.4 Analysis of the driving data

As already mentioned in **Section 2.3** the driving data chosen for this study are operational analysis and forecasts of the **IFS**. In their analysis the **ECMWF** includes as many

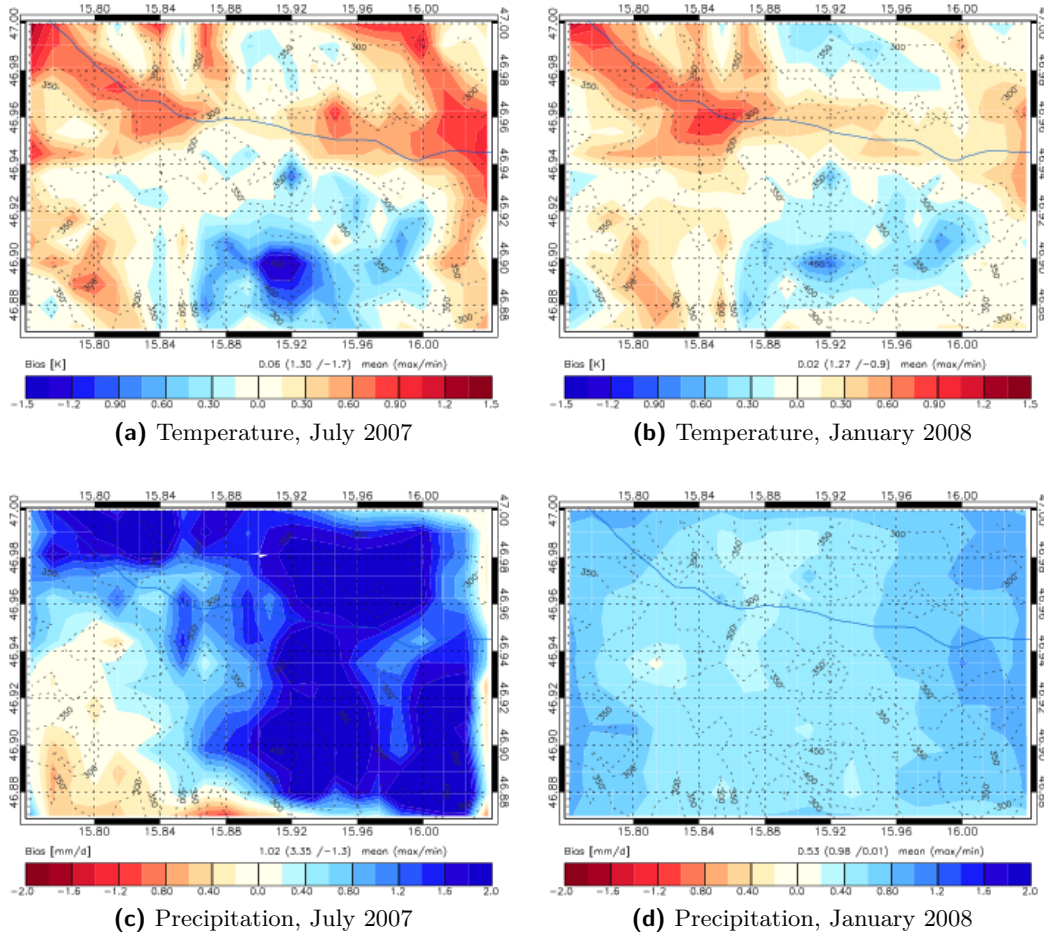


Figure 2.5: Deviations of monthly mean temperature [K] (upper row) and monthly mean precipitation [mm/day] (lower row) of *INCA* from gridded WegenerNet observations with 1 km×1 km grid spacing.

observations as possible to get the best available estimate of the distribution of global atmospheric variables. But at least in the short-term forecasts, like every other model also this one shows biases from observations, especially when it comes to high resolution details which — by design — can not be included in global models. In order to get a better picture of the quality of the driving data the authors also analyze differences between the driving data and the main correlative dataset, *INCA*.

The only parameter available for comparison is 2 m air temperature, since this is the only analyzed parameter in the *IFS* among the three parameters chosen for evaluation in this study. Precipitation amount is only available as a forecast parameter, and the authors did not want to evaluate forecasts of the *IFS*. Surface downward shortwave

radiation (a.k.a ‘global radiation’) is not available at all. In the temperature analysis a height correction as discussed in Suklitsch et al. (2008) has been applied in order to balance differences in the surface altitude of the two datasets.

The difference plots between **IFS** and **INCA** are shown in Figure 2.6 for both months, July 2007 and January 2008. At the first glance there is a big difference between these two months, partly the bias is even inverted. In July (Figure 2.6a) temperatures are overestimated by **IFS** in the mountains and underestimated in the inner alpine valleys. Plains are simulated too warm, too. Looking into more detail is a bit dangerous since the differences in the details may be attributed to both datasets. Doing so one sees that the western flanks of the mountains are particularly warm biased in **IFS** (or too cool in **INCA**). In January (Figure 2.6b) the picture is a whole different one: Mountains are too cold in **IFS** and valleys are too warm. If the height correction using a constant lapse rate of -6.5 K/km is left out the bias characteristics are inverted in winter (i.e., mountains are suddenly too warm in **IFS**) and enhanced in summer (not shown). This indicates that in winter the lapse of -6.5 K/km should be reconsidered in future work.

In context with the findings in Subsection 2.4.3 this means that the temperatures simulated by **IFS** in July are very accurate. In January there seem to be cumulating problems with the vertical temperature gradient from both datasets which makes a clear statement impossible.

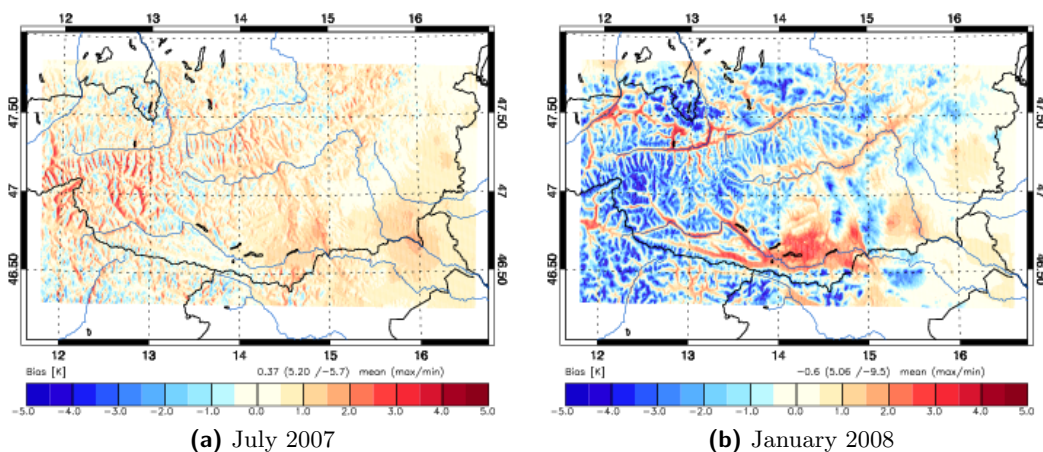


Figure 2.6: Deviations of monthly mean temperature [K] of **IFS** from **INCA** analysis. A height correction of -6.5 K/km has been applied. Positive values equal to a too warm **IFS** model.

2.5 Synoptic overview

At this point the authors give an overview of the climatic conditions and overall synoptic situations during the full simulation period. Like the simulations this analysis focuses on the two test areas in south eastern Styria (abbreviated ‘D4a’ in the following) and the Hohe Tauern region (‘D4b’), although a situation report for the whole Eastern Alpine Region is given to get the broader picture and the connection between the two focus regions. This discussion is given in [Subsection 2.5.1](#). Furthermore, the two test months which most simulations were conducted for, July 2007 and January 2008, will be discussed in more detail than the rest of the year in [Subsection 2.5.2](#) and [Subsection 2.5.3](#). The synoptic analysis is based on the [E-OBS \(E-OBS\)](#) dataset, [ZAMG](#) station data and publicly available re-analysis data of the [Global Forecast System \(GFS\)](#) of [National Centers for Environmental Prediction \(NCEP\)](#).

2.5.1 General overview

The year 2007 started with a very warm January. The temperature deviations from the climate mean in this month in the eastern Alpine region were at least 3.0 K, the maximum deviation was about 6.5 K. Similar, but not that large, deviations also occurred in February (differences to the climate mean between +2.5 K and +4.5 K). This very mild atmospheric conditions were possible because of prevailing westerly flows which advected warm air masses from the Atlantic to the Alpine region. There were virtually no northerly or northeasterly flows which at that time of the year would bring cold polar air masses to the Alps. The months from March to August show subsequently decreasing positive deviations from the climate mean. During these months westerly and southwesterly flow regimes and gradient weak conditions prevail. The remaining four months are slightly cooler than in the climate mean with differences ranging from -0.2 K to -2.0 K. These months, especially September, show many days with synoptic conditions which enable the advection of rather cool air masses to the Alpine region, e.g., northwesterly flows. January 2008, although starting out rather cool, was again warmer than in the climate mean. Deviations topped +4.5 K at some places in the Eastern Alps, in the inner-alpine region they partly did not exceed +2.5 K.

The monthly numbers for the two focus regions read: temperature deviation in D4a between -1.1 K and +5.6 K, in D4b between -1.9 K and +5.3 K, precipitation deviation in D4a between -90 % and +92 %, in D4b between -95 % and +52 %. The deviations of the annual mean temperature is +1.9 K in D4a and +1.3 K in D4b, respectively, the deviations of the annual mean precipitation amounts to -5 % in D4a and -8 % in D4b.

2.5.2 July 2007

The first main evaluation period is the month July 2007. The two evaluation regions show quite different deviations from the climate mean which is why they are treated separately below.

The first main evaluation period is the month July 2007. Several cold fronts pass the Alps during this month. The most important ones occur around July 9 and July 30. Both cold fronts trigger thunderstorms and locally heavy precipitation events. In the middle of the month, starting July 17, persistent advection of hot air masses results in a heat wave which cumulates to the hottest day of the year on July 20. For example, the highest temperature measured by the WegenerNet that day was 37.8 °C. More detailed information on these weather events follows in [Section 2.6](#).

The temperature deviation in this particular month was 1.2 K in D4b region and 2.4 K in D4a region, respectively. The values for precipitation deviation from the climate mean read -15 % in D4a and -6 % in D4b, respectively.

2.5.3 January 2008

The second main evaluation period is the month January 2008. This month started with low temperatures which were possible through persistent low level clouds preventing insolation, and advection of cold air from the east. However, no noteworthy precipitation event occurred. Starting around the middle of the month more and more warm air is advected from the Atlantic or the Mediterranean which avoids very cold days and nights during this period. A stormy northwesterly flow associated with the passage of a low pressure system further north induces heavy precipitation at the northern flanks of the Alps, also affecting the D4b region at its northern side. More details follow in [Section 2.6](#).

January 2008 exhibited strong deviations from the climate mean: Temperatures were around 3.6 K above normal in the D4a region and about 3.4 K in the D4b region. With respect to precipitation the D4b got only slightly less precipitation than in the climate mean (-11 %) while the D4a region ran dry since hardly any precipitation event crossed that area (-86 % compared to the climate mean).

2.6 Interesting weather events

As discussed earlier in this section two simulation periods were chosen on purpose: the authors wanted to have one month with strong convective events on the one hand and one month with a predominantly stratified atmosphere. After browsing through the weather records of recent history the choice was made for the already noted July 2007 and December 2008 for being the evaluation periods. In the next paragraphs ‘interesting’ weather events that took place in these periods shall be discussed in more detail.

July 2007: This summer month was a very hot one. Three heavy precipitation events occurred in the D4a region. In this region the month started out moderately warm with temperature maxima hardly above 30 °C. In the night turning July 4, a low pressure system passed north of Austria. The associated cold front passed the region in the morning of this particular day and, caused by the time of the day, induced only moderate thunderstorms which at some points produced precipitation of about 6.5 mm/h. A more appropriate setting for heavy precipitation events occurred only 5 days later, on July 9. After the cold front passage mentioned above the atmosphere heated up again quite fast, the maximum temperature on July 9 nearly reached the 30 °C mark. Insolation on this day was very strong, there were no clouds which could decrease radiation input, and the soil was still moist from the previous precipitation event and therefore could evaporate an appropriate amount of water. In the evening of July 9 another low pressure system passed by the Alps and the associated cold front reached the region around 20:30 UTC. That evening multiple thunderstorms crossed the region and produced precipitation amounts of up to 3.5 mm in 5 min. The total amount of this event lies between 19 mm and 37 mm.

January 2008: In case of the D4a region this month is characterized by an enormous dry spell: the region received less than 20 % of the normal precipitation amount. Instead of generally cold and often nebular days there were very sunny and comfortably warm ones. The most prominent weather feature in that month was a strong low pressure system which affected the two test regions mainly on January 27 and January 28. That low pressure system caused severe winds with gusts up to 165 km/h, the highest measured wind speed in the test regions was 115 km/h in SE Styria and 155 km/h in Hohe Tauern.

3 Results

At the beginning of this chapter the authors want to give a short overview on the evaluation concept (Section 3.1). In this section the various plots used in the course of the evaluation are shortly described, and the strategy persecuted in the evaluation is laid out. The actual results are then subdivided into three sections according to the three sets of simulations that have been conducted. There is the evaluation of the ‘preliminary cloud resolving climate simulations’ (S1) in Section 3.2, followed by the results of the ‘longer term cloud resolving climate simulations’ (S2) in Section 3.3 and the ‘sensitivity experiments at the cloud resolving scale’ (S4) in Section 3.4.

Each of these sections is further split up in two subsections reflecting the two test regions since the results, as will be shown, are as different as the synoptic conditions themselves (which has been laid out in Section 2.5). For each of these groups there will be an evaluation of the parameters 2 m air temperature and precipitation amount, in case of the S4 experiments the parameter global radiation will be evaluated, too.

This chapter includes many plots. The authors therefore chose to cumulate them in the appendix, since otherwise they would disturb the reading process.

3.1 Evaluation concept

The overall evaluation strategy for the simulations conducted in this study is to compare all model results, regardless of their respective horizontal resolution, on the grid of the reference dataset INCA (see Subsection 2.4.1). This makes a comparison of the results easier. However, one has to be careful when bringing the partly considerably coarser model resolution to the fine grid of the observation dataset. The method used to achieve that is called ‘resampling’ and conserves area mean values. The method is described in more detail in Suklitsch et al. (2008). An additional height correction for temperature has generally not been applied in this study.

The overall goal of this evaluation is to find out whether or not there is an ‘added value’ of cloud resolving climate simulations, where an ‘added value’ can manifest itself in different ways. Another goal is to find out which model components have what kind of effect on the results, and which ones are crucial with respect to climate simulations at cloud resolving scales.

The evaluation is based on three categories briefly described below with hourly data as the basis. A more detailed description can be found in Prein et al. (2010a). The

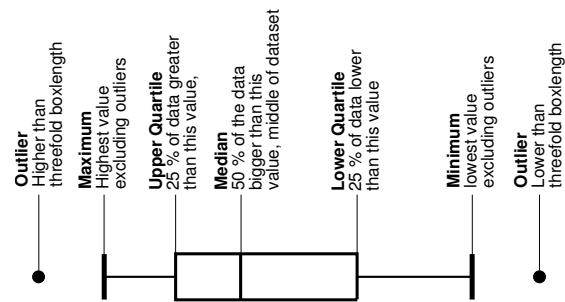


Figure 3.1: Statistical values behind the box-whisker plot. The line within the box shows the median of the considered sample. The upper end of the box shows the 25 % quantile and the lower end the 75 % quantile of the sample. The length of the whiskers are one and a half of the length of the box tops. All points which are outside this distance are outliers and are displayed as diamonds.

performance of the RCMs might differ in each of the categories, and so an added value of the cloud resolving simulations may surface.

3.1.1 Evaluating the Performance in Mean Climate

Box-Whisker Plots are used to display the error ranges of the bias on a half-daily basis.

First, the data is spatially averaged and twelve hourly data are calculated for the daytimes night (18 UTC until 6 UTC) and day (6 UTC until 18 UTC). This means that every daytime consists of 31 time slices in each evaluation month. From the distributions of these points the boxes and whiskers are generated. The background statistics for the present box-whisker plot is shown in [Figure 3.1](#). If outliers (denoted with open diamonds) lie outside the range of the axis the number of outliers in that direction is above the corresponding simulation.

Conditional-Quantile Plots: In this kind of plots certain aspects of the joint distribution of the reference data and the simulation data are shown. The plot is therefore separated in two parts. The first one shows the conditional distribution, while the second one presents the unconditional distribution of the data.

The conditional distribution is derived by separating the range between the minimum and the maximum value of a considered variable of the reference dataset into 100 parts of equal distances ('bins'). Next, at each time slice those grid points in the reference dataset which are within a certain range of the considered slice (e.g., for 2 m temperature between 10 K and 11 K) are searched. Afterwards, at exactly the same grid points and the same time slices the values of the simulated dataset are taken and the 50 % quantile is calculated and plotted against the mean value of the considered slice of the reference dataset. The 50 % quantile of a perfect simulation will therefore lie exactly on the 1:1 diagonal line.

The second part of the plot is the unconditional distribution and shows the density functions of the reference data and the simulations.

A more detailed description of conditional-quantile plots can be found in Prein et al. (2010a), Wilks (2005) and Stevenson (2006).

Error Portrait Diagrams will be used to sum up the whole evaluation in Chapter 4. These plots show the mean bias of each individual simulation in a tabular manner, where the x-axis corresponds to the horizontal resolution and the y-axis corresponds to the simulation setup. As a result, when reading lines of these plots one can determine whether the bias of the RCM within the same simulation chain (i.e., same model setup, different horizontal resolution) increases or decreases, when reading columns one can see the better or worse setups and RCMs at the same horizontal resolution.

3.1.2 Evaluating the Spatial Performance

Spatial Taylor Diagrams display three statistical properties in one single plot as shown in Figure 3.2. The correlation coefficient R is the arccosine between the x-axis and the simulated data point. The normalized standard deviation of the observed data σ_o is the distance between the origin and the observed data point (and equals, by design, always to zero), while the normalized standard deviation of the simulation data σ_s is the distance from the origin to the simulated data point. The distance between the simulated data point and the observed data point shows the centered root mean squared error E' . For a detailed description of the Taylor diagram see Taylor (2001).

In this report, two kinds of Taylor diagrams are shown. The first displays the spatial statistical parameters of the temporal averaged fields. The second contains the spatial statistical values of each hourly time slice. The density of these points in the Taylor diagram is then shown as contours where dark colors mark regions with a high density. This method not only shows the spatial performance of the simulations but also contains information on the ability of the RCMs to capture spatial characteristics on hourly basis.

Fractional Skill Score (FSS): Evaluating the spatial characteristics of precipitation in a high temporal and spatial resolution is one of the toughest tasks in the verification of atmospheric simulations. This is due to the fact that precipitation fields feature high spatial variability and are partly discontinuous, partly continuous within a region. Looking at very high resolutions, precipitation features on grid point basis may get non-deterministic and unpredictable (e.g., intermittent convective rainfall).

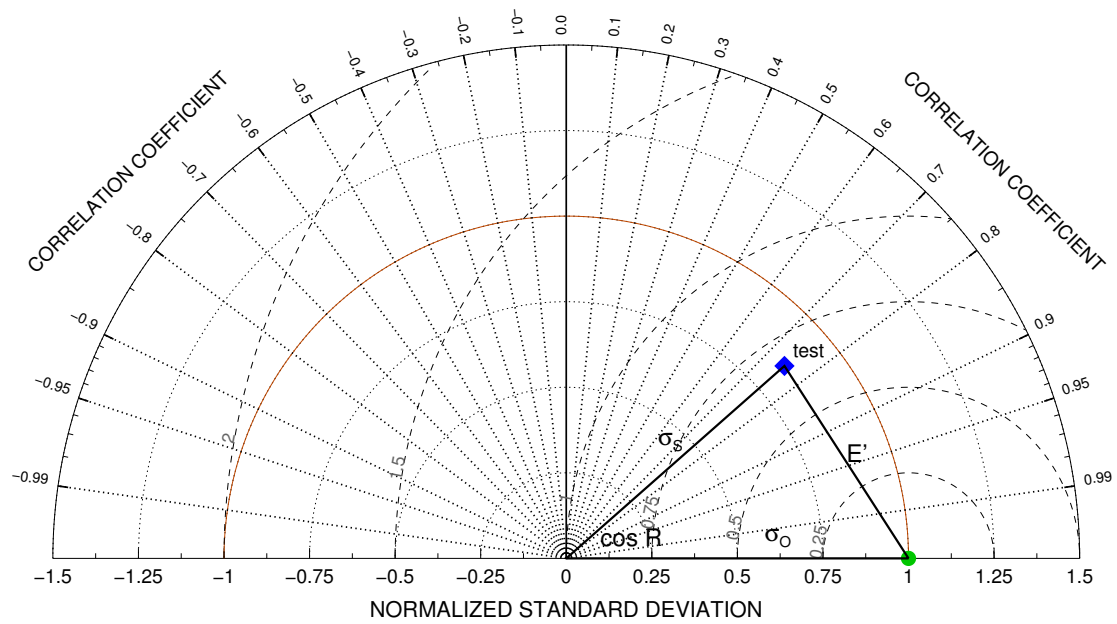


Figure 3.2: Exemplary Taylor diagram for a test field. The black triangle shows the relation between the correlation coefficient R , the normalized standard deviation of the test data σ_s and the reference data σ_o (which, by design, equals to 1), and the centered root mean square error E' .

Therefore, evaluating spatial precipitation fields with traditional statistical methods often leads to the so-called ‘double penalty’ problem, because certain features are observed but not simulated while others get simulated but are not observed. That is why special methods were developed which are discussed in Prein et al. (2010a).

In this report the **fractional skill score (FSS)**, a method which is often used in the evaluation of **NWP** models, is used. It was published by Roberts and Lean (2008) and is based on the assumption that a useful simulation has a similar frequency of precipitation events as the observation. In the **FSS** method multiple neighborhood sizes and precipitation thresholds are used to evaluate the dependency of skill on spatial scales and rainfall intensity.

3.1.3 Evaluating the Temporal Performance

Temporal Taylor Diagrams: As in **Subsection 3.1.2** Taylor diagrams are also used for the temporal evaluation of the cloud resolving climate simulations. Again two kinds of Taylor diagrams are presented. One shows the spatially averaged temporal statistical values. It essentially shows the ability of the **RCMs** to reproduce the mean time series of the whole domain. The other kind of Taylor diagrams displays

the temporal statistical values on grid basis as a contour plot. It gives an insight on how accurate the RCMs are able to simulate temporal characteristics in different parts of the considered domain.

3.2 Preliminary cloud resolving climate simulations

3.2.1 Evaluation in the D4a region

2 m temperature

Figure A.1 shows the conditional quantile (CQ) plots for the evaluation in the summer and the winter month at all three horizontal resolutions separated by RCM. The first thing that strikes the eye is the 0 °C peak of the COSMO-CLM in the winter month which is largest in the 10 km simulation. Nearly 10 % of all grid points and time slices (further called the ‘sample’) have that value. This peak gradually decreases with each increase of the horizontal resolution to about 4.5 % of the sample at 1 km horizontal resolution. This is still too much compared to the observations and is a hint that something might be going wrong in the snow related processes. MM5 and WRF do not show this peak behavior at all. In the winter month all simulations underestimate higher temperatures. COSMO-CLM because of its 0 °C peak already at temperatures above 0 °C, MM5 and WRF for temperatures above about 4.5 °C. Additionally all models have in common an overestimation of the lowest temperatures in the observation dataset. But the overestimated low temperatures occur too seldom to have an impact on the overall bias which lies at about -1.8 K (averaged over all simulations at 1 km horizontal resolution). The simulations of the summer month in that region perform better in all aspects: Because of the generally higher temperatures and low altitudes there is no 0 °C peak in the COSMO-CLM, but it still tends to simulate too low temperatures. Interesting enough, the 10 km simulation in that case performs better than the two simulations with higher horizontal resolution. The latter fail at reproducing the higher temperatures which might be related to problems with insolation.

Figure A.2 shows box-and-whisker plots for all simulations separated into RCM, horizontal resolution, as well as daytime and nighttime. These plots reveal that all three RCMs show a pronounced cold bias during nighttime (the median bias roughly lies between -1.5 K and -2.8 K), while during daytime only COSMO-CLM has a similar strong cold bias. Most simulations show a slight increase in temperature (decrease of cold bias or even switch to small warm bias) with increasing horizontal resolution. In winter all MM5 and WRF simulations show a good performance with the median bias being close to zero, except M58 which is the simulation with reduced vertical resolution. COSMO-CLM shows a strong cold bias, both during nighttime and daytime, which is mitigated by increasing the resolution to 1 km. The error range of one simulation chain is nearly the same at all horizontal resolutions.

A comparison of spatial and temporal Taylor diagrams for temperature for this region (cf. Figure A.3) at a first glance shows that in general the temporal correlation is reproduced much better than the spatial one. While the spatial correlation ranges from 0.1 to 0.5, depending on RCM, resolution and month, the temporal correlation ranges from 0.82 to 0.97. The temporal correlation does not vary much for COSMO-CLM at the different resolutions. MM5 and WRF on the other hand show better temporal correlation in their 3 km simulations in summer (Fig. A.3c). In winter (Fig. A.3d) the picture is slightly clearer: MM5 and WRF show an improvement in terms of temporal correlation with increasing horizontal resolution, COSMO-CLM on the other hand captures the temporal evolution of temperature less good with each further nesting step. The differences for all RCMs, however, are rather marginally. The temporal variability is captured very good both in summer (Fig. A.3c) and winter (Fig. A.3d) by MM5 and WRF, slightly less well by COSMO-CLM which underestimates the temporal variability. The spatial variability is strongly overestimated by all RCMs in summer (cf. Fig. A.3a). All models also show an improvement with increasing horizontal resolution both in terms of spatial variability and spatial correlation. For example, while COSMO-CLM shows nearly twice as much variability as the reference dataset at 10 km horizontal resolution this overestimation decreases to about 1.5 times at 3 km and to 1.25 times at 1 km. At the same time the spatial correlation increases from 0.28 to 0.31 to 0.42. In the winter month (cf. Fig. A.3b), when the diurnal cycle in this region is generally dampened compared to summer months, the spatial correlation is less good than in the summer month, but the variability is reproduced with acceptable accuracy (ranging from 0.85 to 1.25).

Precipitation amount

Displayed in Figure A.4 are the CQ plots for precipitation during both test months in the D4a region. These plots show that COSMO-CLM is the only model which produces precipitation events in the summer month in compliance with INCA (in agreement with both time and location; cf. Figure A.4a). An opposite performance provide MM5 and WRF. These two models perform better in the winter month (cf. Figures A.4d and A.4f) where they capture some precipitation events correctly but they do not capture the precipitation events in summer (cf. Figures A.4c and A.4e). The density function parts in Figure A.4 show that in summer only MM5 is able to capture the full spectrum of precipitation rates at all resolutions. COSMO-CLM on the other hand produces no precipitation events with more than 7.5 mm/h at 10 km horizontal resolution which is improved with increasing horizontal resolution. WRF does not produce precipitation events with more than 14 mm/h at any resolution.

The plots of the fractional skill score shown in Figure A.6 (for summer) and Figure A.7 (for winter) show a rather interesting feature. This type of analysis reveals that especially in summer MM5 does reproduce weak precipitation events less good when its horizontal resolution is increased. In winter the situation is slightly better: if the thresh-

3 Results

old is set to exclude events with less than 0.5 mm/h the simulations with 1 km horizontal resolution perform slightly better than the ones with 3 km horizontal resolution which in return perform equally well as the simulations with 10 km horizontal resolution. For **WRF** the results are similar. In summer the increase of horizontal resolution from 10 km to 3 km yields better results when disregarding precipitation of less than 2 mm/h, a further increase of resolution to 1 km the improve in the results is not noteworthy. The same is true for the winter case, but here the threshold is 0.5 mm/h. Below these thresholds, when lower precipitation rates are regarded in the analysis, the coarser resolved simulation performs better, especially in small scale events. Much improvement between 10 km and 3 km as well as between 10 km and 1 km horizontal resolution is shown by the **COSMO-CLM**. **COSMO-CLM** can also further increase its skill in the resolution step from 3 km to 1 km horizontal resolution for precipitation events with more than 2 mm/h. However, its skill is at the same time reduced for precipitation events below this threshold. In winter the **COSMO-CLM** does perform best at 10 km horizontal resolution and worst at 3 km horizontal resolution.

The Taylor diagrams for spatial and temporal correlation are given in **Figure A.8**. They show that there is hardly any correlation between observation and simulation at all, the correlation coefficient mostly lies around 0 or 0.1. There is no clear clustering of the results, each sensitivity experiment ‘interprets’ the precipitation events in its own way, which is mostly wrong either in space or time.

3.2.2 Evaluation in the D4b region

2 m air temperature

Figure A.9 shows the **CQ** plots for all S1 simulations in the D4b region for both the summer month and the winter month. Similar to the other region there is a 0 °C peak in the summer month in **COSMO-CLM** and a shift in the distribution function of the **COSMO-CLM** simulations in all resolutions towards lower temperatures. Also, while in the summer month both the 3 km simulation and the 1 km simulation have a nearly identical distribution function the 1 km simulation shows improvements in winter. In the winter month all **COSMO-CLM** simulations show too low temperatures at all resolutions. **MM5** and **WRF** on the other hand in winter overestimate sub-zero temperatures and underestimate temperatures above roughly 0 °C. For all three **RCMs** one can see an improvement with increasing horizontal resolution: the deviation of the **CQ** curves from the ideal one become smaller from one nesting step to the next.

The box-and-whisker plots in **Figure A.10** show that all three **RCMs** are cold biased during nighttime in the summer month (where **WRF** has the smallest bias and **COSMO-CLM** the largest one). During daytime the bias of both **MM5** and **WRF** are nearly zero, **COSMO-CLM** on the other hand stays strongly cold biased at all three horizontal resolutions. This difference between the two American models and the European one is

even more pronounced in the winter month where **COSMO-CLM** produces a cold bias of about -5 K at 3 km horizontal resolution while the other two **RCMs** are slightly warm biased (roughly +1 K). It is important to notice, however, that in that case **COSMO-CLM** manages to reduce its enormous cold bias at 3 km by 2 K to about -3 K at 1 km.

The spatial Taylor diagrams (Figure A.11) reveal a better performance by all models at all resolutions in summer than in winter. Also, the results for the summer month are more clustered than in winter. In summer (Fig. A.11a) the correlation increases with each resolution step and reaches values around 0.8 at 1 km horizontal resolution with a normalized standard deviation of roughly 0.9, i.e., the variance in the temperature field is also captured well at that resolution. The lower resolution simulations underestimate the variance to a higher extent. In winter (Fig. A.11b) the variance is overestimated at a horizontal resolution of 3 km or less and the correlation coefficient reaches 0.75. The temporal correlation of the simulations for the D4b region is overall better in summer than in winter. In summer (Fig. A.11c) the temporal correlation coefficient increases for all models when the horizontal resolution is increased from 10 km to 3 km but decreases again for the next nesting step to 1 km horizontal resolution. **COSMO-CLM** has the best correlation coefficient of the model ensemble with values above 0.94. The variability in this month is captured equally well by all models at all resolutions. In winter (cf. Fig. A.11d) the best temporal correlation is achieved by the simulations at 3 km horizontal resolution. At the same time the variance in the simulated temperature field varies the most at this resolution (between 0.9 and 1.25). A further increase of the resolution renders worse temporal correlation than at 10 km horizontal resolution.

Precipitation amount

The **CQ** plots for precipitation amount in the D4b region (cf. Figure A.12) show that **MM5** and **WRF** do perform equally well in summer. In conjunction with Figure A.13 one can see that both models also produce slightly too much precipitation. **COSMO-CLM**, on the other hand, tends to underestimate precipitation. In winter the performance of all models is much better. Of the three **RCMs** **COSMO-CLM** captures the precipitation events spatially and temporally best which is confirmed by the Taylor diagrams described in the next paragraph. Also, the inter-quartile range (the difference between the first and the third quartile) is smallest for this model. The density function shows that **COSMO-CLM** produces too many precipitation events with less than 2 mm/d. With increasing intensity and finer resolution the density function is reproduced more accurately. **MM5** and **WRF** both overestimate the precipitation events.

The Taylor statistics (cf. A.15) reveal that **COSMO-CLM** performs best of the three **RCMs** in terms of spatial correlation and variability — but at a very low level, the spatial correlation lies below 0.1 in summer and between 0.1 and 0.3 in winter. Temporal correlation is slightly better, but as in the D4a region the simulations at 3 km horizontal resolution perform better than the ones at 1 km horizontal resolution. Especially in

3 Results

summer **MM5** produces way too much temporal variability, its symbols are even outside the range of the Taylor diagram at about 2.5 times the reference standard deviation.

A similar picture can be drawn from the **FSS** plots shown in [Figure A.14](#). The **FSS** of **COSMO-CLM** decreases with increasing horizontal resolution in summer for most threshold values and spatial scales. Especially the step from 3 km to 1 km horizontal resolution does not improve the results in this particular month and region. In winter **COSMO-CLM** does benefit mainly from the 1 km horizontal resolution. The 3 km simulation has a lower **FSS** than the simulations at the other two resolutions. The differences of the **FSS** for **MM5** between the different horizontal resolutions are not overwhelming. There is a slight improvement for precipitation events between 2 mm/h and 10 mm/h in summer from 10 km to 3 km horizontal resolution, the next resolution step does not improve much on the **FSS**. For lower precipitation rates there is a slight decrease of the **FSS** with increasing horizontal resolution. In winter **MM5** has a weak spot for precipitation rates between 2 mm/h and 3.5 mm/h at big spatial scales where its **FSS** drops by up to 0.06. Higher precipitation rates are again reproduced better with increasing horizontal resolution.

3.2.3 Concluding remarks

The S1 experiments show distinct model characteristic biases: while **COSMO-CLM** is cold biased in both test months and both test regions **MM5** and **WRF** partly show a warm bias as well. In terms of precipitation **MM5** and **WRF** both are strongly dry biased in the summer month, **COSMO-CLM** shows a less pronounced dry bias. In the winter month **WRF** performs best with respect to precipitation, where ‘best’ means that its dry bias is less strong than that of the two other models.

With the results achieved the authors settled on the setups of C50 and M55a for the one-year simulations. C50 was the least cold biased setup and as such as good as the median of all S1 experiments in terms of bias and standard deviation (not shown). The differences between the single **MM5** setups in terms of bias was rather small, but M55a featured the more ‘correct’ setup by using shallow convection at the cloud resolving scale. **WRF** had to be dropped because, at that time, it had to be run with a very small time step in order to avoid a crash.

3.3 Longer term cloud resolving climate simulations

As already mentioned in [Section 2.3](#) these simulations were conducted for the period January 2007 to February 2008. However, since **INCA** data is only available from June 2007 onwards the authors only consider the period June 2007 to January 2008 for evaluation.

3.3.1 Evaluation in D3

The box-and-whisker plots displayed in [Figure A.16](#) show that both [COSMO-CLM](#) and [MM5](#) exhibit a rather uniform temperature bias throughout the day. The only exception is [COSMO-CLM](#) which has a stronger cold bias in the evening hours. The biggest outliers occur during daytime in [MM5](#) and in the midday hours in [COSMO-CLM](#). In terms of precipitation there are more outliers, and the error range is biggest in the evening hours. For both parameters applies that the inner-quartile range is narrower for [COSMO-CLM](#) than for [MM5](#), even if the absolute bias might be bigger for [COSMO-CLM](#).

The [CQ](#) plot for temperature (cf. [Figure A.17a](#)) again reveals the 0 °C peak of the [COSMO-CLM](#). Apart from that both models reproduce the shape of the distribution function reasonably well. [MM5](#) tends to overestimate temperatures below roughly 2 °C. In terms of precipitation (cf. [Figure A.17b](#)) [COSMO-CLM](#) has too low precipitation rates throughout the spectrum. On the other hand it partly captures precipitation events on time and location, which [MM5](#) does not. [MM5](#) in turn better reproduces the density function for precipitation in the evaluation period.

One kind of skill of the two models in reproducing precipitation is shown in [Figure A.18](#). The [FSS](#) for the [COSMO-CLM](#) is given in absolute values for the two horizontal resolutions as well as the difference between these two. The skill of [COSMO-CLM](#) (cf. [Figure A.18a](#)) rises when increasing the horizontal resolution from 10 km to 3 km as can be seen in the right panel. For some threshold/spatial scale combinations the gain exceeds 0.1. The skill score of [MM5](#) (cf. [Figure A.18b](#)) do not show this improvement. They are nearly identical at both resolutions, about 0.1 to 0.3 lower than that of [COSMO-CLM](#) at each corresponding threshold/spatial scale pair.

3.3.2 Comparison with evaluation in the two test regions D4a and D4b

[Figure A.19](#) shows a comparison of spatial correlation and variability achieved with the S2 simulations of [COSMO-CLM](#) and [MM5](#) between the evaluation in the biggest possible evaluation domain for simulations at 3 km horizontal resolution (sub-figure a) and the evaluation in the two test regions (b) and (c). When evaluated over the bigger domain the two models show only small differences in both correlation coefficient and variability, with the tendency to achieve higher correlation and less scattering of variability in the higher resolved simulations. Evaluated only in the D4b region both [COSMO-CLM](#) and [MM5](#) show the same pattern: there is an increase in correlation with increasing horizontal resolution and less scattering of variability. Additionally, the correlation of [COSMO-CLM](#) at both resolutions (0.75 at 10 km and 0.81 at 3 km) lies between the correlation of the two [MM5](#) resolutions (0.7 and 0.9 at 10 km and 3 km, respectively). The evaluation in the D4a region, however, shows that the spatial correlation of the [COSMO-CLM](#) simulation at 3 km horizontal resolution drops considerably to around 0.45 from originally 0.84 at 10 km, at the same time the spatial variability also is un-

derestimated by a factor of about 2. **MM5**, although the correlations of the single time slices are more scattered than in D4b region, achieves higher correlation at 3 km horizontal resolution than at 10 km horizontal resolution and — on average — reproduces the variability with acceptable accuracy.

Much better is the accordance between the evaluation domain for the temporal correlation and variability (cf. [Figure A.20](#)): Regardless of the evaluation domain the performance of **COSMO-CLM** is always better than that of **MM5**, the correlation coefficient in all cases is about 0.5 higher and the temporal variability is near to the one of the reference dataset.

Spatial and temporal correlation coefficients for precipitation are also not heavily dependent on the evaluation domain (not shown). They are generally very low — usually around 0.1 (**MM5**) and 0.3 (**COSMO-CLM**).

3.4 Sensitivity experiments at the cloud resolving scale

3.4.1 D4a region

2 m air temperature

The **CQ** plots for the two **RCMs** (cf. [Figure A.22](#)) show that the distribution functions of both **RCMs** are much smoother than the observation in the summer month, the pronounced valley in the sample size around 16 °C is not contained at all in the simulations. Both models show also deficits in the winter month, where they both give too low temperatures above roughly 0 °C. **COSMO-CLM** additionally exhibits a strong 0 °C peak which is mended with each additional nesting step and virtually straightened out at 1 km horizontal resolution. Generally one can deduce from these plots that higher resolution simulations tend to perform better than their coarser resolved brothers.

The box-and-whisker plots in [Figure A.21](#) show that **MM5** seems to have a diurnal cycle in the temperature bias in summer which is not apparent in the winter month. This might be related to **PBL** processes which are not captured correctly in summer. Simulation M59 is the best in this respect, since it features the weakest median bias in both months and both daytime periods, yet it shows the largest error range of the **MM5** simulations in the winter month. Another visible feature in summer is that during daytime the temperature bias in **MM5** is increasing with increasing horizontal resolution while in the **COSMO-CLM** simulations the bias increases in the second nesting step (3 km horizontal resolution) and decreases again in the last nesting step. Judging from the median bias, all **COSMO-CLM** simulations are warm biased throughout the day in summer and cold biased in winter. One cause might be that the soil dried out in these simulations leaving too much energy for the sensible heat flux which in return increased the near surface temperature. In winter the simulations are also less cold biased than in the S1 set which is another indicator that the changing of the soil generally increased the

temperature in the current simulations. Further, the increase of the horizontal resolution mitigates the cold bias to some extent in the winter month.

The Taylor statistics shown in Figure A.23 give an overview on the spatial and temporal correlations of the sensitivity experiments at each horizontal resolution as well as their variances compared to the reference dataset. They show that the spatial correlation is in general lower than the temporal one, and while the differences in spatial correlation between the two months are marginal the temporal correlation is higher in the winter month than in the summer month. Further, COSMO-CLM shows much higher spatial correlation in the summer month than MM5 (cf. Figure A.23a). In terms of spatial variability both RCMs are better in winter than in the summer month at all horizontal resolutions. In Figure A.23c one can see that in summer the COSMO-CLM captures the temporal variability well, while MM5 overestimates it. In the winter month, on the other hand, COSMO-CLM underestimates the temporal variability and MM5 reproduces it well. In any case the increase in horizontal resolution improves both the spatial correlation and variability, whereas this is not true for the temporal correlation/variability.

Precipitation amount

Figure A.24 shows that during nighttime the error characteristics of the MM5 simulations do not change much with resolution. An interesting fact is that the simulation that performed ‘best’ in terms of temperature bias shows the strongest precipitation bias during nighttime and the smallest one during daytime (particularly at 1 km horizontal resolution). The COSMO-CLM simulations are mainly dry biased, especially during daytime, and the increase of horizontal resolution to 1 km worsens the result. As mentioned in Section 2.5 the winter month was very dry with hardly any precipitation. The RCMs also do not produce much precipitation which is a good thing. But the timing is not correct: while there is a small wet bias during nighttime there is a small dry bias during daytime. There is one notable exception, though: M62 at 10 km horizontal resolution. This simulation features ‘slope effects on radiation’.

Figure A.26 shows the difference FSS plots for precipitation for both models in both months in the D4a region. From Fig. A.26a it is clear that in summer the higher horizontal resolution of the COSMO-CLM helps to improve the skill of the model to reproduce precipitation events of the correct size and magnitude. Both the 3 km and the 1 km resolution simulations perform better (in terms of the FSS) than their 10 km parent simulation. However, the increase in resolution from 3 km to 1 km again worsens the skill (which is, as we have seen in the last paragraph, related to a strong underestimation of precipitation as well). In winter (cf. Fig. A.26b) the skill does only improve for a very narrow band of precipitation rate between 0.5 mm/h and 1 mm/h. The skill of the model decreases with increasing horizontal resolution for precipitation rates below 0.5 mm/h. It has to be kept in mind, though, that this month was very dry and there has been hardly any precipitation event at all in that region. MM5 shows the opposite

3 Results

behavior. In summer (Fig. A.26c) there is no additional skill for the higher resolved simulations, on the contrary, the skill decreases slightly. There is hardly any difference between the two cloud resolving simulations. In winter (Fig. A.26d) the higher resolution helps **MM5** to better capture the low precipitation events while it has a negative effect on the higher precipitation rates.

Expectedly the correlation, both spatial and temporal, of precipitation is very low. Figure A.27 shows that summer spatial correlation (see Fig. A.27a) partly even becomes negative, the mean of the correlation coefficients of each **RCM**'s ensemble lies around 0.5. The spatial variance is also spread over a wide range, from 0.4 standard deviations to well over 2 standard deviations of the reference. In winter (Fig. A.27b) it is only marginally better than before, and spatial variance is even more overestimated by both models, particularly by **COSMO-CLM** at 1 km horizontal resolution. Temporal correlation is slightly better than the spatial one in terms of absolute values. But the single sensitivity experiments are far more spread across the Taylor diagram in both summer and winter. In this respect it would be optimistic to speak of an improvement at higher horizontal resolutions. What's more, there is no improvement of the results due to higher resolution.

Global radiation

The **CQ** plots in Figure A.29 show an interesting behavior which can be seen most prominently in the **COSMO-CLM** evaluation for the summer month: the distribution function of simulated global radiation has several peaks, their amplitude increasing with each nesting step. These peaks also appear in **MM5** in summer and in both **RCMs** in winter. The difference to the first case is that here the peaks do not increase in amplitude, plus they are less pronounced. Another striking feature is the peak in **MM5** summer global radiation at around 920 W/m^2 which is higher than the global radiation in the reference dataset. Contrary to that the highest summer global radiation in **COSMO-CLM** is roughly 790 W/m^2 .

Accordingly the biases of the two **RCMs** differ considerably as can be taken from Figure A.28. The minimal bias during nighttime is clear, since between 18 UTC and 06 UTC the insolation in the region is marginal. During daytime, however, **MM5** generates too much radiation (median bias between $+40 \text{ W/m}^2$ and $+80 \text{ W/m}^2$, with the bias increasing with each nesting step), while **COSMO-CLM** receives too few radiation at the surface (bias of roughly -90 W/m^2). In the winter month the nighttime bias is virtually zero, since this time of the day has no sunlight at all, the median of the daytime bias is now negative in both **RCMs** — but still, **COSMO-CLM** has a larger bias.

Correlation coefficients between reference data and simulated global radiation is comparable to that of precipitation. Mean spatial correlation (cf. Figures A.30a and A.30b) lies between 0.05 (summer) and 0.1 (winter) for both **RCMs**, but **COSMO-CLM** captures the spatial variability better than **MM5**. Hardly any differences can be seen for temporal

correlation and variability (see Figures A.30c and A.30c) in summer and winter. One distinctive feature in this respect is the behavior of the temporal correlation in winter: while the correlation coefficient for COSMO-CLM increases with each nesting step it at the same time decreases for MM5 by the same amount leaving both roughly at the same level of 0.85.

The horizontal resolution does not seem to have any measurable effect on the RCMs' performance with respect to global radiation: there is no change in the mean bias, and both temporal and spatial correlation do not vary much with resolution.

3.4.2 D4b region

2 m air temperature

The box-and-whisker plots of the temperature evaluation in the D4b region show that in summer (Fig. A.31a) both RCMs are cold biased during nighttime (where one MM5 simulation, M59, sticks out with a weaker cold bias than the rest). The inner-quartile range (being the interval between the 25 % and the 75 % percentile hardly exceeds the 0 K line. During daytime, however, the biases of both RCMs are scattered around zero, one MM5 simulation (M60), is now predominantly warm biased. In general, COSMO-CLM exhibits the biggest error range at 3 km horizontal resolution, while the error ranges of the MM5 simulations are rather equal at all horizontal resolutions. In winter (cf. Fig. A.31b) COSMO-CLM shows its pronounced cold bias, even the upper whiskers (denoting $1.5 \times$ the standard deviation) hardly exceeds the zero bias line both during nighttime and daytime. This might be related to the snow cover in that region, which consumes too much energy (see also next paragraph). MM5 on the other hand is predominantly warm biased, partially even more than in summer.

The density distribution function for temperature is captured well by MM5 in both months, as can be taken from Figure A.32. COSMO-CLM also captures the density distribution good in summer, but in winter it is somehow distorted for the two coarser resolutions, 10 km and 3 km: These simulations have the 0 °C peak on the one hand (but less pronounced than elsewhere due to the overall conditions in this region) and a pronounced 'valley' at around -1 °C. In case of the 10 km simulation there is another peak at about -3 °C. In winter both models show a small shift in the density distribution, COSMO-CLM to lower temperatures, MM5 to higher temperatures than observed. In these plots one can also see that the CQ curves get nearer to the reference line with each nesting step.

The Taylor diagrams for temperature in the D4b region, depicted in Figure A.33, reveal that in summer there is good accordance between the single sensitivity experiments in their respective horizontal resolution. Figure A.33a shows the spatial correlation and variance which is nearly exemplary for how the simulations should improve on their details: with each nesting step the variance between the single experiments becomes

smaller (the contours get smaller), the correlation increases monotonically, and the normalized standard deviation converges to 1. In winter (cf. Fig. A.33b) the results of the sensitivity experiments are more widespread, there is no clear clustering, and the **COSMO-CLM** simulations with 3 km horizontal resolution perform worse both in terms of correlation and variability than the one with 10 km. Temporal correlation in summer, as shown in Fig. A.33c, is uniform for both models and all horizontal resolutions, **COSMO-CLM** (correlation: 0.95) performs slightly better than **MM5** (correlation: 0.92). In winter (Fig. A.33d) temporal correlation increases with the nesting step to 3 km but then, in case of **MM5**, drops below the correlation of the 10 km simulations at 1 km horizontal resolution.

Precipitation amount

The box-and-whisker plots displayed in Figure A.34 show that the median bias of all simulations, regardless of the **RCM**, is very close to zero in the summer month. Notable exceptions from this rule are the simulations C79 and, to some extent, also C78. These two simulations feature a setup using a diagnostic treatment of precipitation (i.e., there are no prognostic equations used to calculate the contents of rain, snow and ice) and a microphysics scheme including graupel, respectively. Also clearly visible are the huge whiskers of simulation M61. This **MM5** simulation also features a microphysics scheme including graupel. But unlike in the **COSMO-CLM** where such a scheme increases the amount of precipitation in **MM5** it merely increases the temporal variability of the bias, i.e., the timing of precipitation events gets disturbed. Such a simulation would be off the chart in Taylor diagrams. In winter (Fig. A.34b) nighttime precipitation is captured rather well by both **RCMs** (judging by the median bias). Daytime precipitation is generally overestimated by both **RCMs**, with two notable exceptions, M62 and C79. So, with regard to **COSMO-CLM** a setup which produced the ‘worst’ result in summer now produces the ‘best’ one, where the term ‘best’ has to be treated with care. Generally, there are hardly any differences between each nesting step, i.e., the bias does not vary much with resolution. An exception is **COSMO-CLM** which has a more pronounced wet bias at 1 km horizontal resolution during daytime in the winter month.

The **FSS** plots for both models and both months in Figure A.35 show, for example, that there is neither improvement nor decline in terms of skill between the three horizontal resolutions for **MM5** in summer. In the same month **COSMO-CLM** can at least improve its skill compared to the 10 km horizontal resolution, but there is a slight decline from 3 km to 1 km horizontal resolution. In winter (Figures A.35b and A.35d) the results are rather complex: In **COSMO-CLM** the skill is improved from 10 km to 3 km as well as 1 km horizontal resolution for precipitation rates below 1 mm/h. For the narrow band between 1 mm/h and 1.5 mm/h there is a slight decline, stronger precipitation events are captured better mainly at 1 km horizontal resolution. In **MM5** the biggest improvement in skill occurs in the nesting step from 10 km to 3 km horizontal resolution, a further

increase in resolution decreases the skill, especially for precipitation events with more than 2.5 mm/h.

Global radiation

In terms of global radiation one can deduce from [Figure A.39](#) that **MM5**, like in the D4a region, simulates too high values for global radiation whereas **COSMO-CLM** simulates too low values. In the summer month peaks appear in the density distribution function, but less pronounced than in the D4a region. For **COSMO-CLM** the increase in horizontal resolution helps to improve the results, most notably in the summer month.

This statement is strengthened by the box-and-whisker plots of global radiation displayed in [Figure A.38](#). In [Fig. A.38a](#) it can be seen that the underestimation of radiation is strongly reduced between 10 km and 3 km resolution, the further nesting step to 1 km only slightly reduces it once more. Besides the non-existent biases during nighttime the overestimation of radiation in **MM5** is also clearly visible. In **MM5** the overestimation even increases with each nesting step. On the other hand, in the winter month both **RCMs** show a much less pronounced bias, **MM5** even reduces it nearly to zero. In **COSMO-CLM** a slight overestimation of radiation occurs.

4 Discussion

In the previous chapters the authors introduced the results obtained in altogether 26 simulations at cloud resolving scales with the three **Regional Climate Models (RCMs)** **COSMO model in CLimate Mode (COSMO-CLM)**, **Fifth-Generation Mesoscale Model (MM5)** and **Weather Research and Forecasting model (WRF)**. These models were run in various configurations which should tackle potential shortcomings or benefits of the **RCMs**. The simulations show distinctive differences, which partly can be traced back to specific model setups which will be discussed in this chapter.

Figure 4.1 and **Figure 4.2** show a comparative evaluation of all sensitivity experiments conducted in the course of the project **Non-Hydrostatic Climate Modelling (NHCM-1)** for temperature and precipitation, respectively. These plots give a condensed overview on the mean (relative) biases of each simulation and can be used to elaborate effects of different model setups. For both plots one singularity of the **COSMO-CLM** simulations has to be recalled in advance: at a horizontal resolution of 10 km only one experiment has been conducted in both the S1 and the S4 set of simulations. Therefore the bias displayed in the first column of each corresponding row in the two figures is identical (also denoted by the acronym C34 and C71S4, respectively).

Figure 4.1 shows that for **MM5** the transition from the fresh soil initialization to the ‘balanced’ soil initialization brings a smaller cold bias in D4a in the summer month. The same effect can be seen for the summer month in D4b. The signal in the winter month in D4a is inconclusive, while in D4b there is the tendency to an increased warm bias in case of a balanced soil initialization. The use of less vertical levels has a weak warming effect in **MM5** in winter (M58), while the ‘z-diffusion’ in the same month has a weak cooling effect (M60). One simulation sticks out from the rest at 10 km horizontal resolution, M59. This simulation differs from M55 by the use of a different **planetary boundary layer (PBL)** scheme and, of course, the altered soil initialization. Since the other S4 simulations perform very similar to the S1 ones it can be concluded that the warming effect comes from the **PBL** scheme. The fact that it mainly affects the 10 km resolution is a hint that scale dependent interactions are causing this behavior.

So, both sets of **MM5** simulations show very similar biases. Median and inner-quartile range are only slightly different. This indicates that **MM5** is very robust to changes in the setup. Interesting is the fact that, even if the differences are rather marginal, the simulation with 40 model levels (M57) is colder than the one with 20 model levels (M58), i.e., where the 40-level-experiment is cold biased the 20-level-experiment is less cold biased, where the 40-level-experiment is warm biased the 20-level-experiment is

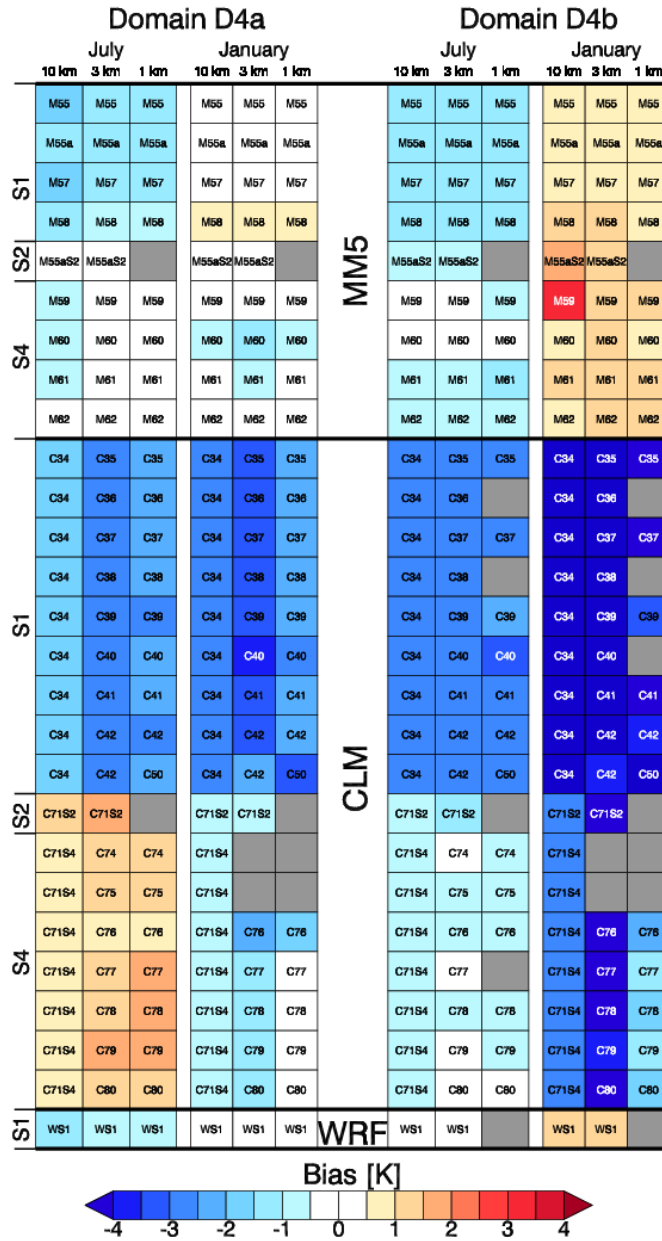


Figure 4.1: Comparative evaluation of all NHCM-1 sensitivity experiments for the parameter 2 m air temperature. The statistical value displayed is the mean bias with INCA as the reference dataset. Red values indicate a warm biased simulation, blue colors indicate a cold biased simulation. Grey blocks indicate that the corresponding simulation was either not carried out or did not succeed. Rows indicate the same simulation chain (identical model setup, varying horizontal resolution), columns indicate the different model setups at the same horizontal resolution.

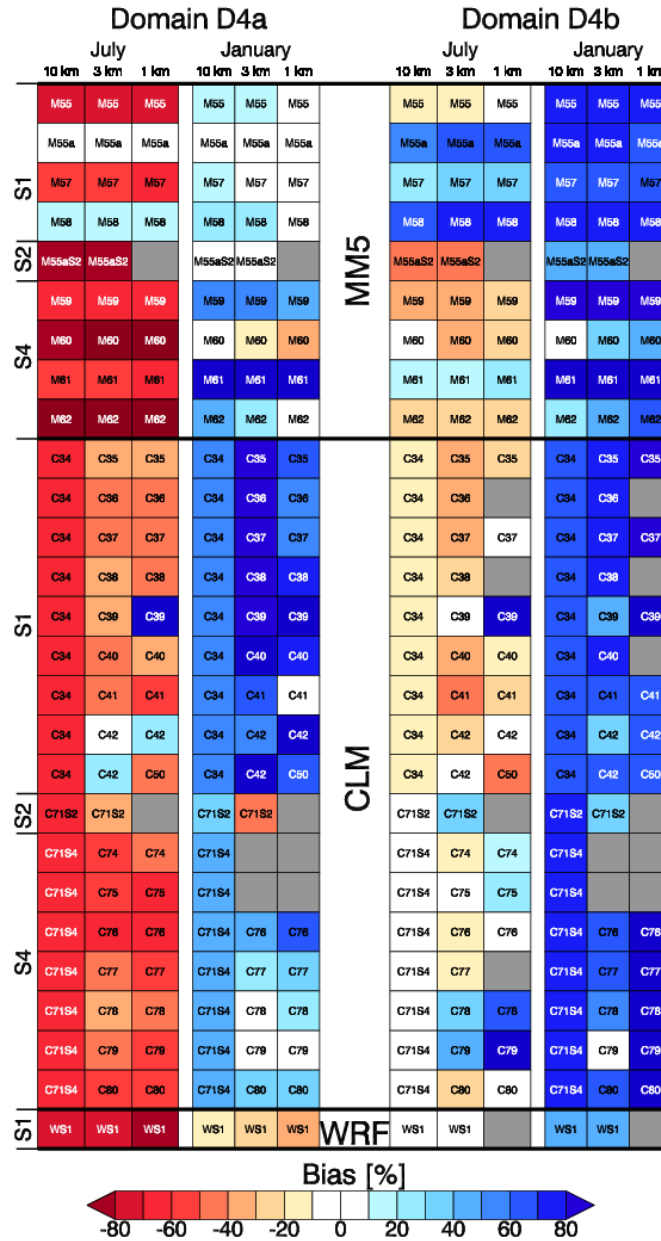


Figure 4.2: Comparative evaluation of all NHCM-1 sensitivity experiments for the parameter precipitation amount. The statistical value displayed is the mean relative bias with INCA as the reference dataset. Red values indicate a dry biased simulation, blue colors indicate a wet biased simulation. Grey blocks indicate that the corresponding simulation was either not carried out or did not succeed. Rows indicate the same simulation chain (identical model setup, varying horizontal resolution), columns indicate the different model setups at the same horizontal resolution.

more warm biased. It is said that with an increase in horizontal resolution also the number of vertical layers should be increased to roughly preserve the shape of the three-dimensional grid boxes. So, a theoretically more correct spatial setup results in a less accurate reproduction of temperatures. The same is true for the **COSMO-CLM** as will be shown below.

For **COSMO-CLM** the S1 simulations are strongly cold biased. The cold bias in D4b in the winter month is off the chart. Still, one can see that the simulation with an extended domain performs slightly better there. In the summer month the cold bias is less pronounced, and it is also less pronounced in D4a in both months. With respect to D4a it is interesting to see that the cold bias is largest at 3 km horizontal resolution and again reduced at 1 km, partly even below the corresponding bias value at 10 km horizontal resolution. The transition to the initialization with a balanced soil completely changes the error characteristics. In D4a the initial cold bias is even converted into a warm bias, which partially increases with increasing horizontal resolution. An exception from this general statement are the simulations at 3 km horizontal resolution in D4b, which are still largely cold biased. From this plot it has to be concluded that at that particular resolution there are some interactions which are preventing the model to ‘unfreeze’. As with **MM5** there is one simulation which is slightly different from the rest as a whole, C76. This simulation is slightly cooler than the other S4 simulations. Its setup uses a ‘3D turbulence’ scheme.

A plain look at the ensemble results show that the cold bias in the S4 simulations is reduced by about 1.5 K. The box-and-whisker plots of the two sets of simulations (Figure A.2 and Figure A.10 for S1, Figure A.21 and Figure A.31 for S4, respectively) show clearly that **COSMO-CLM** more or less completely changes its error characteristics from the one set to the other. Especially in winter **COSMO-CLM** is rather cold biased in the S1 simulations. This cold bias is dramatically reduced in the S4 simulations, partly the model is now even warm biased. The most likely cause for this tremendous change of characteristics in **COSMO-CLM** is something connected to the soil model, since this is the most prominent difference between the two sets of simulations. As explained in Section 2.3 the S1 simulations were initialized ‘from scratch’, soil moisture and temperature were taken from the driving global model. The S4 simulations used the soil parameters from the longer term cloud resolving simulations, S2. They therefore should have started with a more balanced state of the soil. Without further analysis it seems to be clear that there was less moisture in the soil of the S4 simulations. As a result more energy was available for heating the surface and its vicinity rather than for evaporation, i.e., there has been more sensible heat flux than latent heat flux.

Further prominent effects on temperature are related to the surface and/or boundary layer scheme. Turbulence is a key factor for the exchange of heat between the surface and higher altitudes. If something goes wrong here it surely results in overestimation or underestimation of the near surface temperature. Related to that is another issue, namely the correct simulation of temperature inversion layers, cold air pools and alike.

RCMs do not have many model levels within the boundary layer and therefore show difficulties in reproducing such features. But also the vertically higher resolved **COSMO-CLM** simulation did not show obvious differences to other model runs regarding the model errors (in terms of bias, correlation, . . .). From comprehensive simulations at a horizontal resolution of 10 km the authors know that in case of the **COSMO-CLM** vertical resolution and domain size have the biggest impact on the model results. This is obviously not the case for the cloud resolving simulations since the experiments dealing with that kind of settings do not show notable deviations from the other ones. Of course, this as well might be due to the fact that the model domains are rather small here and the models do not have much ‘room’ to develop their own climate equilibrium.

With **WRF** the authors only performed one simulation. As can be taken from the plots there have been problems with this model in D4b, where even a ridiculously short time step of 1 s resulted in a model crash. The cause for this, as has been found out much later, was that there has not been any horizontal or vertical diffusion which would keep the flow stable. However, the results that were managed to achieve are very similar to those of **MM5**. For example, the temperature bias of **WRF** is well within the range of temperature biases of **MM5**, both models show a slight warm bias at 3 km horizontal resolution while the two other resolutions are cold biased. Also the error characteristics in precipitation are very similar between the two models.

Figure 4.2 shows the comparative evaluation of all simulations conducted in this study for the parameter precipitation amount. From this plot one can deduce that most simulations feature a rather strong dry bias in the summer month in D4a. Partly this dry bias also occurs in D4b in the summer month, but here the signal is rather inconclusive. Contrary, in the winter month most simulations show a wet bias, which is pronounced in D4b. M55a and M58 stick out because they produce much more precipitation than the other S1 simulations of **MM5**. The first of these two simulations has shallow convection turned on while the other one features a reduced vertical resolution. The overall effect is obviously the same. Between the S1 and the S4 set of simulations is no clear difference can be seen in case of **MM5**. In S4 the two simulations which produce more precipitation are the ones that use an alternate version of the **PBL** scheme (M59) and the microphysics scheme which includes graupel (M61), respectively. On the other hand, the simulations that feature a large dry bias in the summer month in D4a are the ones which use the ‘z-diffusion’ (M60) and the orographic shading effects (M62), respectively.

In both figures, **Figure 4.1** and **Figure 4.2**, the nested domains (3 km and 1 km grid spacing) show nearly the same biases as their driving mother domain (10 km grid spacing) in the case of **MM5**. This correlation, which is mostly independent from other model perturbations, is a result of the feedback mechanism described in **Subsection 2.3.1**. In the case of **COSMO-CLM**, the feedback does not exist, and hence the nested domains differ much more from their mother domains.

In case of the **COSMO-CLM** simulations a clear difference between the simulations which used a freshly initialized soil and the ones which used a rather balanced soil are

more apparent in the winter month in D4a and in the summer month in D4b. Further, some simulations stick out from the rest through one or another ‘special feature’. C39, for example, shows a weak dry bias in both regions in the summer month at 10 km and 3 km horizontal resolution, while at 1 km horizontal resolution it produces way too much precipitation. This simulation uses the increased domain size. C42 sticks out because it shows a small wet bias in D4a in the summer month, where virtually all other simulations are dry biased. This simulation uses the microphysics scheme which includes graupel. Another interesting feature is that these two simulations show a reduced wet bias at 3 km horizontal resolution in D4b in the winter month. So, for example, the statement that ‘the graupel scheme simply produces more precipitation’ does not hold. Another **COSMO-CLM** simulation worth mentioning separately is C79. This simulation, which features diagnostic treatment of precipitation, shows hardly any bias in D4a in the winter month, its wet bias in D4b in the summer month increases with each nesting step, and while reproducing precipitation in D4b in the winter month correctly at 3 km horizontal resolution it fails doing so at 1 km horizontal resolution.

While the differences in both mean temperature bias and mean precipitation bias within the same month and the same region for the different nesting steps are very small in case of **MM5** and **WRF** this is certainly not true for **COSMO-CLM**. This can be seen in the error portrait diagrams. It is most likely related to the update frequency of the **lateral boundary conditions (LBCs)** and therefore the ‘intensity’ of the coupling between the different nests. As described in the model setup tables the update frequency of **LBCs** is, by design, limited to a maximum of 1 hour in **COSMO-CLM**, contrary in **MM5** and **WRF** the **LBC** update is done with each nest’s time step. This issue becomes more pressing with small domains since vital synoptic information may be lost with an hourly **LBC** update.

With respect to correlations (both temporal and spatial) there is not much change between the S1 simulations (**Figure A.3** and **Figure A.11**) and the S4 simulations (**Figure A.23** and **Figure A.33**). There are of course fluctuations since the various model setups produce different results, but there is no notable or visible difference between these two sets of simulations that catches the eye. The influence of orography on temperature can best be seen in the Taylor diagrams for this parameter. It is much stronger in D4b than in D4a, where there are much higher correlation coefficients visible in both months. Similar is true for the temporal correlation of precipitation (**Figure A.8**, **Figure A.15** for S1; **Figure A.27** and **Figure A.37** for S4). For this parameter, however, a discussion is more complicated since precipitation is very difficult to simulate, let alone correct in time and space. The lack of precipitation during the winter test month is particularly hard to be simulated correctly, since many **RCMs** tend to drizzle. Thus, the differences here might as well be random as determination.

To be correct in time and space, a.k.a ‘the double penalty issue’, strikes hardest in the **conditional quantile (CQ)** analysis and is best visible in the respective plots. There the **RCM** has to produce the correct amount of precipitation or simulate the correct

temperature (both within a certain bandwidth) at the correct grid point according to the reference dataset. Nonetheless it is a valid and valuable analysis since it reveals features such as the 0 °C peak of **COSMO-CLM**. Speaking of which, the 0 °C peak is by far less pronounced in the S4 simulations. The cause for that is most likely that, since this set of simulations is also warmer, there is less snow covering the ground. Less snow also means less energy needed for melting the snow. Less energy needed for melting the snow results in more energy used to heat the atmosphere.

Added value of cloud resolving climate simulations compared to coarser scale simulations have been found in specific analyses, but not in any instance. The analysis of area averaged biases ([Figure 4.1](#) and [Figure 4.2](#)) reveals only few information on added value. However, improvements have been found for **COSMO-CLM**'s cold bias in winter. Hourly temperature distributions and errors related to different observed temperatures reveal consistent improvements in the simulations of temperature, particularly over complex terrain and with regard to specific model deficiencies like a zero-degree peak of **COSMO-CLM**. Most clearly, spatial correlation and spatial variability of 2 m temperature is improved in all models, but there is no improvement in temporal correlation. Also precipitation patterns are not consistently improved.

5 Conclusions

In the previous two chapters the authors presented and discussed results obtained in a series of sensitivity experiments conducted at three different horizontal resolutions with three different **Regional Climate Models (RCMs)**. The three participating **RCMs** were the European **COSMO model in CLimate Mode (COSMO-CLM)**, and the American **Fifth-Generation Mesoscale Model (MM5)** and **Weather Research and Forecasting model (WRF)**. The **RCMs** were run at horizontal resolutions of approximately 10 km, 3 km and 1 km. The first one is the resolution at which today's cutting edge regional climate projections are simulated, the second one is the resolution which likely will become a future standard resolution for climate projections (something between 2.5 km and 5 km seems reasonable), and the third one is the resolution which will be used for many future case studies up to several time slice experiments.

Some major results of the study are listed below:

- Cloud resolving climate simulations on 3 km and 1 km grids produce more detailed and more realistic temperature patterns than simulations on a 10 km grid, and they can improve the simulation of 2 m temperature on an hourly basis.
- The differences between the individual **RCMs** are higher than the differences arising from different resolutions. This statement has to be treated with care, since only 2 **RCMs** performed enough simulations to obtain a meaningful result. However, the authors strongly believe that this statement can be generalized to the lot of existing **RCMs**.
- Proper initialization of the soil or a sufficiently long spin-up time is crucial for the performance of a high resolution climate model. This is of particular importance on the shorter time scale, e.g., in applications like seasonal or decadal simulations.

One issue that has not been discussed but has to be mentioned at this point nonetheless regards the surface boundary conditions. Partly these parameters are outdated, partly they are simply wrong. The quality of the surface boundary conditions may locally significantly alter the results. A simulation with **COSMO-CLM** which tackles this issue is described in Steiner (2010).

After this thorough analysis it seems as if the horizontal resolution of 3 km yields the most promising results while keeping the computational costs at a feasible level. The 1 km resolution brings further improvements in some details, but partially the results also get worse.

5 Conclusions

Finally it has to be addressed what parts of the RCMs have to be improved in order to get more realistic and ultimately more useful results. The list below mainly refers to the COSMO-CLM but may, to some extent, also be passed on to the other RCMs.

- The high sensitivity to soil initialization, which is assumed to primarily act via soil moisture on the atmosphere, indicates that an improved description of soil and surface properties could considerably improve convection resolving simulations. This improvement also influences the interaction of soil moisture and atmosphere.
- Improvements could be expected from a more proper implementation of a 3-dimensional turbulence scheme. The scheme which is currently implemented in COSMO-CLM didn't notably improve the results
- Orographic shading effects, the effect of exposition of slopes, and the proper treatment of vertical and horizontal exchange in terrain following coordinates are generally regarded as important for high resolution simulations. None of the sensitivity experiments related to these issues resulted in clear improvements of the overall results. Also, these schemes should be analyzed with regard to potential improvements. These results are restricted to added value in a climatological context. Further analysis focusing on specific weather events could still prove added value.
- Online nesting (as implemented for MM5 and WRF, but not for COSMO-CLM) is necessary to enable high update frequencies of lateral boundary conditions at reasonable technical expenses.

Many potential improvements that have not been investigated in this project are related to the radiation scheme. First of all, a full 3-dimensional treatment of radiation including interaction with clouds (and ultimately also aerosols) is of utter importance, and even more so at cloud resolving scales. Also, a proper interaction of radiation with snow and graupel is preferable. Further improvements of the results could be achieved by a better (i.e., more detailed) calculation of the soil properties. As mentioned in Section 2.1 the so-called 'tile approach' could mitigate at least of the problems related to soil-atmosphere interaction. Additionally, at very high resolutions (i.e., less than about 3 km) an urban model should be applied to get a more realistic representation of urban heat islands.

Another desirable model component is a river routing scheme, which would considerably facilitate the evaluation of the hydrological cycle of the model. This is of particular importance at high resolution, where suitable precipitation datasets are generally not available and indirect evaluation via runoff from a catchment would provide valuable information.

Besides the potential improvements mentioned above there are further ones which are not necessarily limited to cloud resolving climate simulations but affect results at all scales. Such improvements are often related to model components which have been

introduced some years ago and which have never been updated such as the ‘background aerosol’ which is included in every **RCM**. This constant in time value turned out to be either outdated or simply wrong. An update of such ‘ancient’ model parts would surely alter the results.

In summary, it was demonstrated that **Convection-Resolving Climate Simulations (CRCS)** have comparable quality as conventional climate simulations and that they feature added value in some aspects, particularly regarding spatial patterns, biases related to specific temperatures or precipitation intensities, and partially also regarding overall biases. Model improvement options have been identified that could further enhance the quality of **CRCS**. This demonstrates that the realisation of long-term **CRCS** is already in reach, but currently still at extremely high computational costs. However, technical advances in the field of high performance computing are expected to allow long-term **CRCS** with about 3 km grid spacing at reasonable costs within the next few years.

A Figures of the results

This appendix contains all plots describing the results of every simulation conducted in the framework of this study. For the sake of completeness, it contains even more plots than described in the text.

Important note: In order to keep the file size of this report small the authors chose to include only plots with reduced quality. The appendix including full quality graphics can be downloaded separately from the homepage of the WegCenter Verlag (<http://wegcenter.at/wcv>).

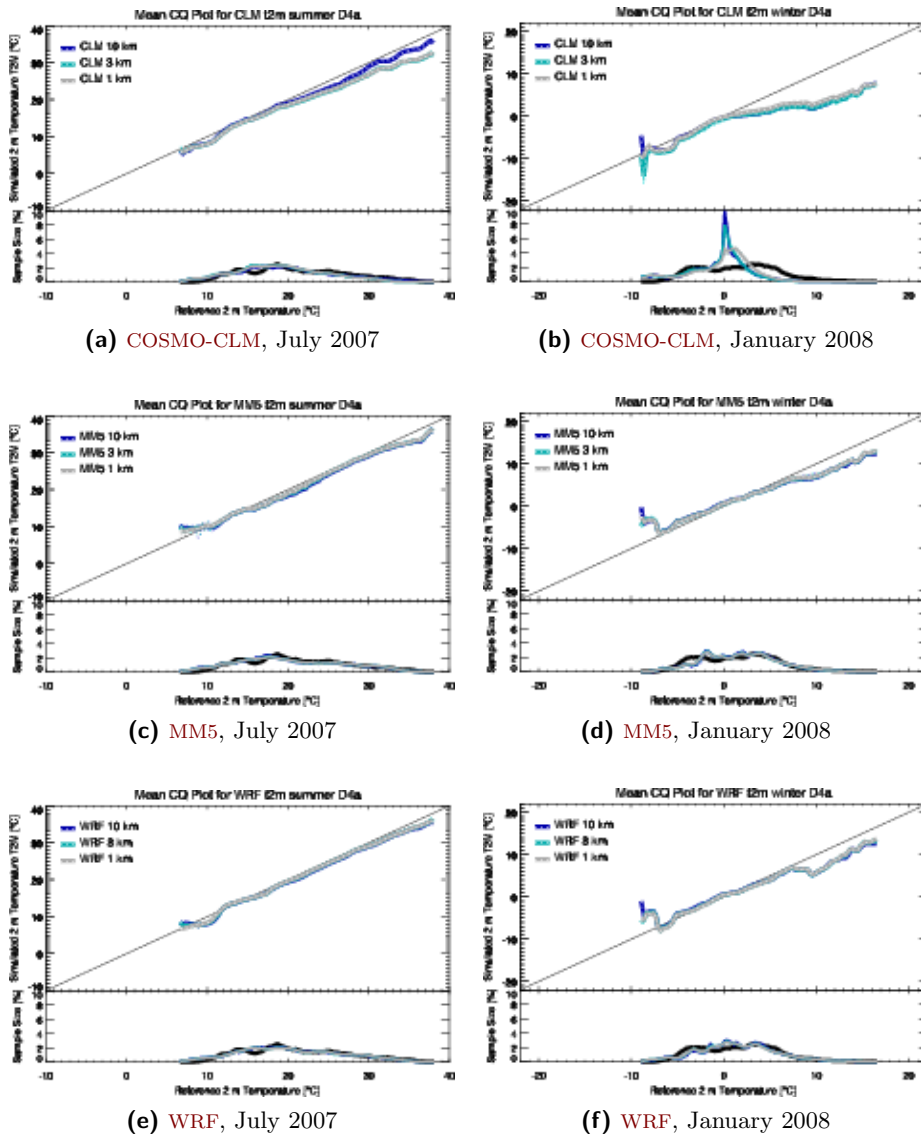
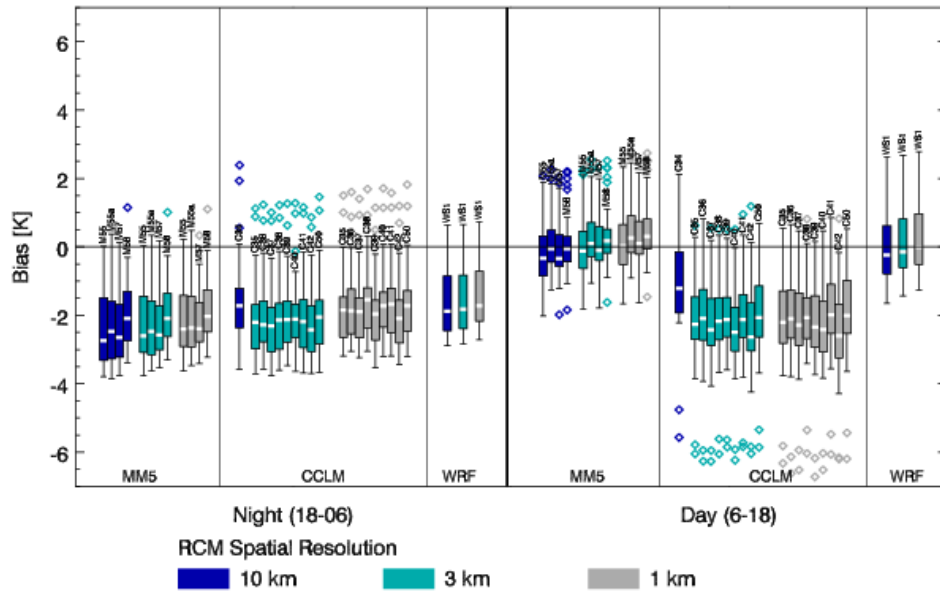
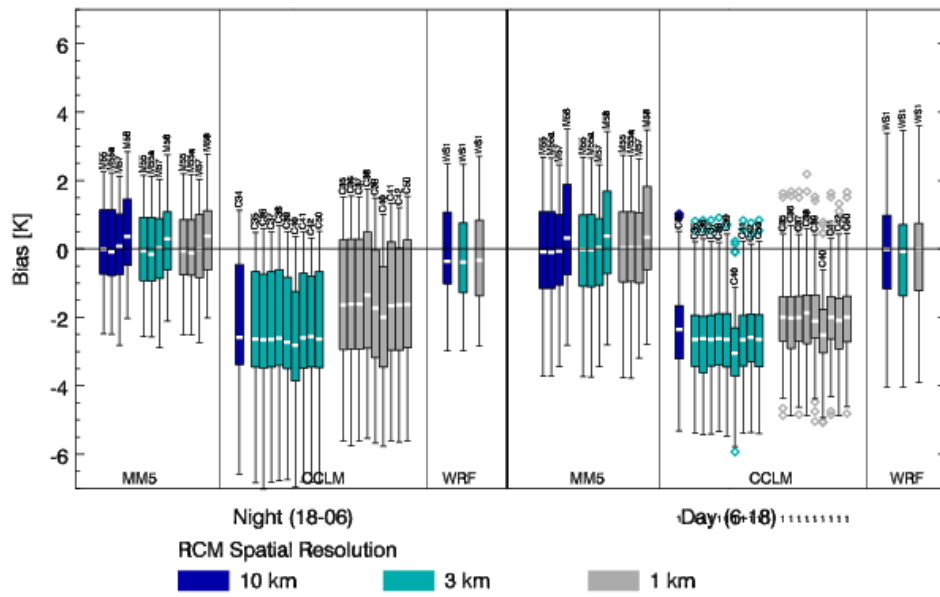


Figure A.1: CQ-Plots of 2 m temperature of all S1 simulations splitted by RCM for both evaluated months. Rows correspond to the three RCMs (COSMO-CLM, MM5 and WRF, respectively); left column: summer month, right column: winter month. Colors correspond to the horizontal resolution, the black curve shows the reference dataset (INCA).

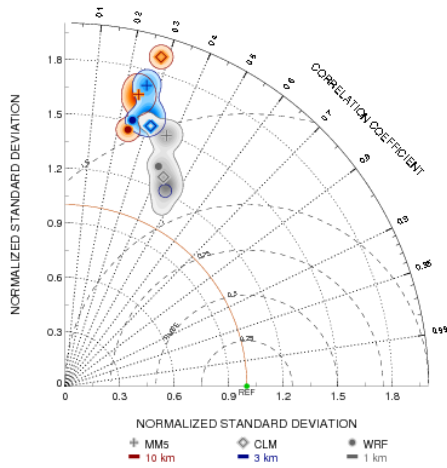


(a) July 2007

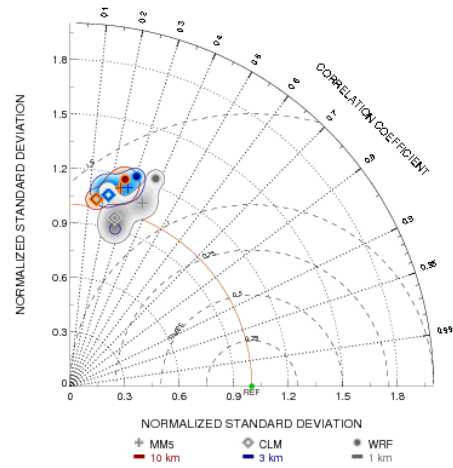


(b) January 2008

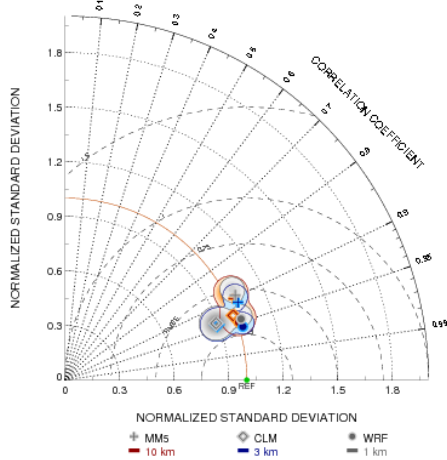
Figure A.2: Box-and-whisker plots for temperature for all S1 simulations separated by RCM and horizontal resolution in the D4a region.



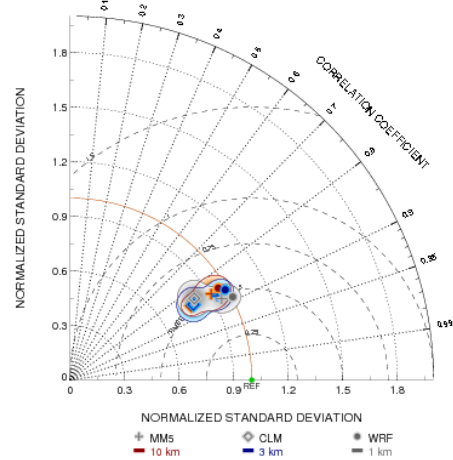
(a) spatial, July 2007



(b) spatial, January 2008



(c) temporal, July 2007



(d) temporal, January 2008

Figure A.3: Spatial and temporal Taylor diagrams of all S1 simulations for the parameter 2 m air temperature in the D4a region.

A Figures of the results

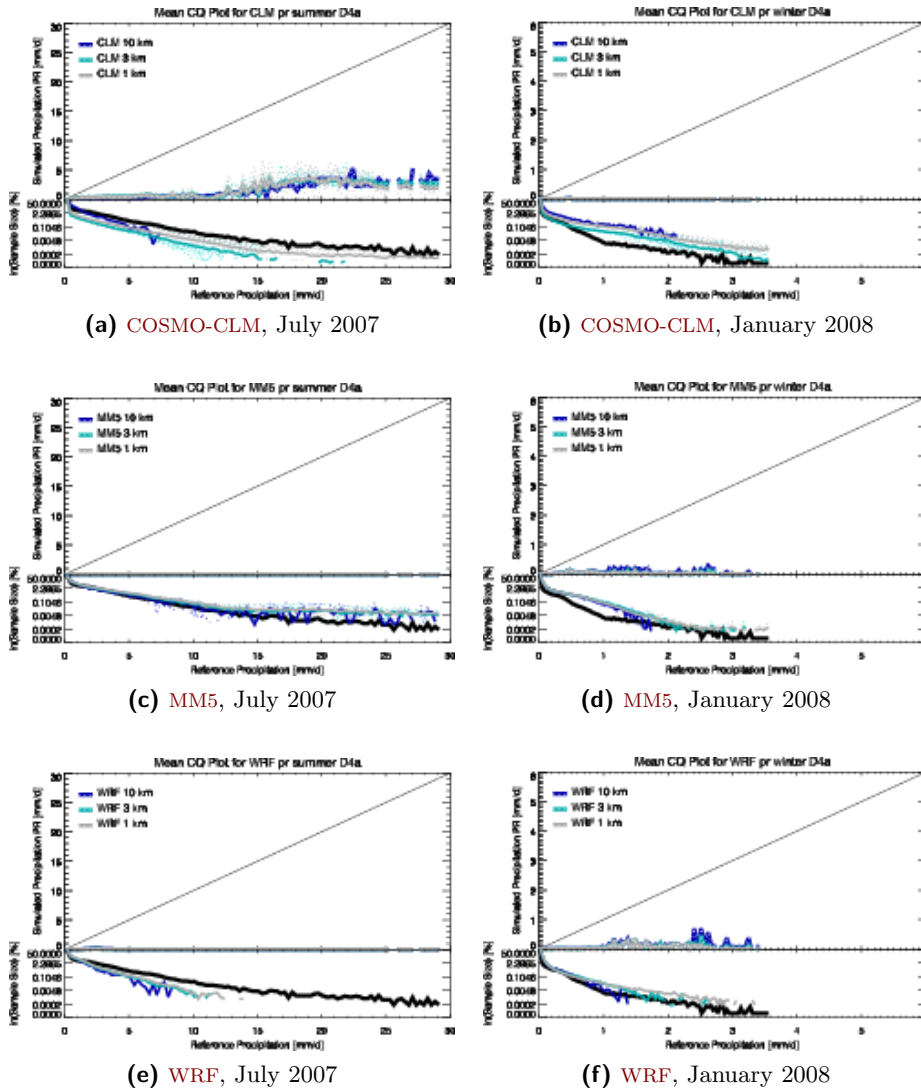
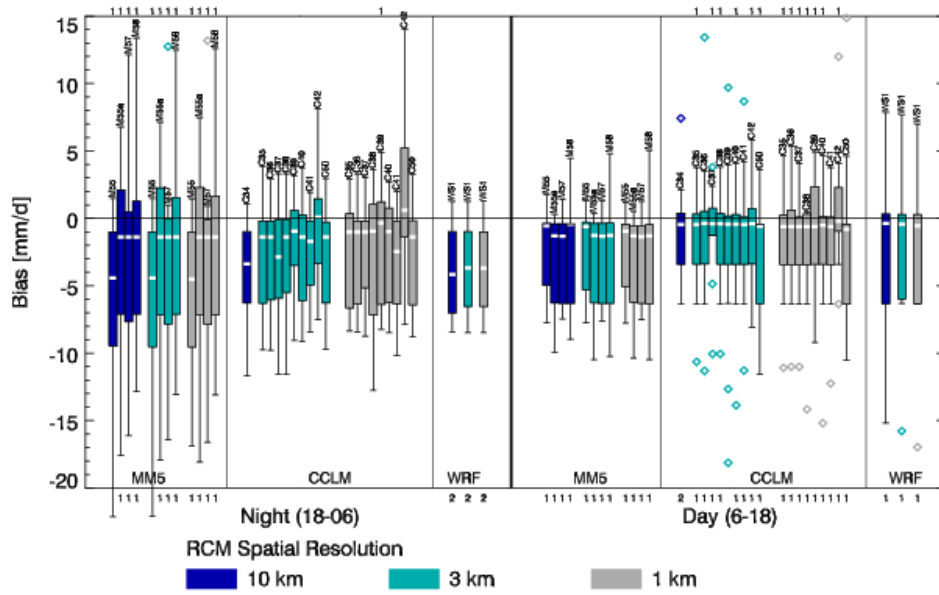
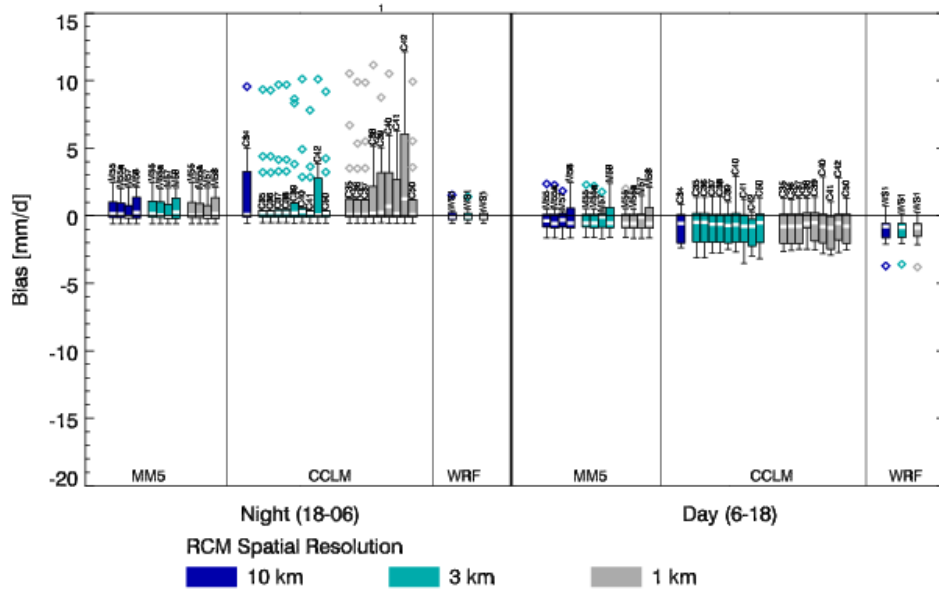


Figure A.4: CQ-Plots of precipitation of all S1 simulations splitted by RCM in the two test months. Rows correspond to the three RCMs (COSMO-CLM, MM5 and WRF, respectively); left column: summer month, right column: winter month.



(a) July 2007



(b) January 2008

Figure A.5: Box-and-whisker plots for precipitation for all S1 simulations separated by RCM and horizontal resolution in the D4a region.

A Figures of the results

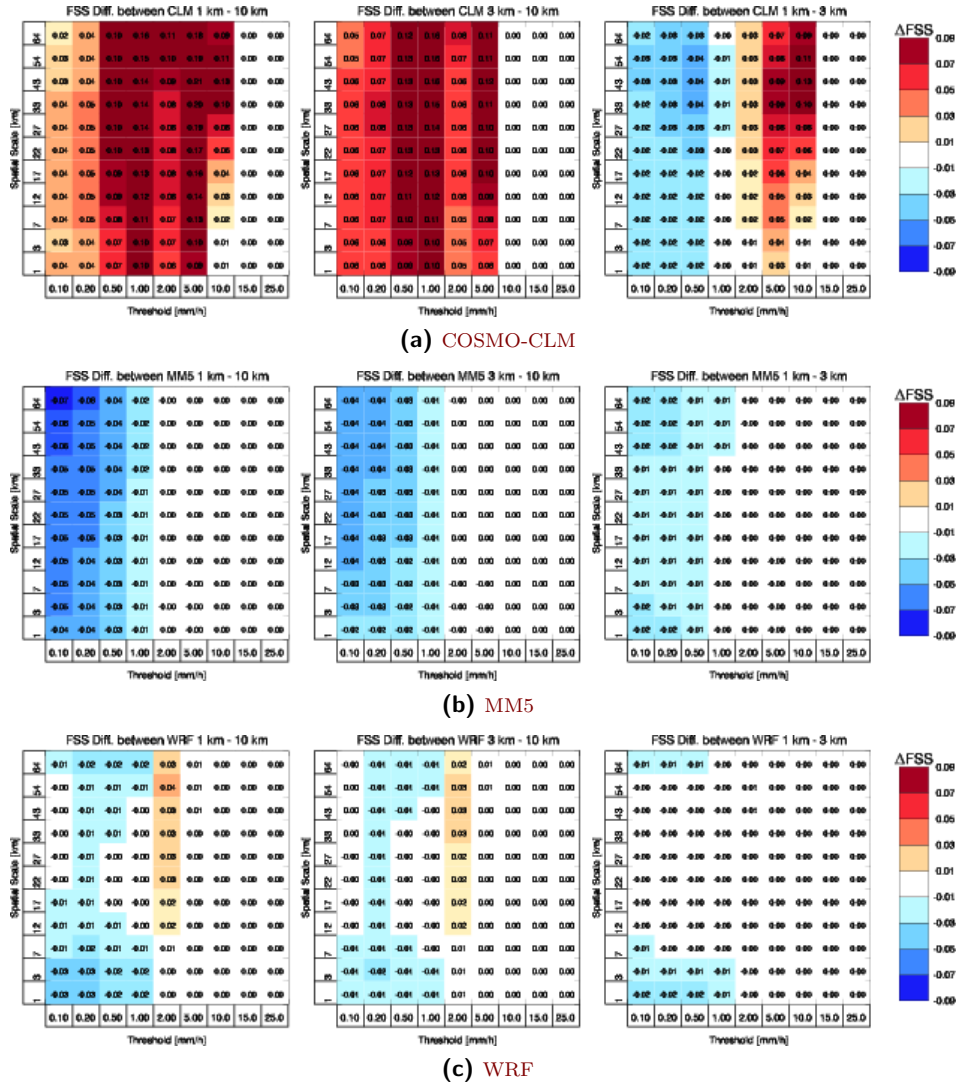


Figure A.6: Difference FSS plots of precipitation of all S1 simulations splitted by RCM in the summer month. Shown are differences in FSS between 10 km and 1 km (left block), between 10 km and 3 km (middle block) and between 3 km and 1 km (right block) horizontal resolution. The rows correspond to the three RCMs (COSMO-CLM, MM5 and WRF, from top to bottom).

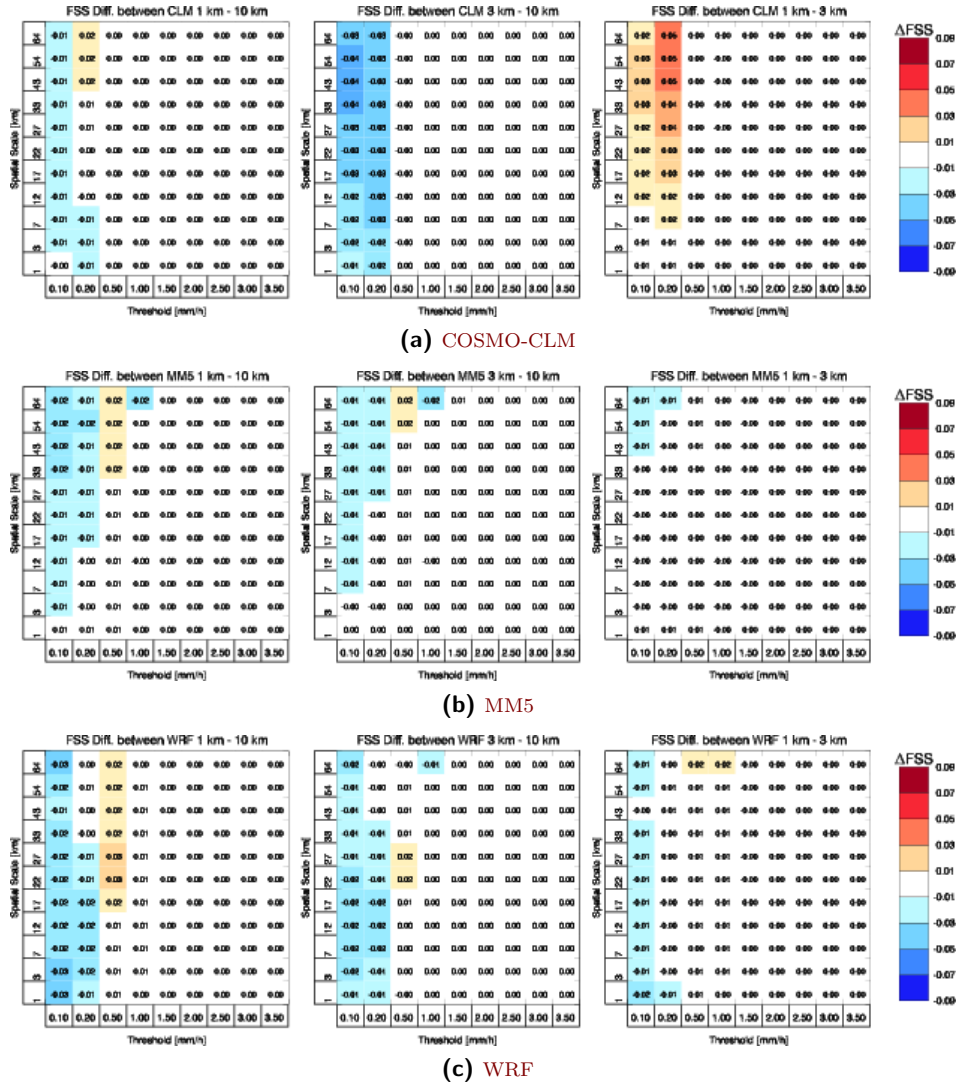


Figure A.7: Difference FSS plots of precipitation of all S1 simulations splitted by RCM in the winter month. Shown are differences in FSS between 10 km and 1 km (left block), between 10 km and 3 km (middle block) and between 3 km and 1 km (right block) horizontal resolution. The rows correspond to the three RCMs (COSMO-CLM, MM5 and WRF, from top to bottom).

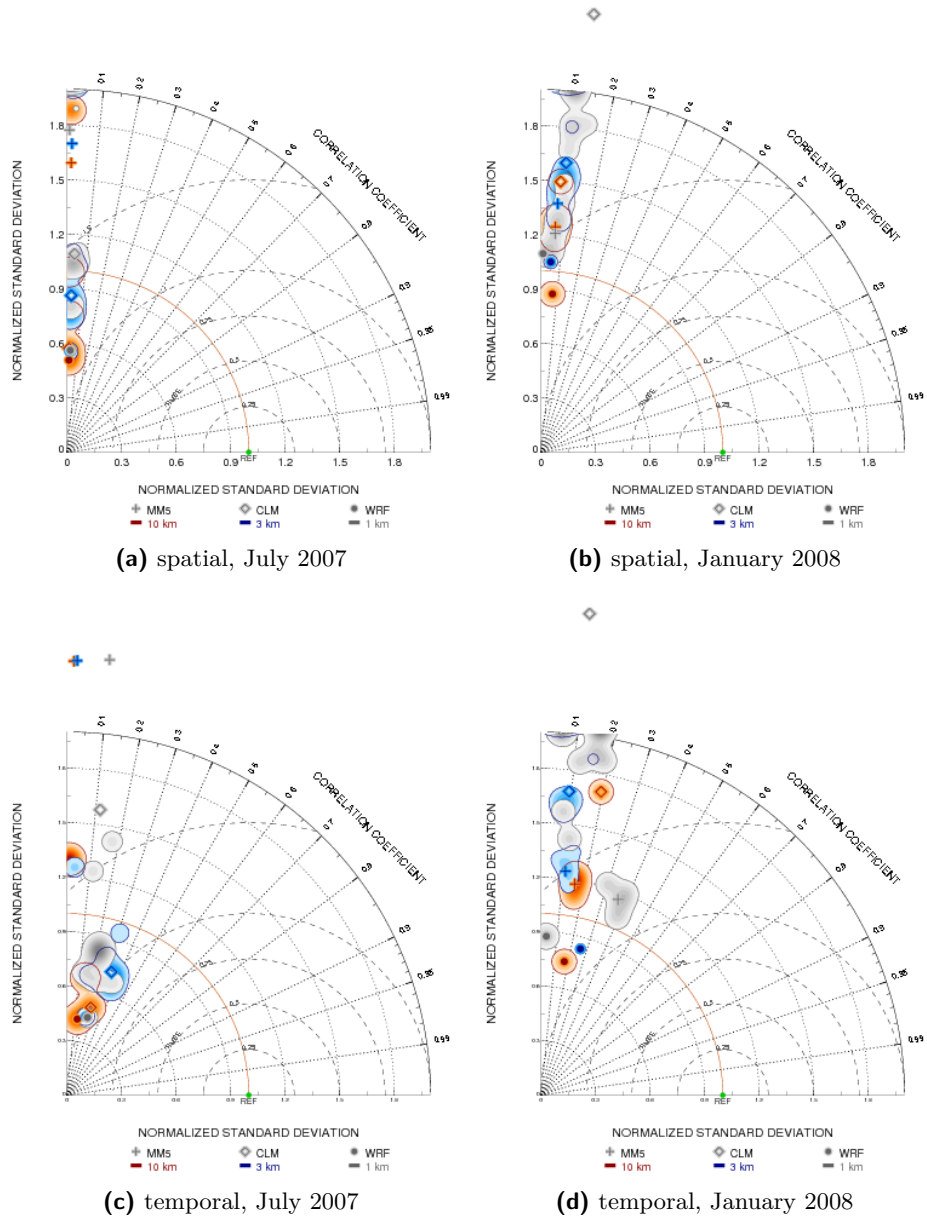


Figure A.8: Spatial and temporal Taylor diagrams for temperature for the S1 simulations in the two test months for the D4a region.

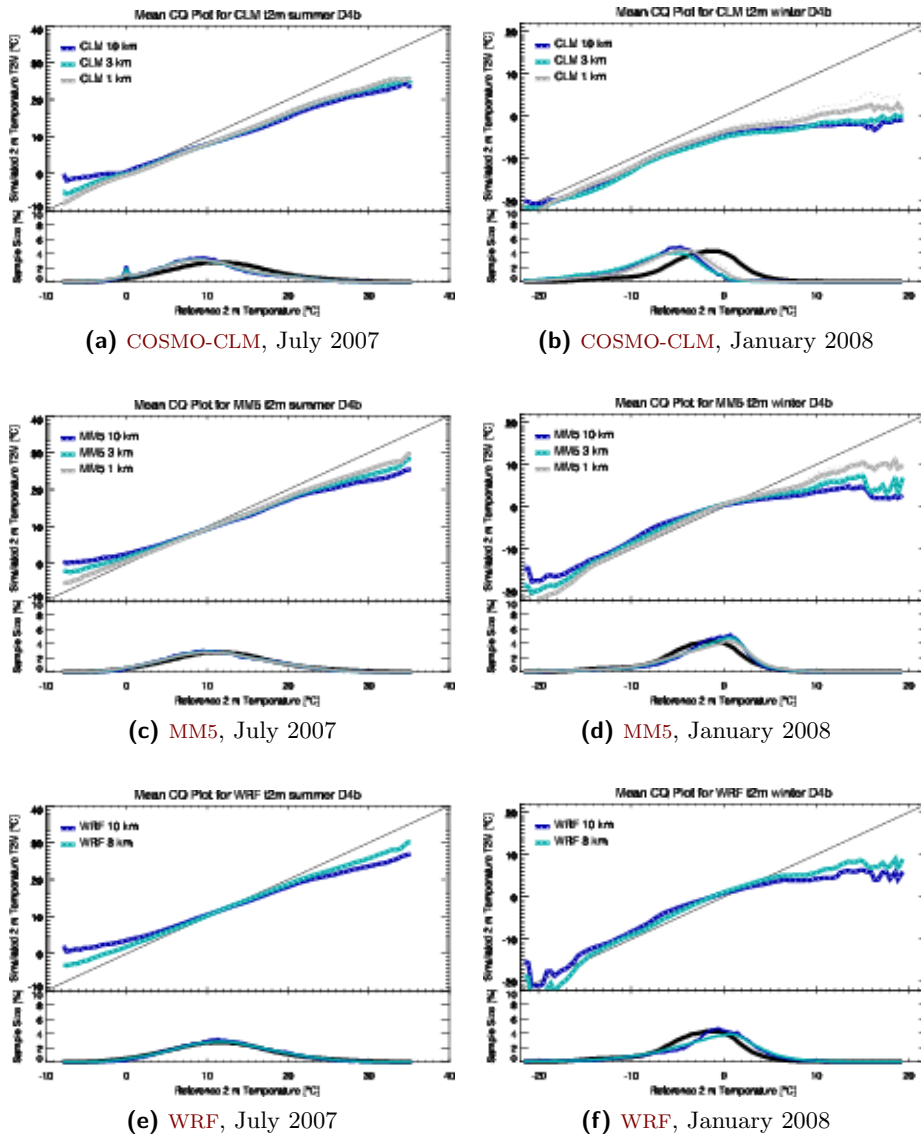


Figure A.9: CQ-Plots of 2 m temperature of all S1 simulations splitted by RCM in the D4b region. Rows: COSMO-CLM, MM5, WRF (top to bottom), left column: summer month, right column: winter month.

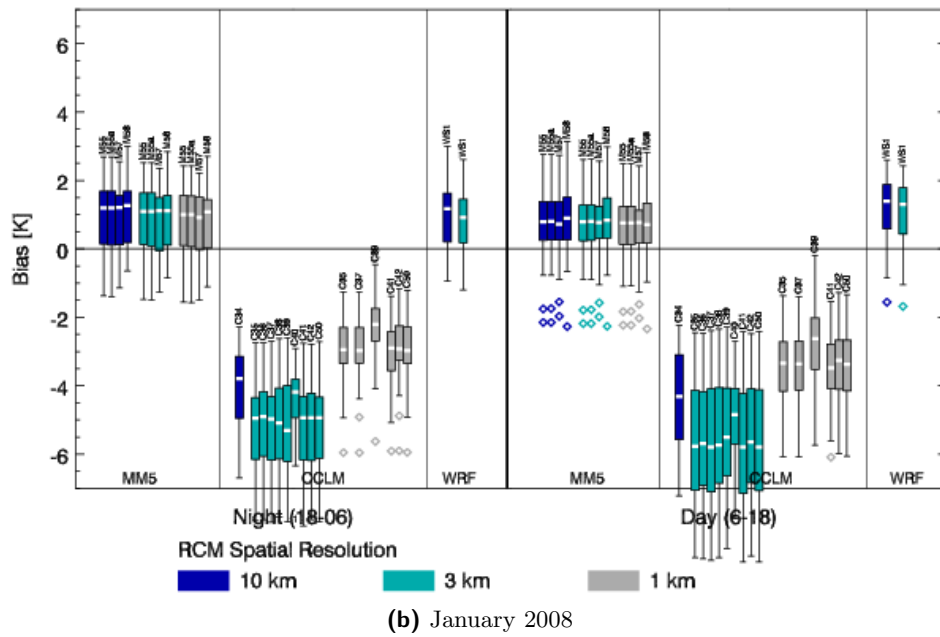
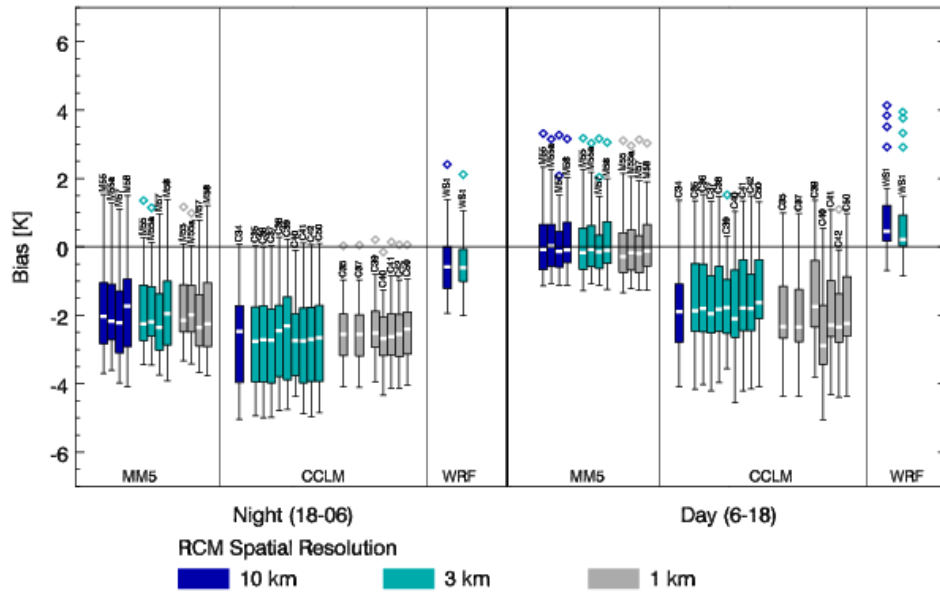
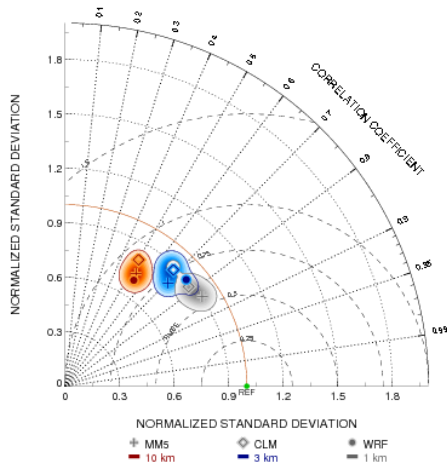
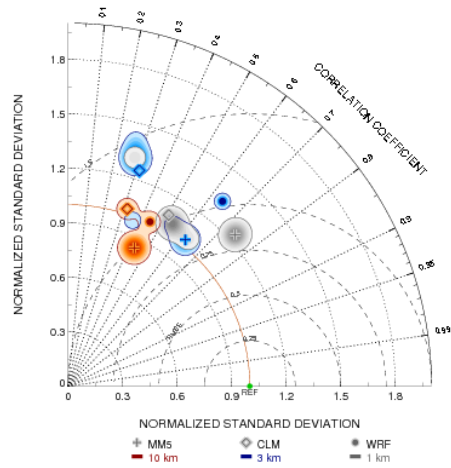


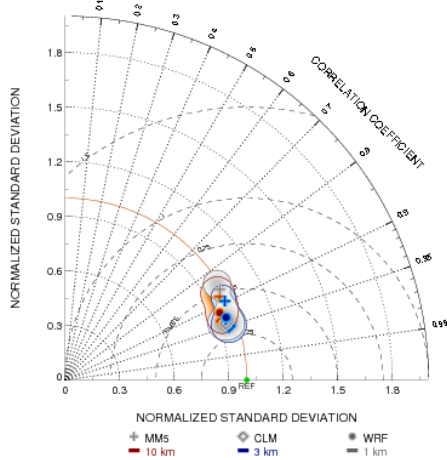
Figure A.10: Box-and-whisker plots for temperature for all S1 simulations separated by RCM and horizontal resolution in the D4b region.



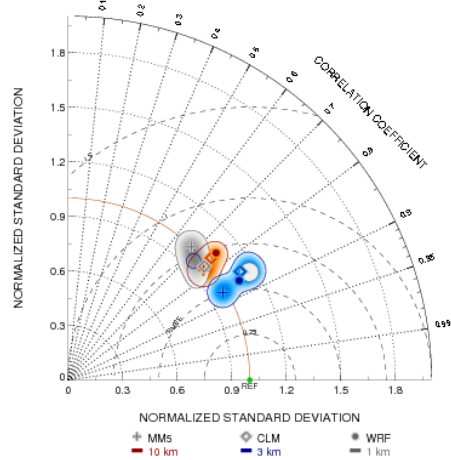
(a) spatial, July 2007



(b) spatial, January 2008



(c) temporal, July 2007



(d) temporal, January 2008

Figure A.11: Spatial and temporal Taylor diagrams for temperature for the S1 simulations in the two test months for the D4b region.

A Figures of the results

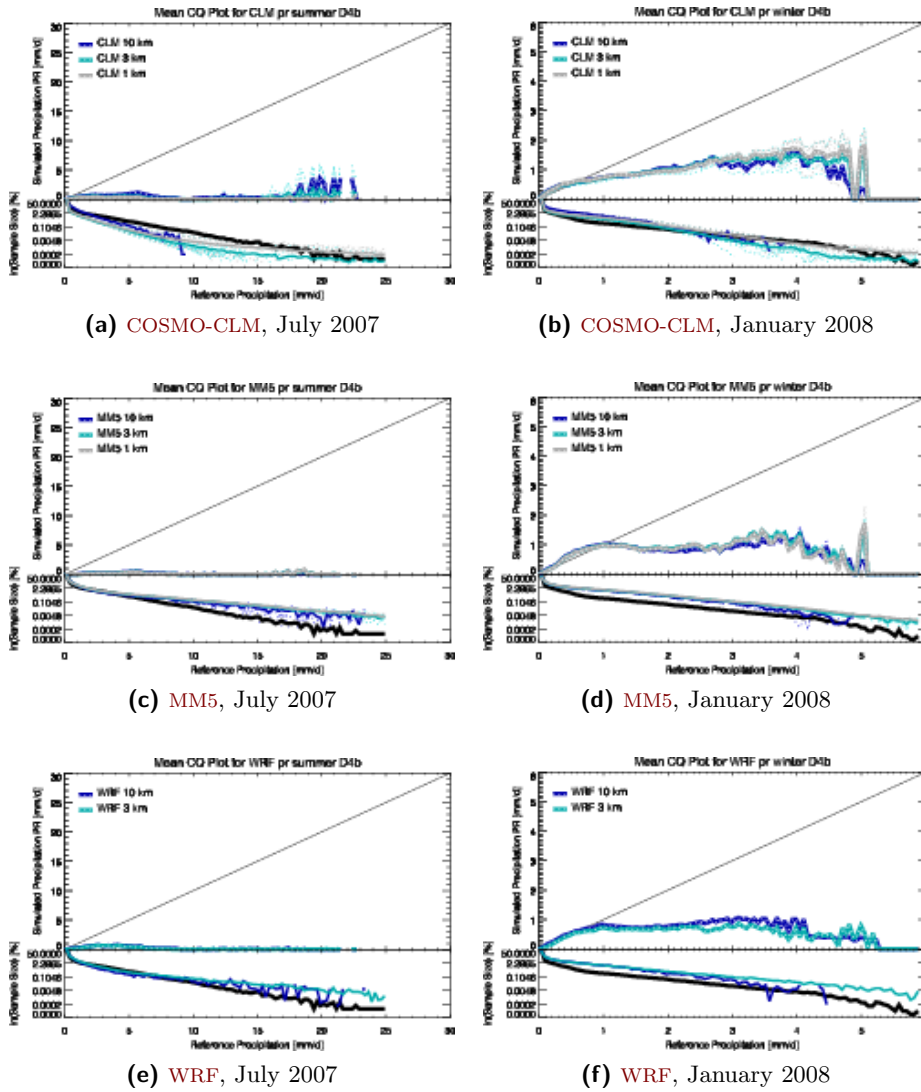
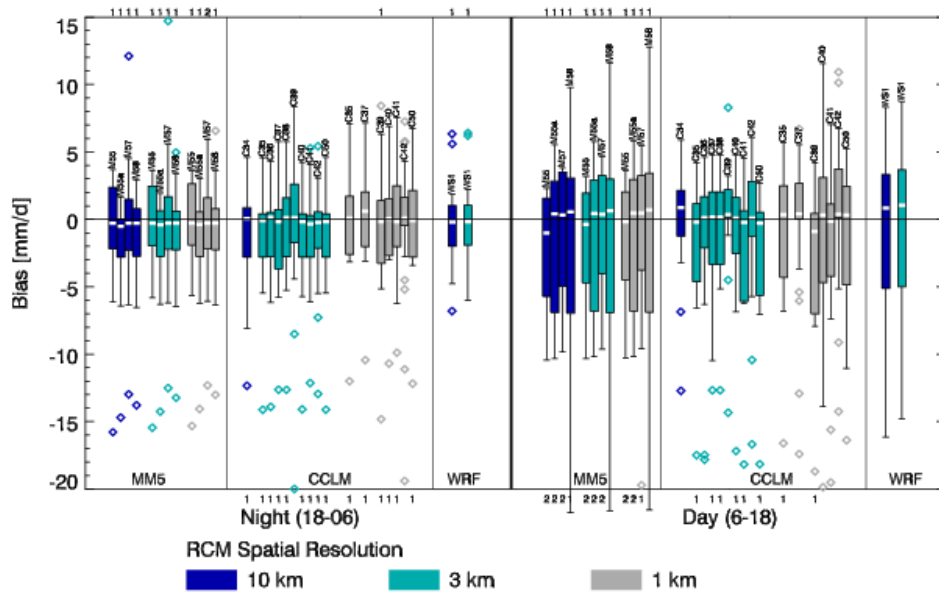
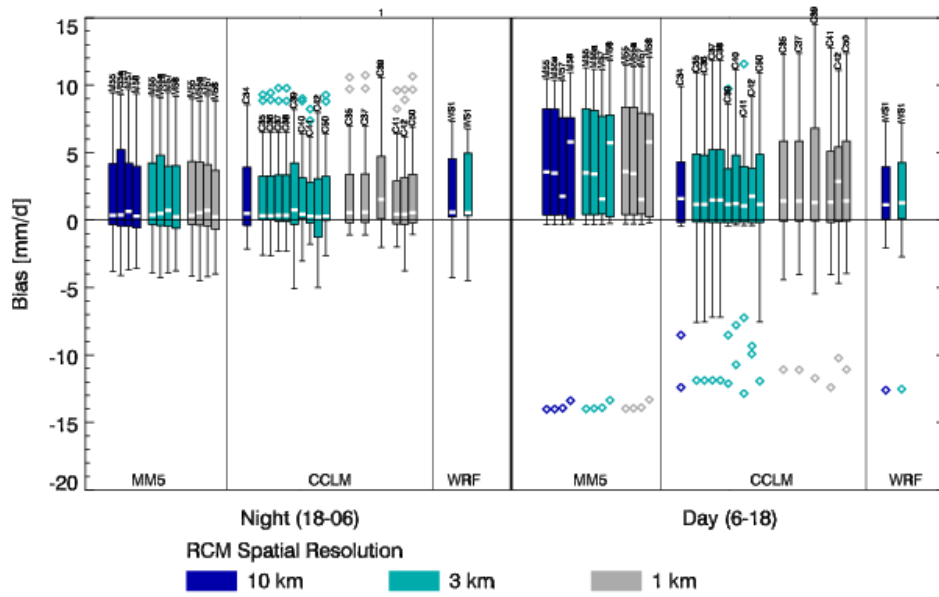


Figure A.12: CQ-Plots of precipitation of all S1 simulations splitted by RCM for both months in the D4b region. Rows: COSMO-CLM, MM5, WRF (top to bottom), left column: summer month, right column: winter month.



(a) July 2007



(b) January 2008

Figure A.13: Box-and-whisker plots for precipitation for all S1 simulations separated by RCM and horizontal resolution in the D4b region.

A Figures of the results

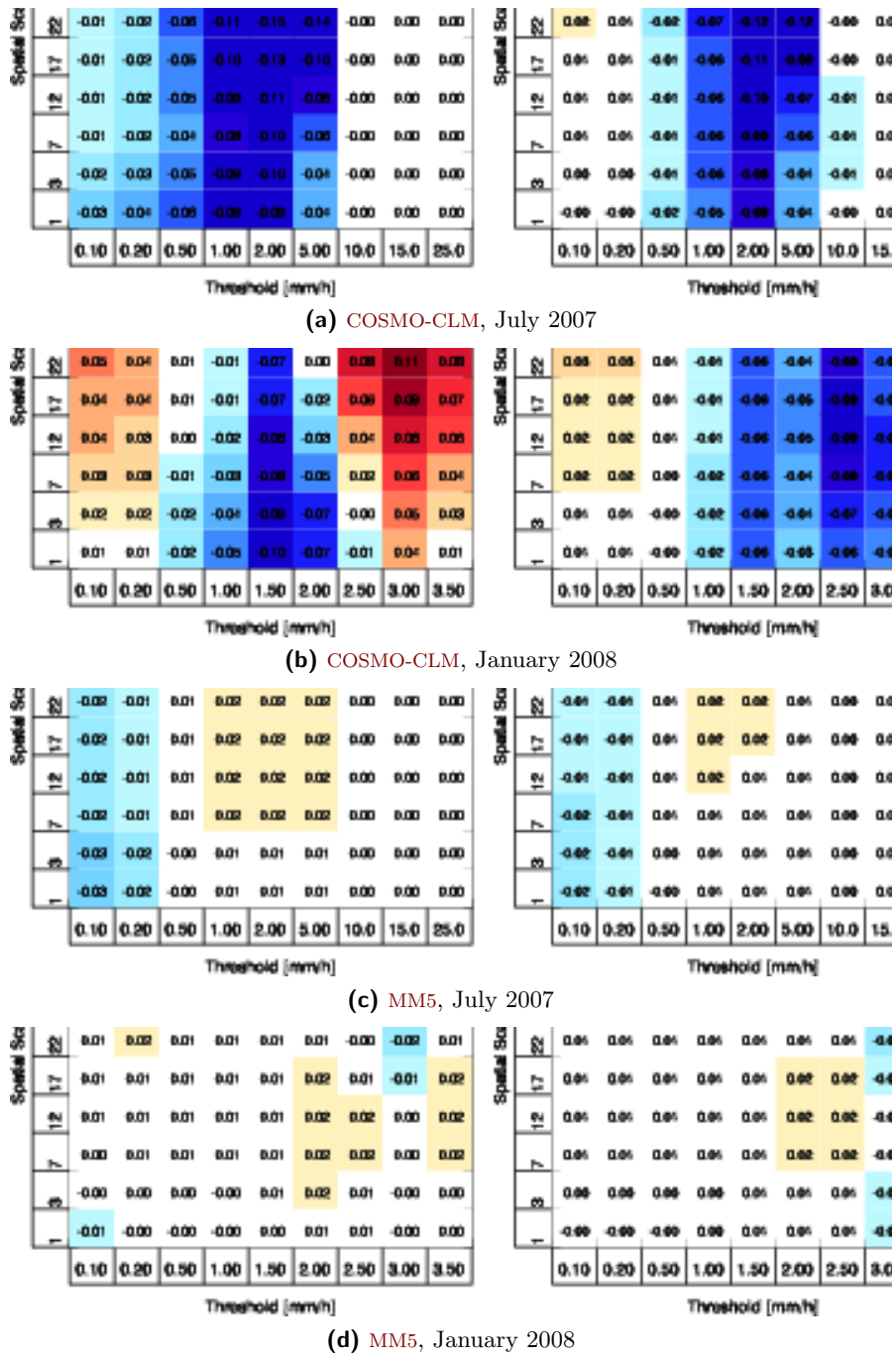
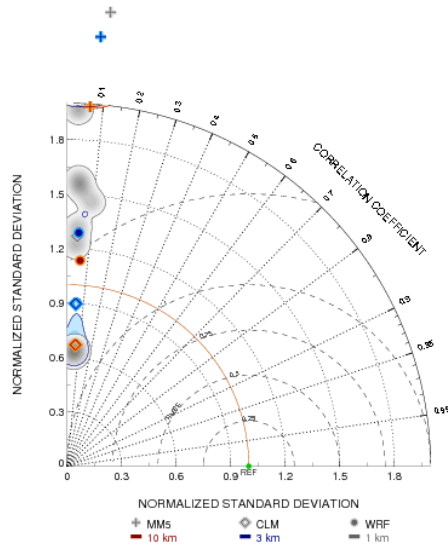
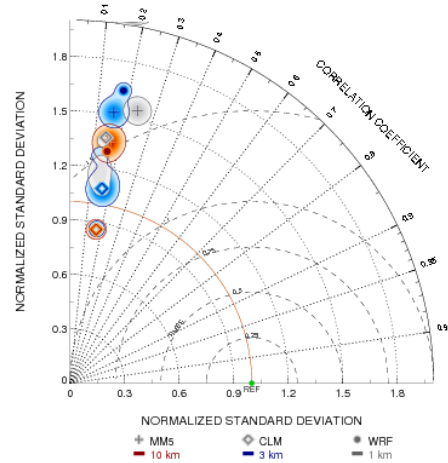


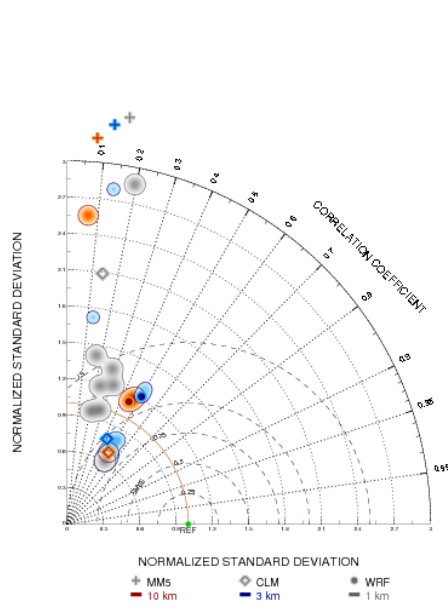
Figure A.14: Difference FSS plots for COSMO-CLM and MM5 for the D4b region. Mind the different thresholds (x axis) for summer and winter!



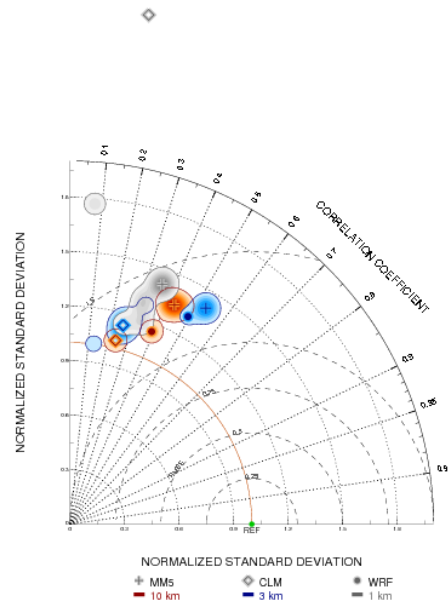
(a) spatial, July 2007



(b) spatial, January 2008

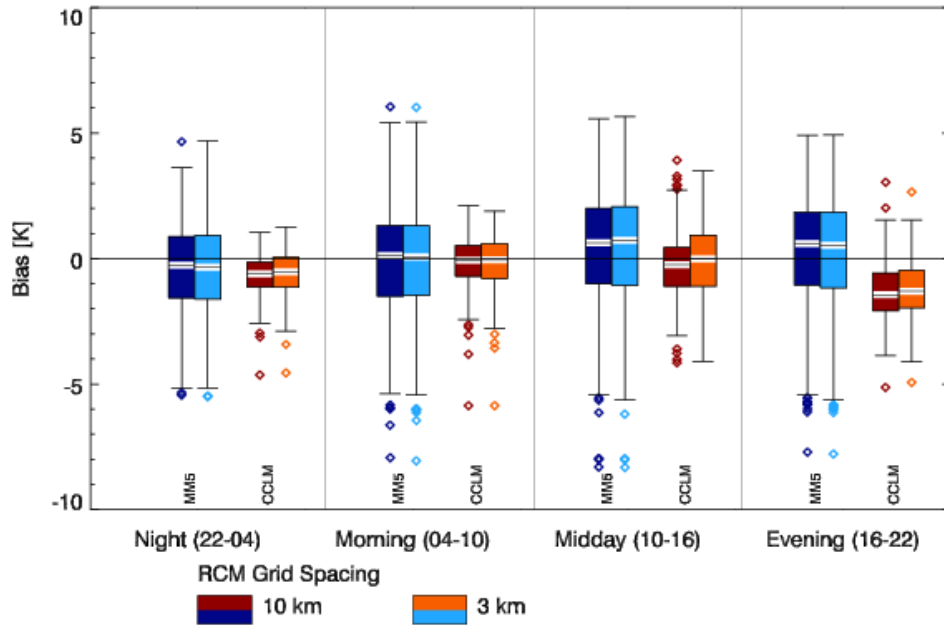


(c) temporal, July 2007

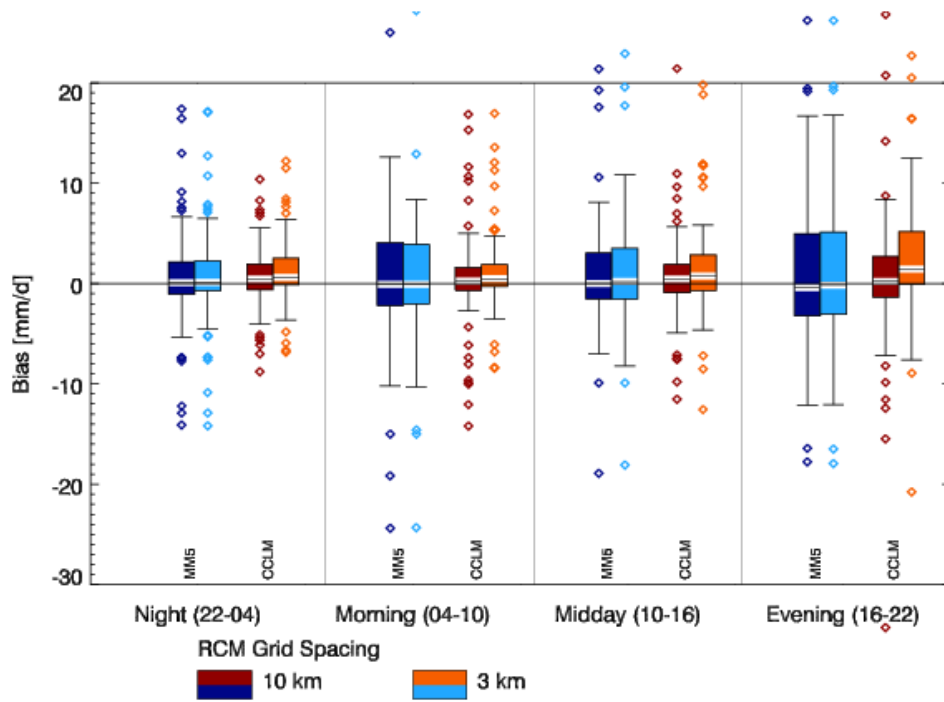


(d) temporal, January 2008

Figure A.15: Spatial and temporal Taylor diagrams for precipitation for the S1 simulations in the two test months for the D4b region.



(a) Temperature



(b) Precipitation

Figure A.16: Box-and-whisker plots for the S2 experiments. Each parameter is evaluated separately for 4 times of day.

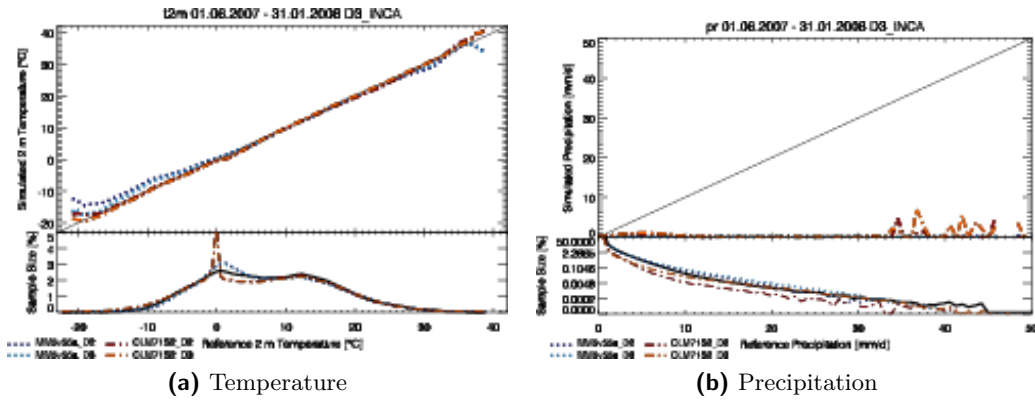


Figure A.17: CQ plots for the S2 experiments.

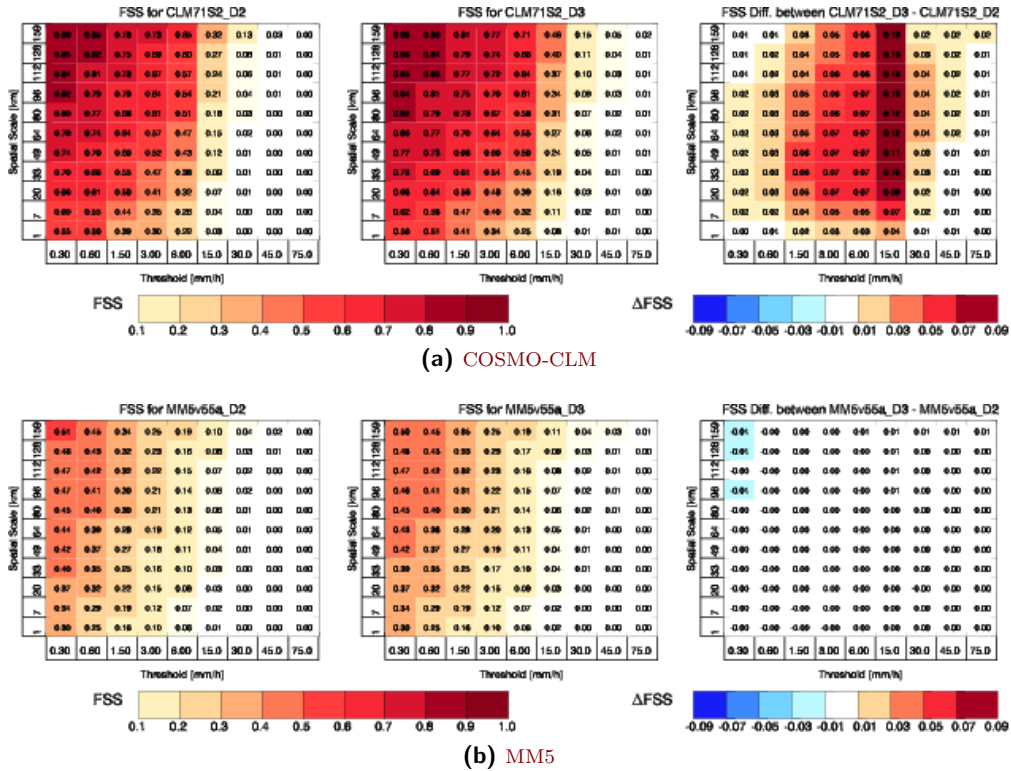


Figure A.18: FSS plots for the S2 experiments of COSMO-CLM (top row) and MM5 (bottom row). Left block: FSS at 10 km horizontal resolution, middle block: FSS at 3 km horizontal resolution, right block: difference between the two (positive values indicate a gain in FSS at the higher resolution).

A Figures of the results

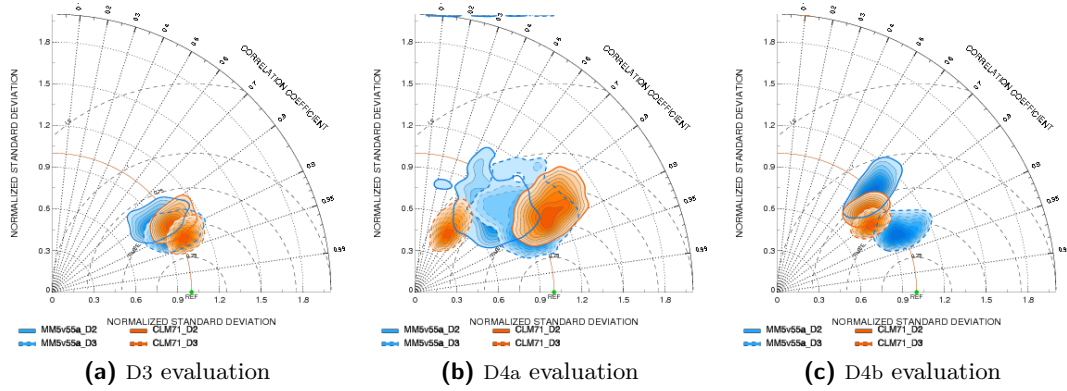


Figure A.19: Comparison of the spatial Taylor diagrams for temperature between the evaluation in D3 and in the two test regions

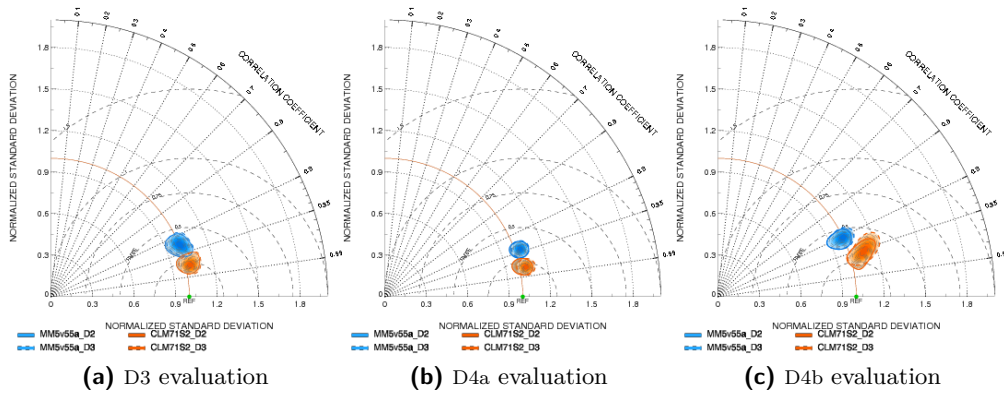


Figure A.20: Comparison of the temporal Taylor diagrams for temperature between the evaluation in D3 and in the two test regions

A Figures of the results

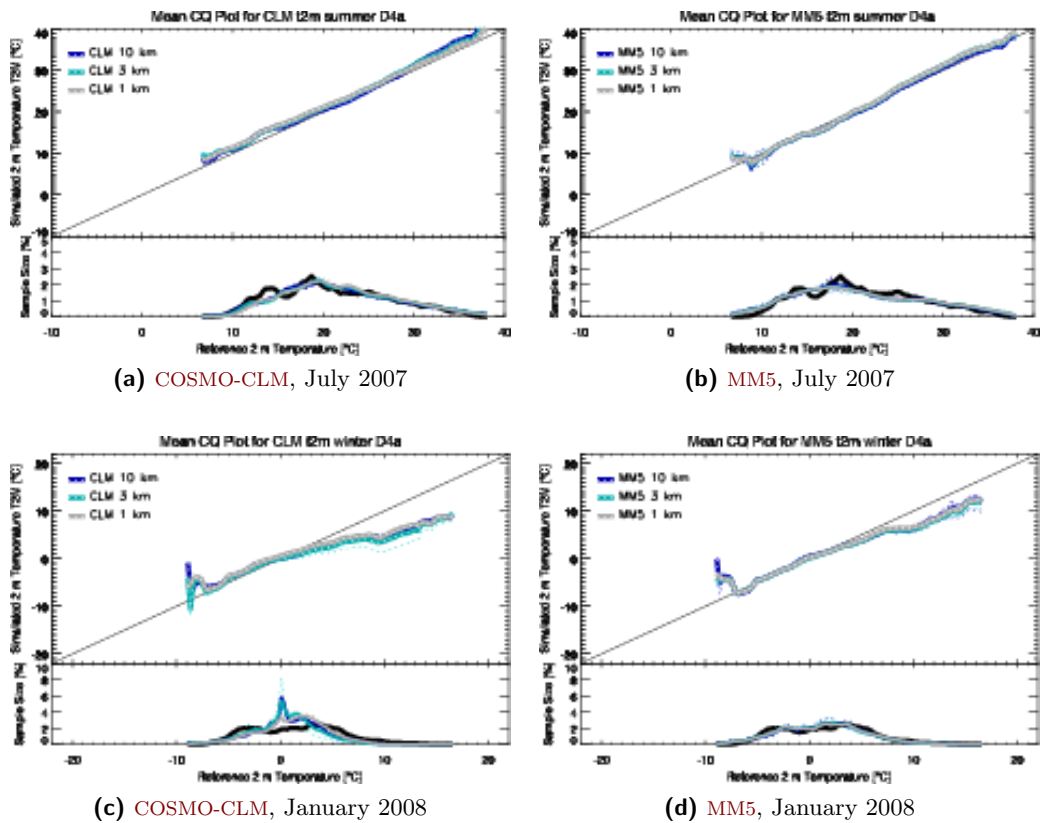
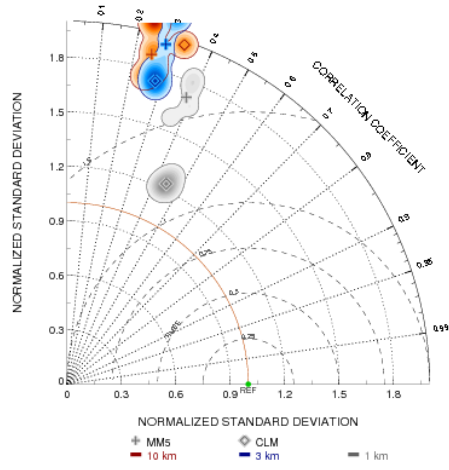
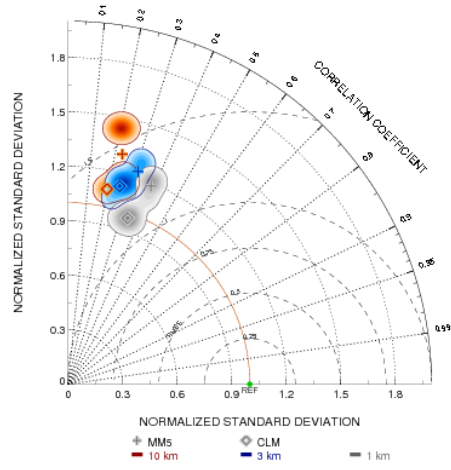


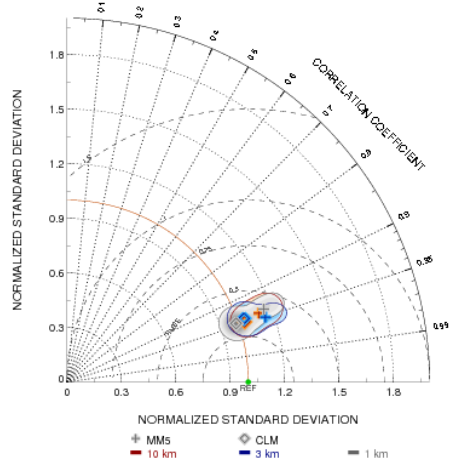
Figure A.22: CQ plots for temperature for all S4 simulations separated by RCM for the summer month (upper row) and the winter month (lower row) in the D4a region. Left column: COSMO-CLM, right column: MM5.



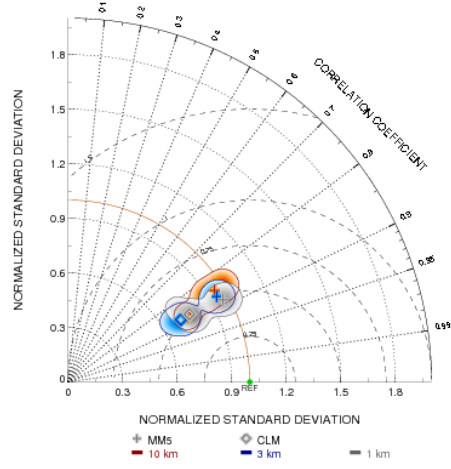
(a) spatial, July 2007



(b) spatial, January 2008



(c) temporal, July 2007



(d) temporal, January 2008

Figure A.23: Spatial and temporal Taylor diagrams for temperature for all S4 simulations in the D4a region.

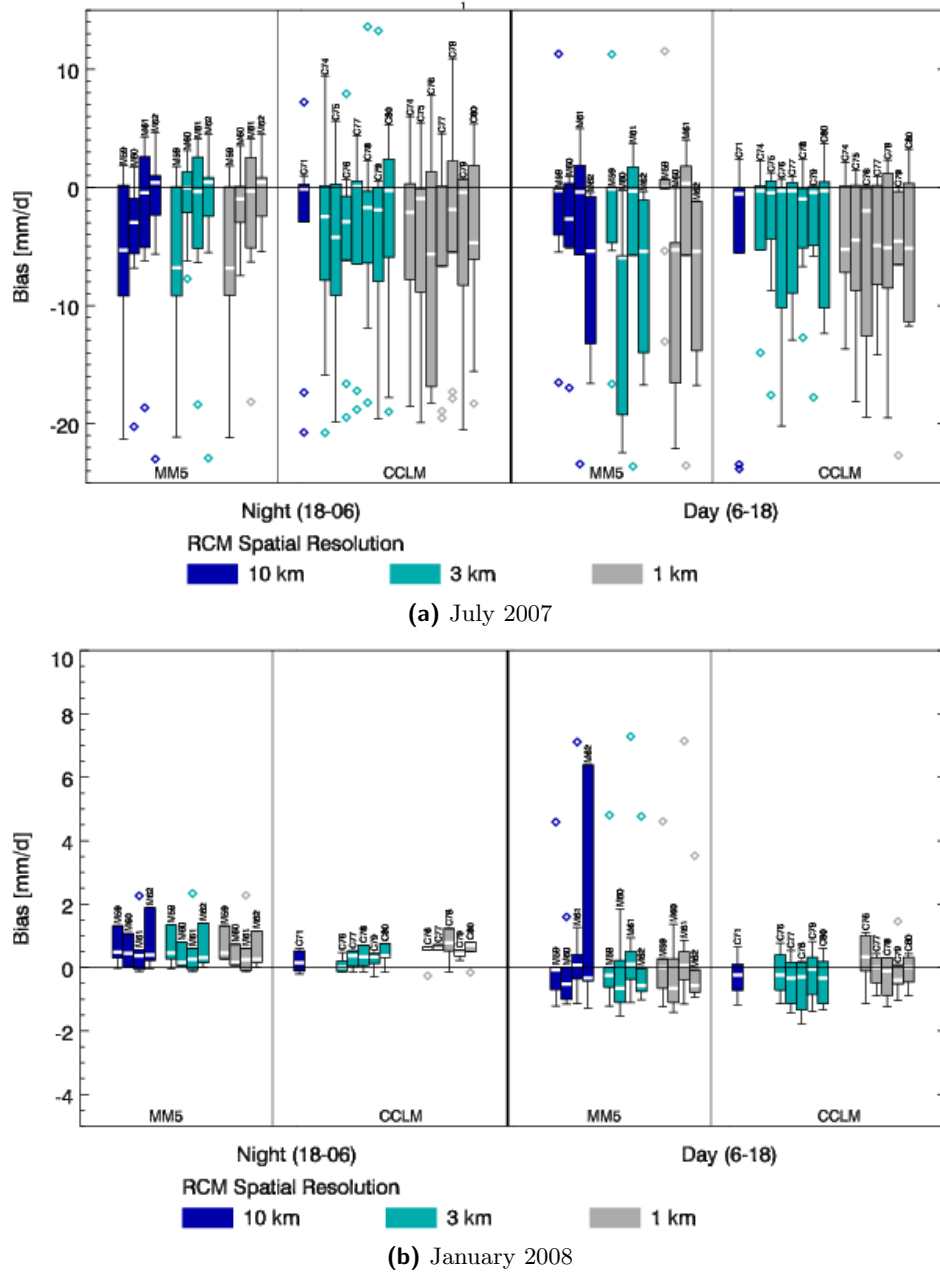


Figure A.24: Box-and-whisker plots for precipitation for all S4 simulations separated by RCM and horizontal resolution in the D4a region.

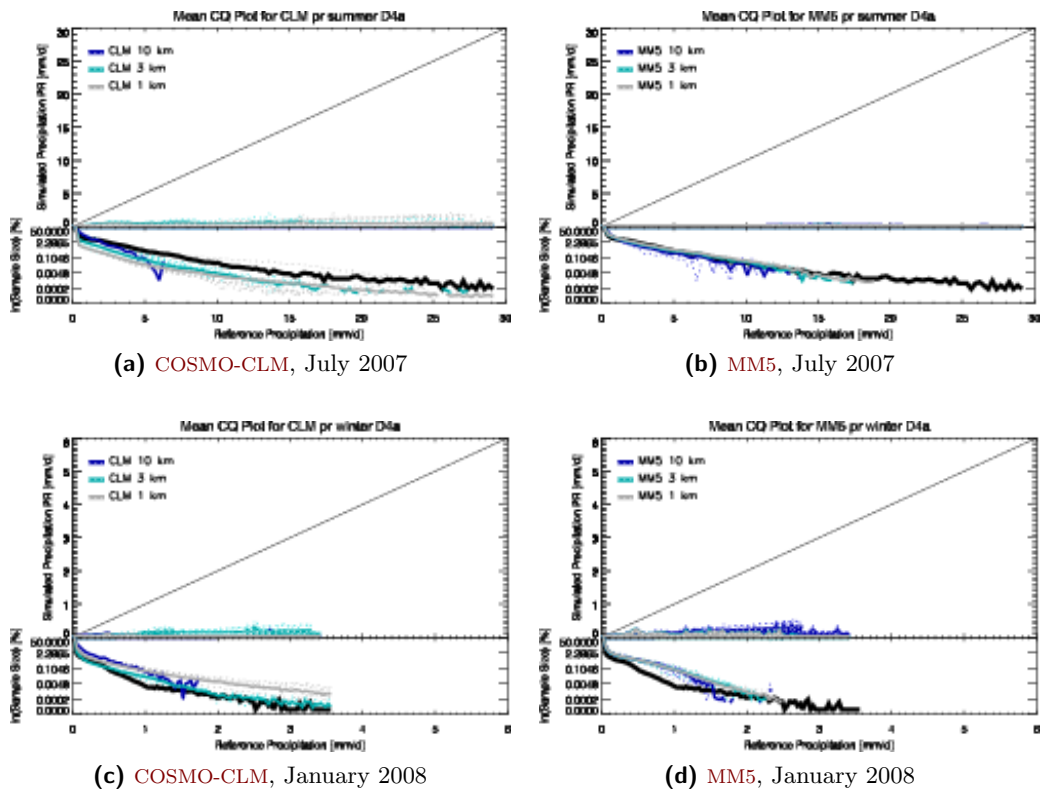


Figure A.25: CQ plots for precipitation for all S4 simulations separated by RCM for the summer month (upper row) and the winter month (lower row) in the D4a region. Left column: COSMO-CLM, right column: MM5.

A Figures of the results

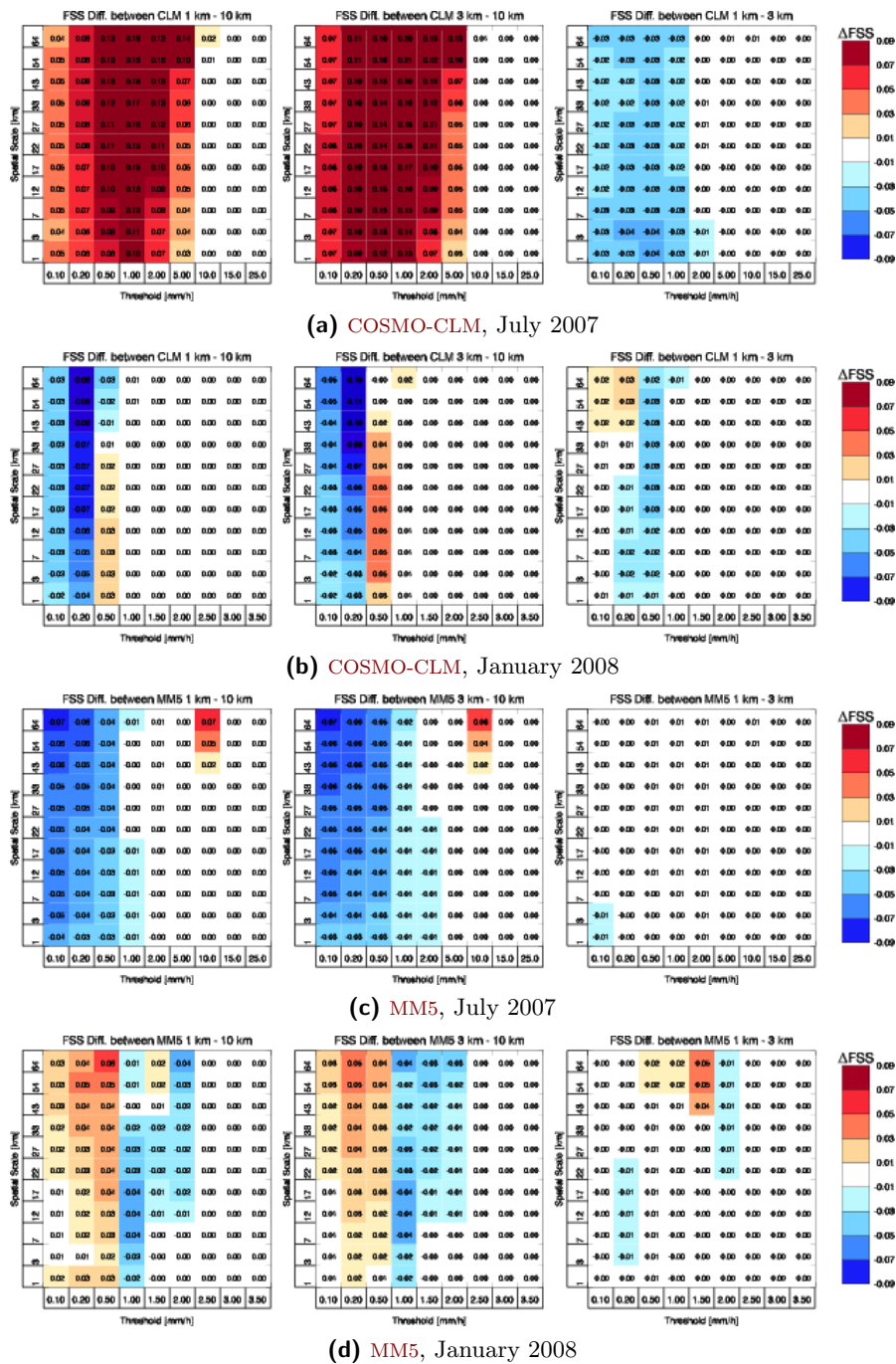


Figure A.26: Difference FSS plots for simulated vs. observed precipitation amount in the S4 simulations of COSMO-CLM and MM5.

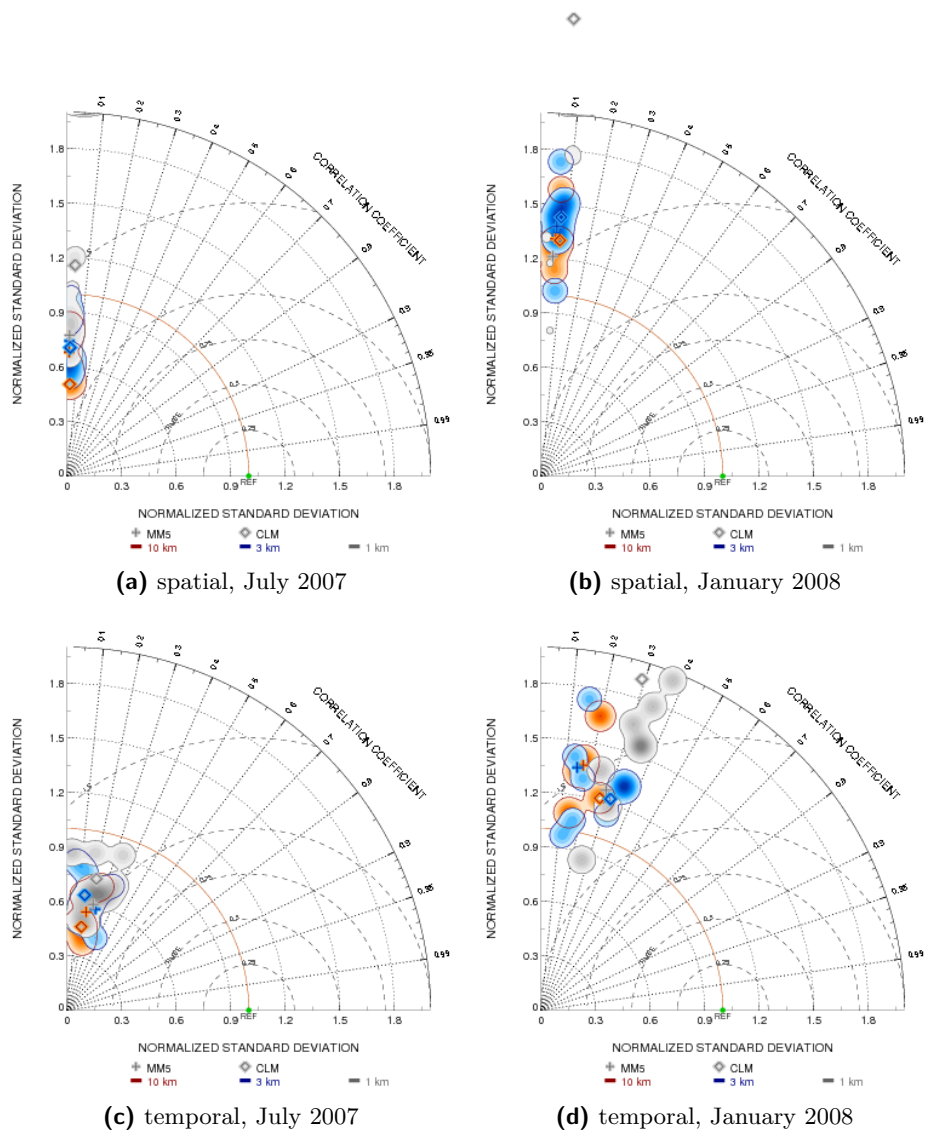


Figure A.27: Spatial and temporal Taylor diagrams for all S4 simulations in the D4a region for precipitation.

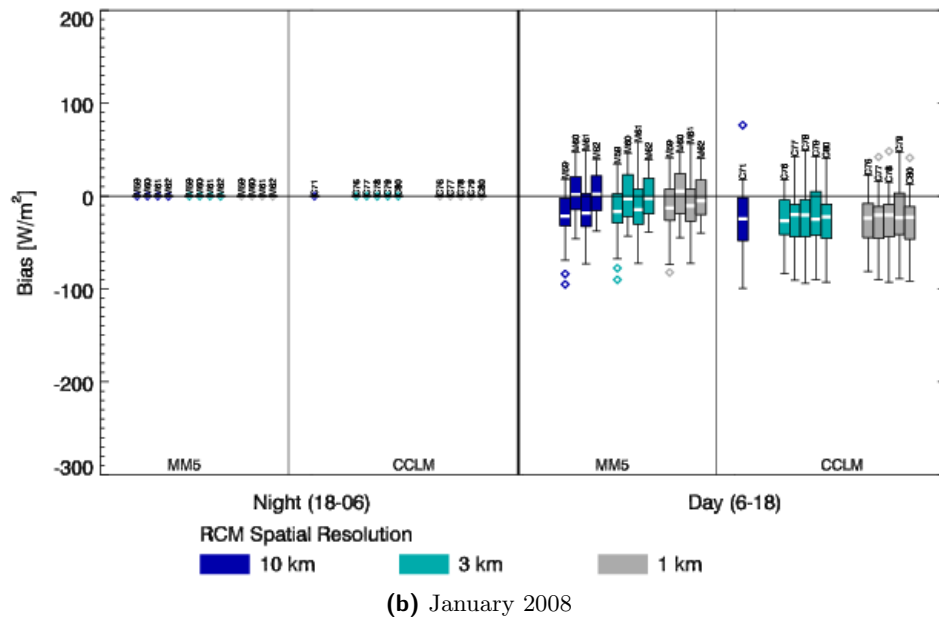
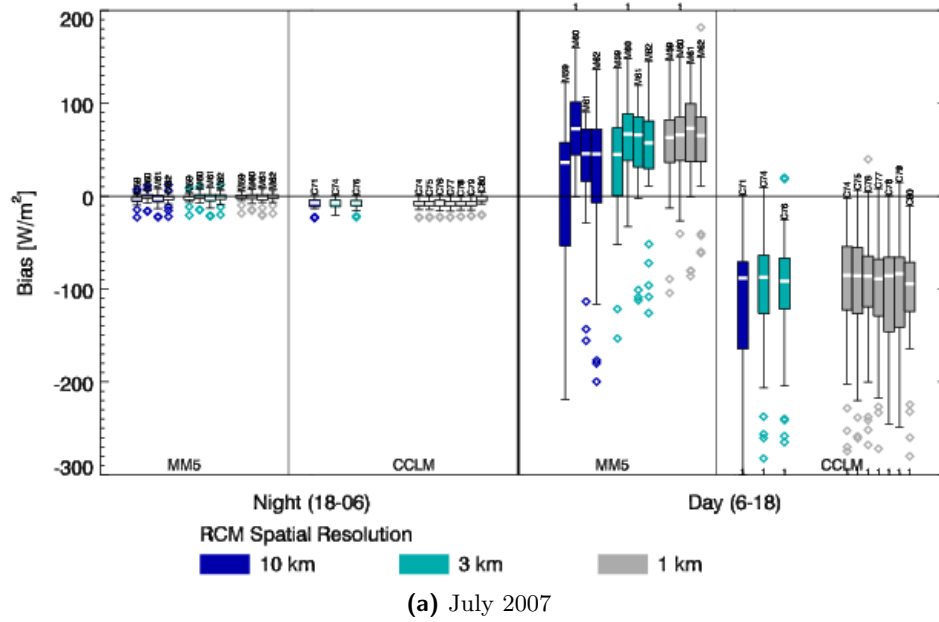


Figure A.28: Box-and-whisker plots for global radiation for all S4 simulations separated by RCM and horizontal resolution in the D4a region.

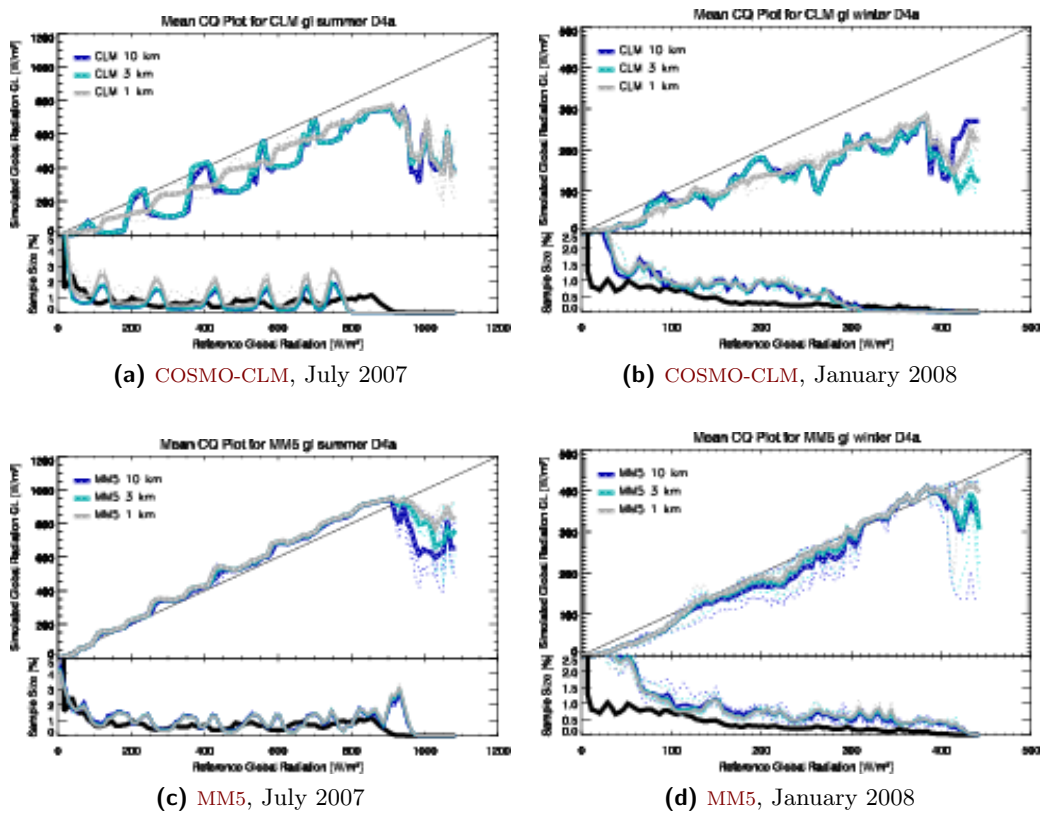


Figure A.29: CQ plots for global radiation for both RCMs and both months in the S4 experiments in D4a region. Top row: COSMO-CLM, bottom row: MM5, left: summer month, right: winter month.

A Figures of the results

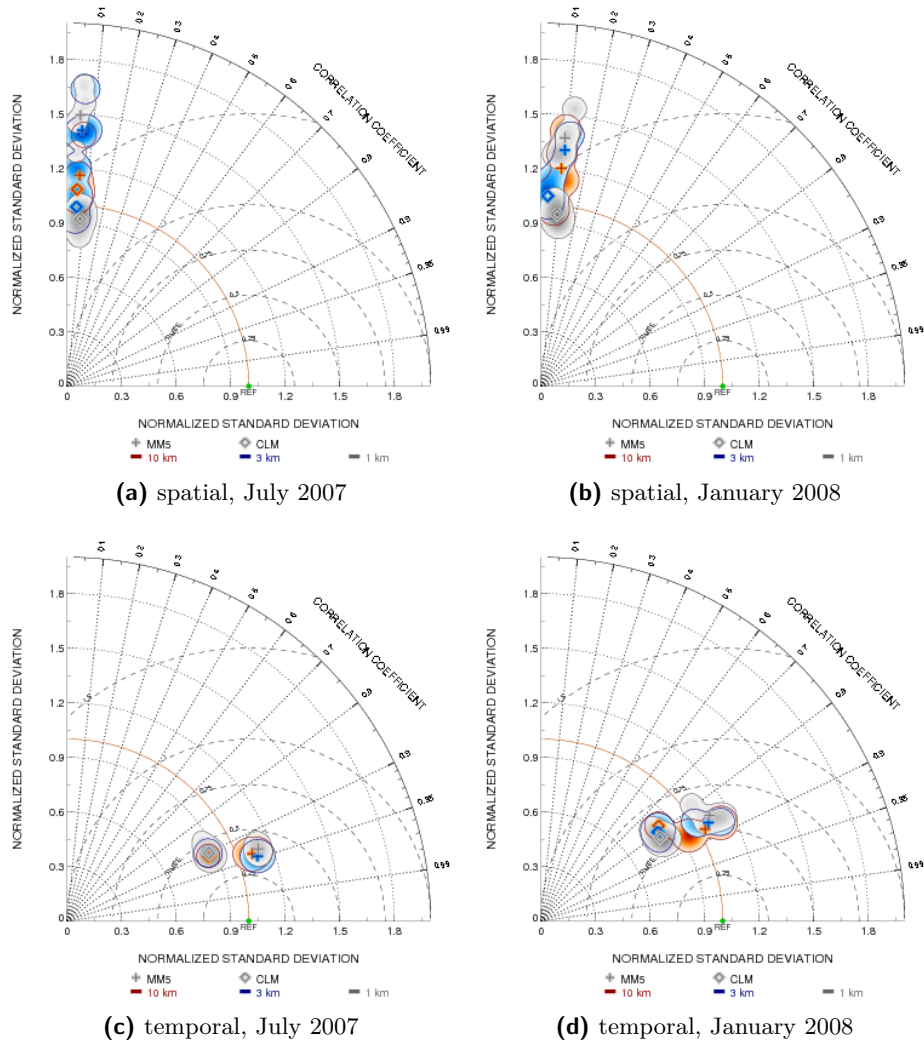


Figure A.30: Spatial and temporal Taylor diagrams for all S4 simulations in the D4a region for global radiation.

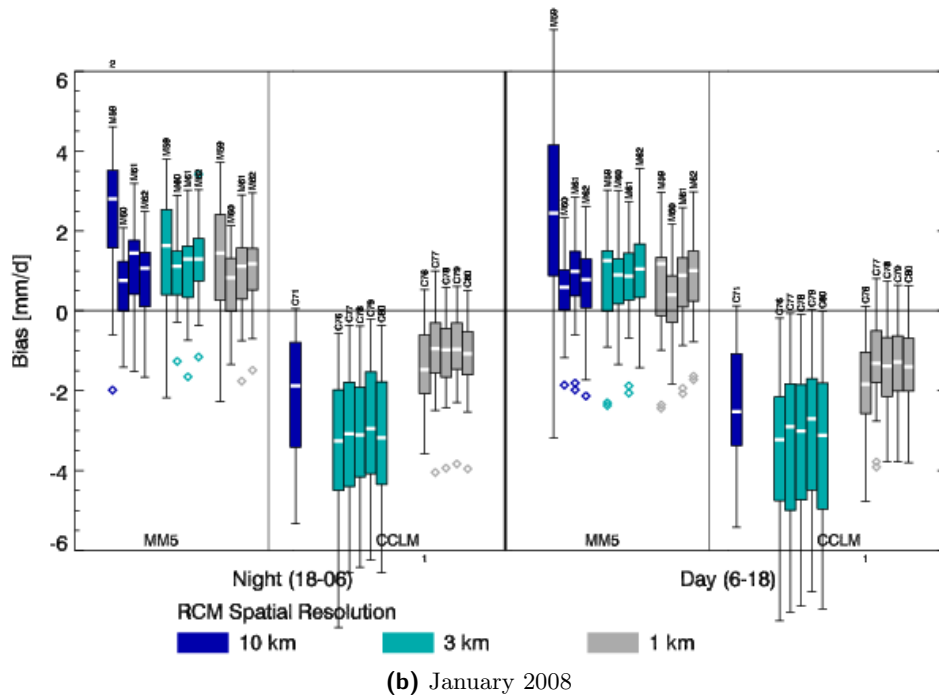
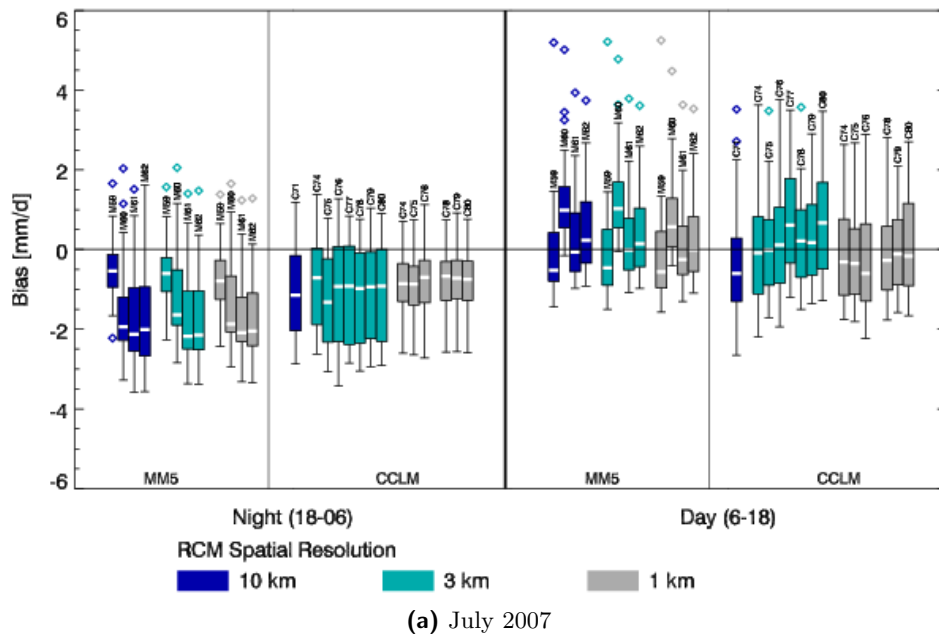


Figure A.31: Box-and-whisker plots for temperature for all S4 simulations separated by RCM and horizontal resolution for the summer month (a) and the winter month (b) in the D4a region.

A Figures of the results

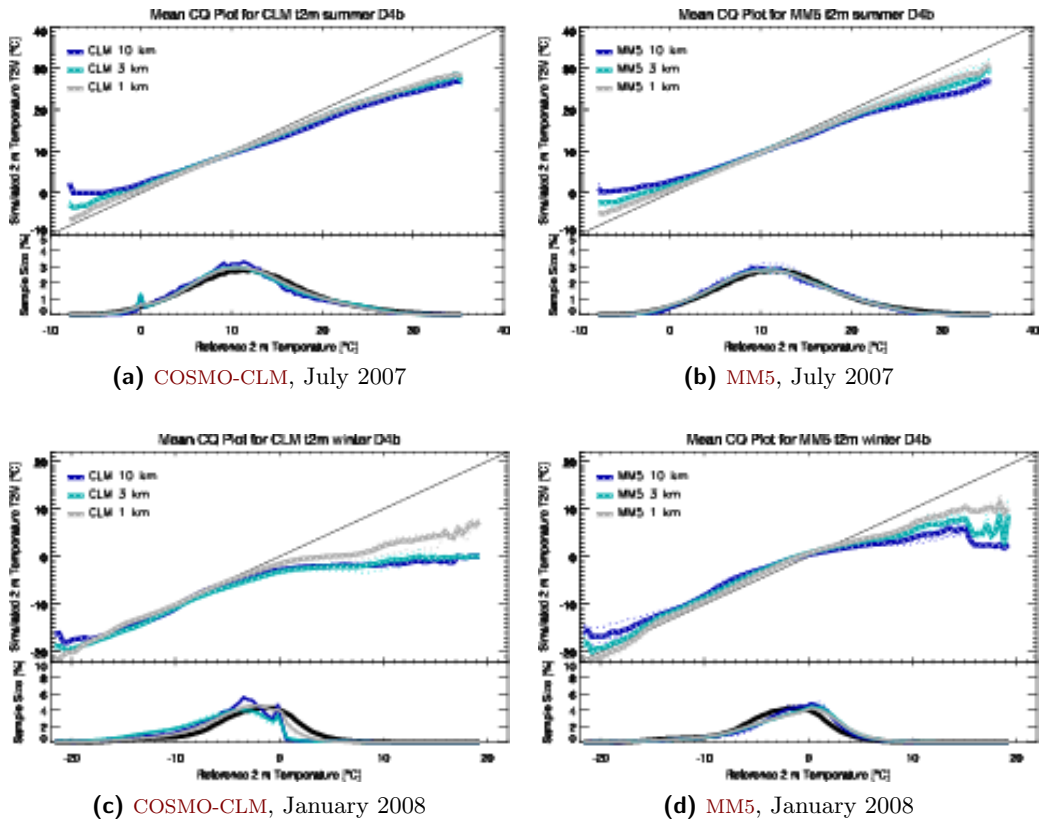
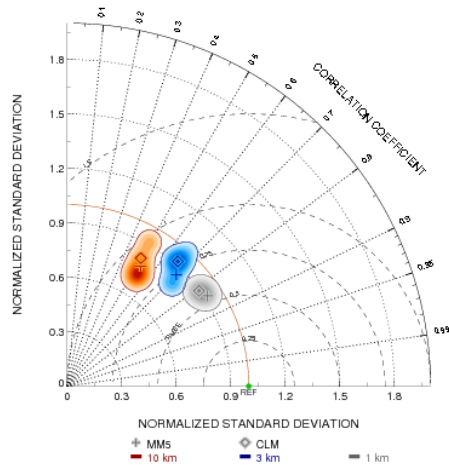
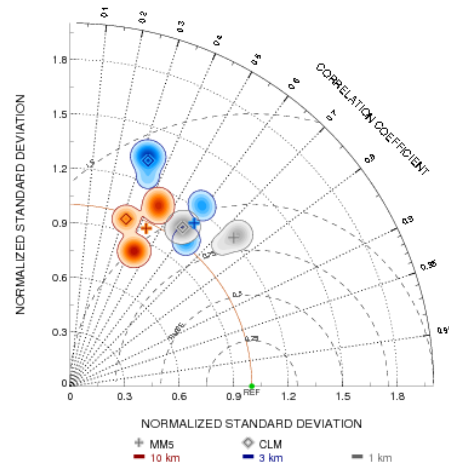


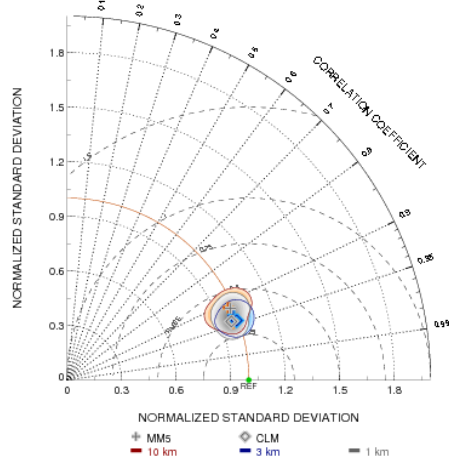
Figure A.32: CQ plots for temperature for all S4 simulations separated by RCM for the summer month (upper row) and the winter month (lower row) in the D4b region. Left column: COSMO-CLM, right column: MM5.



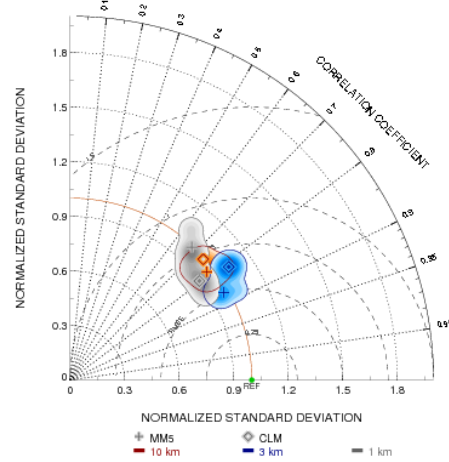
(a) spatial, July 2007



(b) spatial, January 2008



(c) temporal, July 2007



(d) temporal, January 2008

Figure A.33: Spatial and temporal Taylor diagrams for all S4 simulations in the D4b region for temperature.

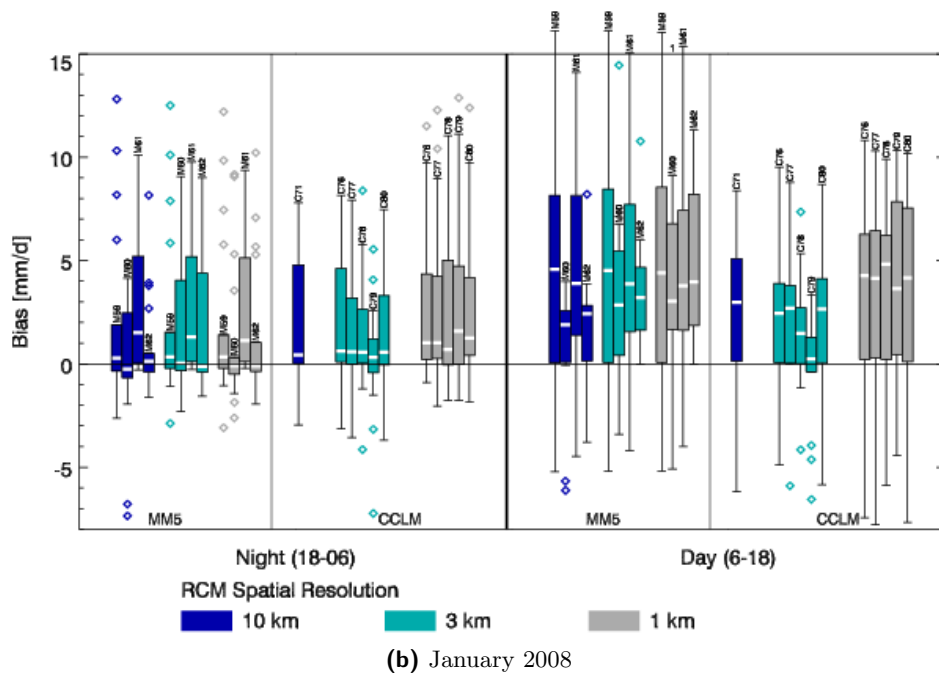
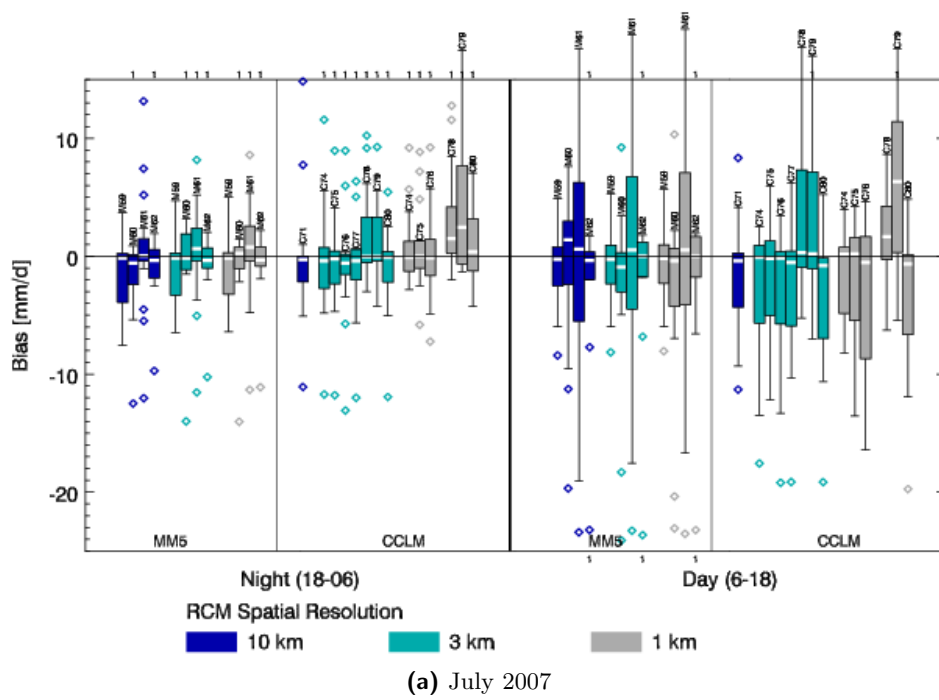
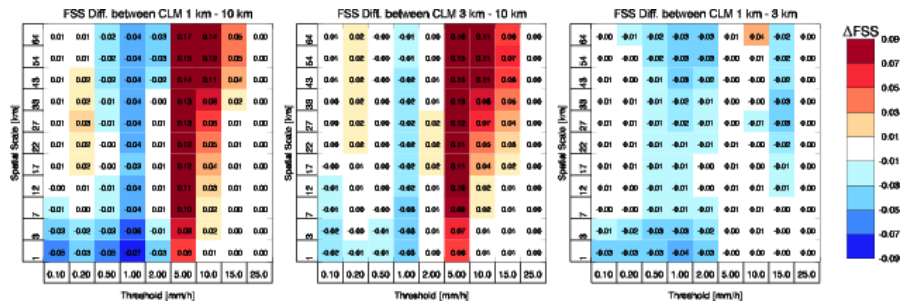
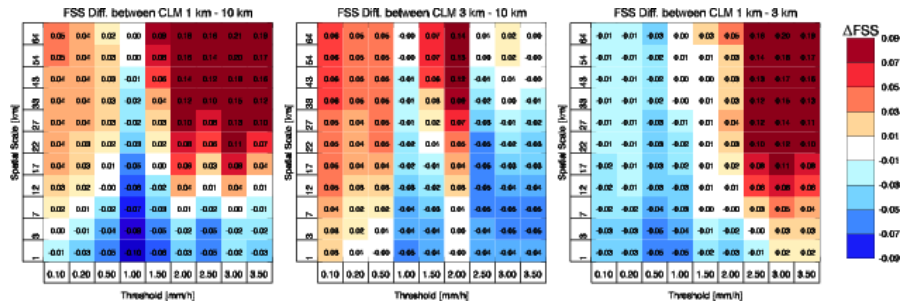


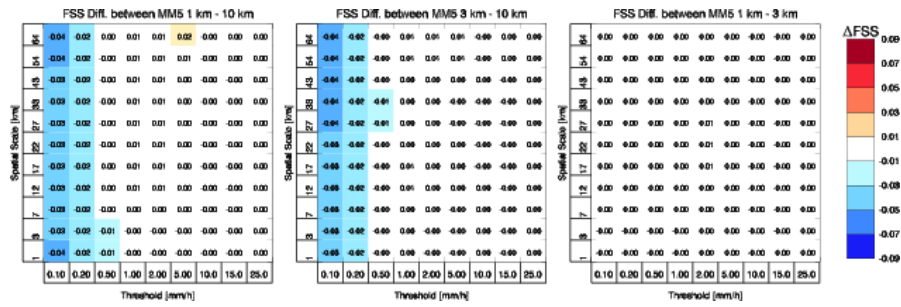
Figure A.34: Box-and-whisker plots for precipitation for all S4 simulations separated by RCM and horizontal resolution in the D4b region.



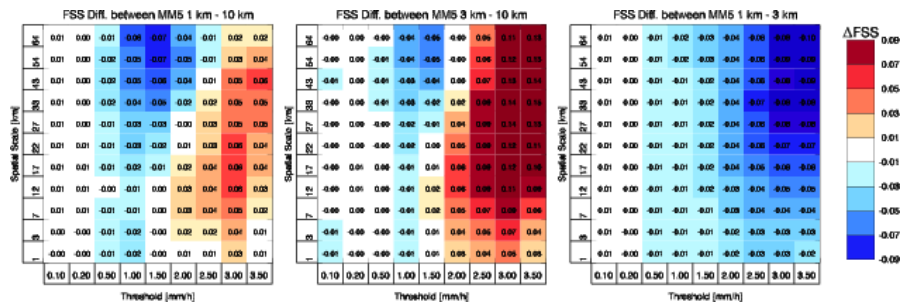
(a) COSMO-CLM, July 2007



(b) COSMO-CLM, January 2008



(c) MM5, July 2007



(d) MM5, January 2008

Figure A.35: Difference FSS plots for simulated vs. observed precipitation amount in the S4 simulations of COSMO-CLM and MM5.

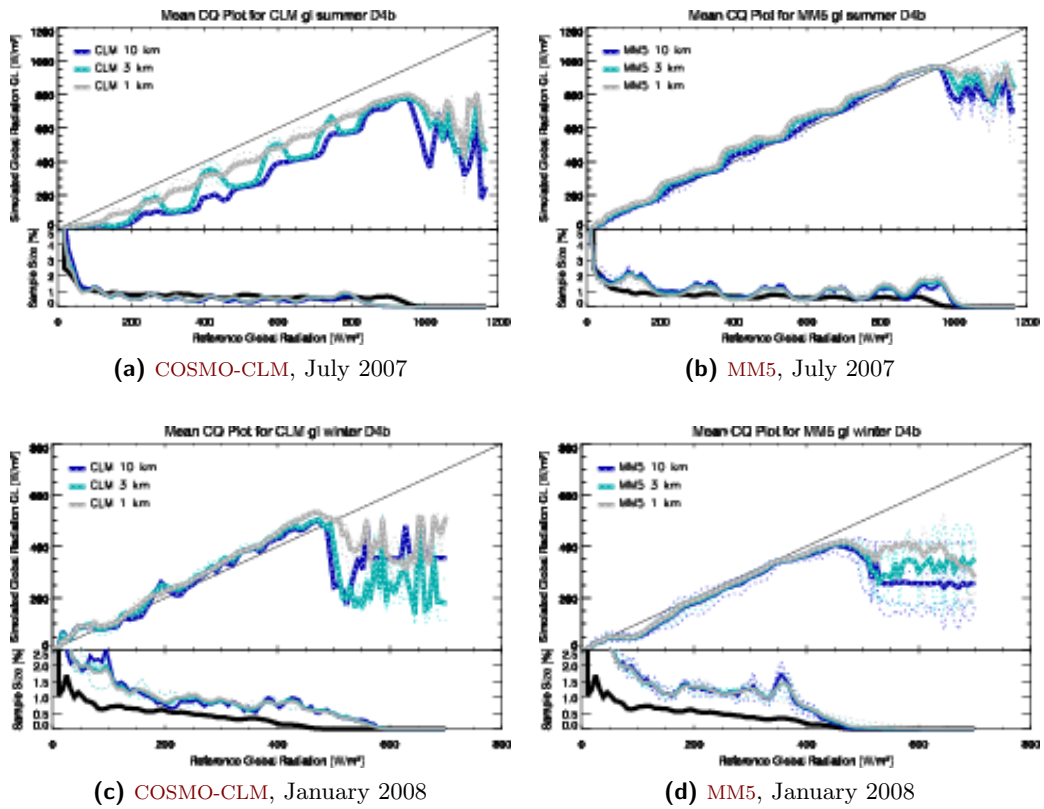


Figure A.36: CQ plots for all S4 simulations separated by RCM for the summer month (upper row) and the winter month (lower row) in the D4b region. Left column: COSMO-CLM, right column: MM5.

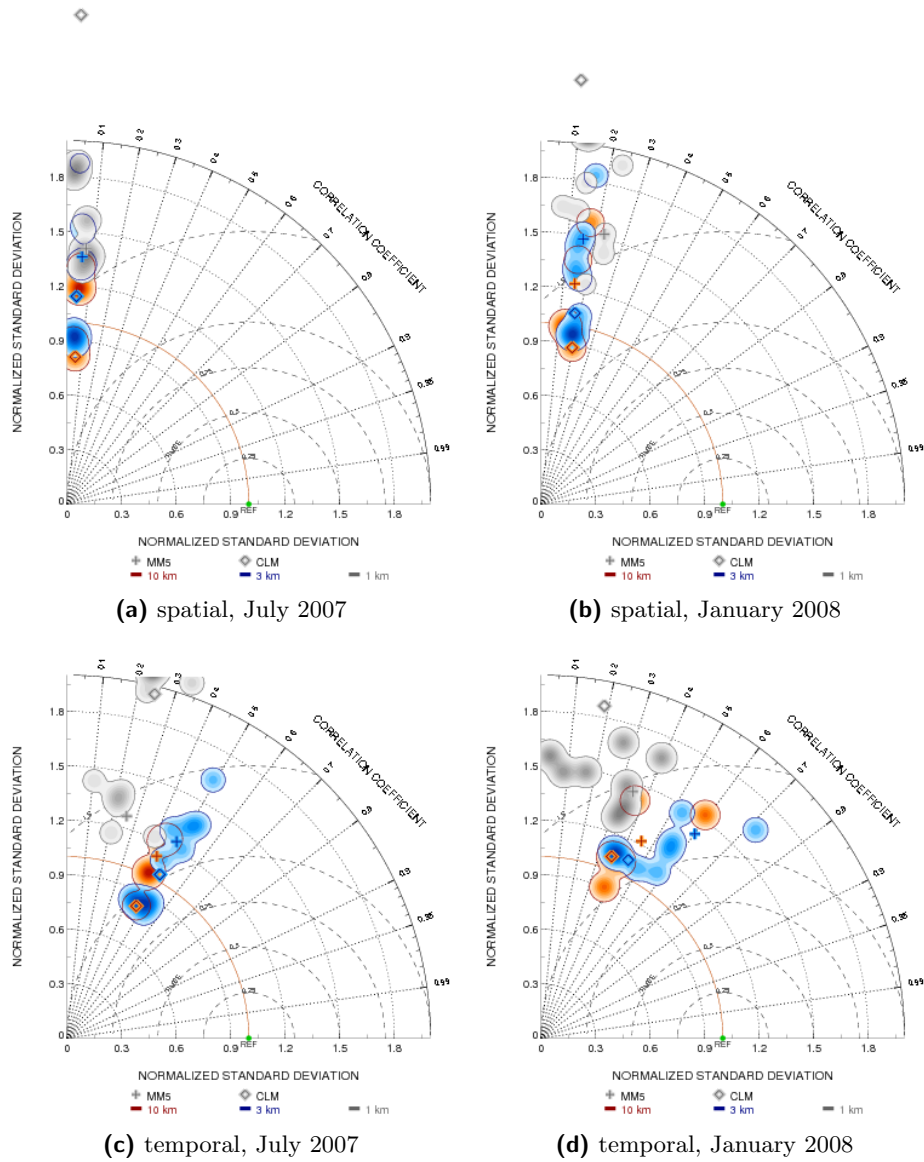
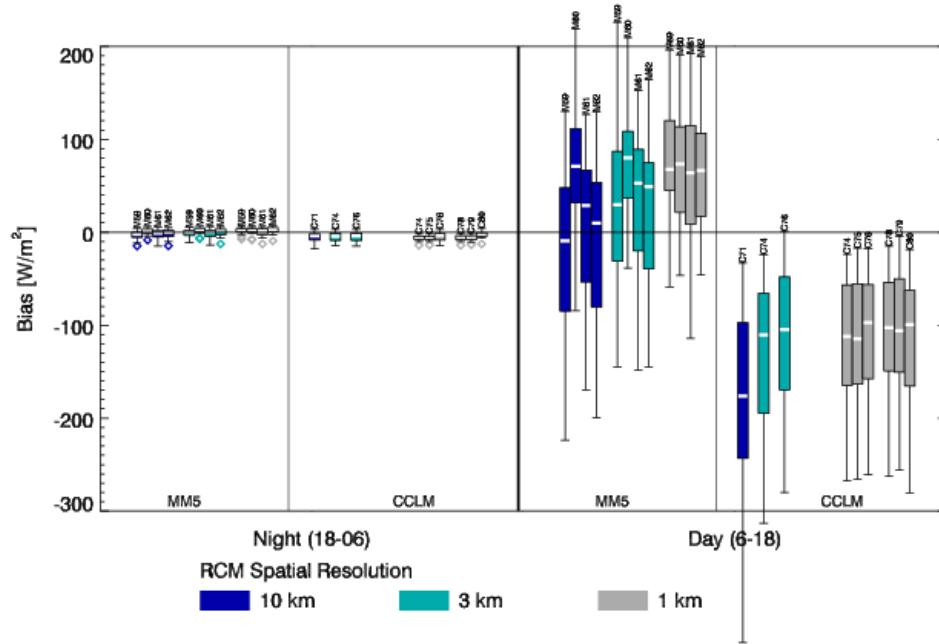
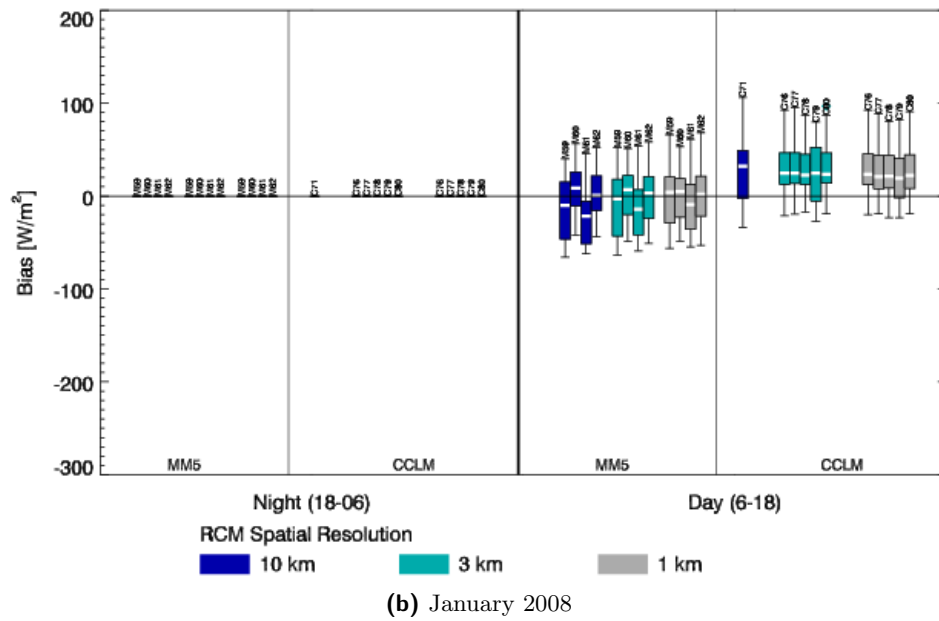


Figure A.37: Spatial and temporal Taylor diagrams for all S4 simulations in the D4b region for precipitation.



(a) July 2007



(b) January 2008

Figure A.38: Box-and-whisker plots for global radiation for all S4 simulations separated by RCM and horizontal resolution in the D4b region.

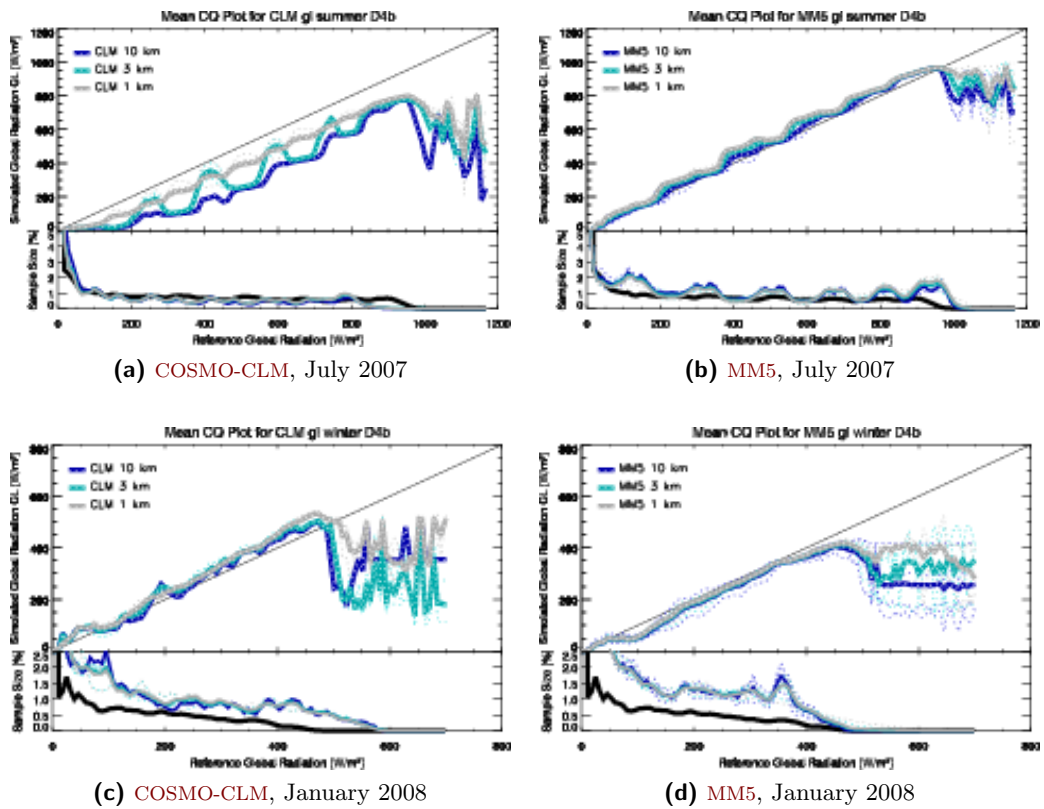
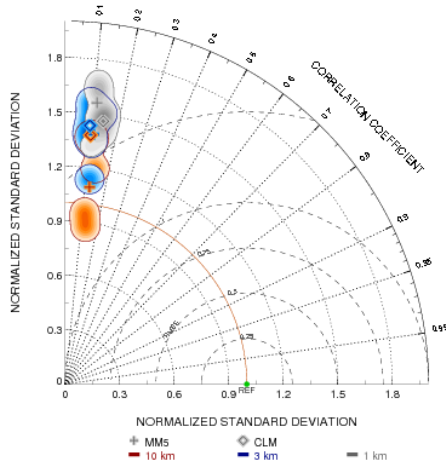
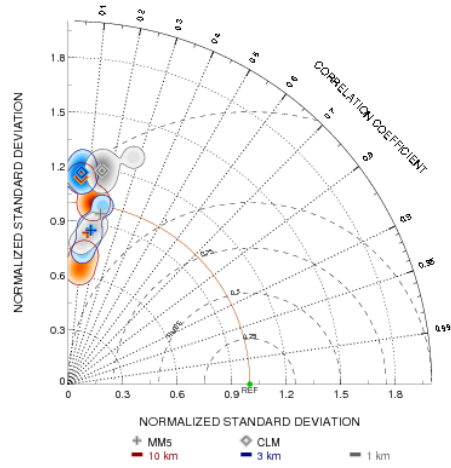


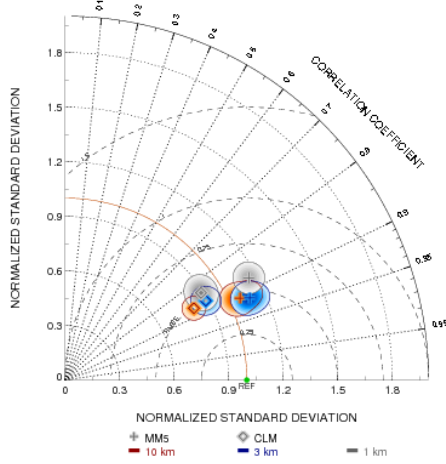
Figure A.39: CQ plots for global radiation for all S4 simulations separated by RCM for the summer month (upper row) and the winter month (lower row) in the D4b region. Left column: COSMO-CLM, right column: MM5.



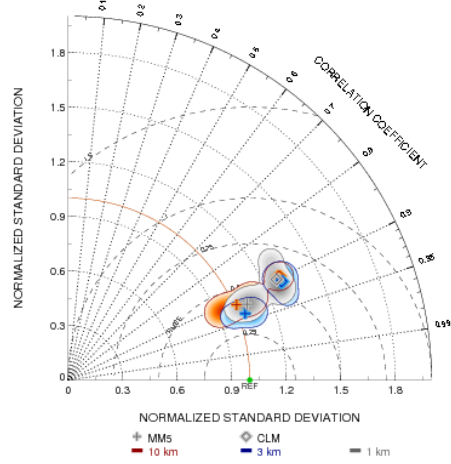
(a) spatial, July 2007



(b) spatial, January 2008



(c) temporal, July 2007



(d) temporal, January 2008

Figure A.40: Spatial and temporal Taylor diagrams for all S4 simulations in the D4b region for global radiation.

List of Figures

2.1	Model domains for CRCS study	19
2.2	INCA orography	26
2.3	INCA stations	27
2.4	WegenerNet stations	28
2.5	INCA temperature	29
2.6	IFS temperature bias	30
3.1	Description of the box-whisker-plot	35
3.2	Exemplary Taylor diagram for a test field	37
4.1	Comparative evaluation of all simulations, 2 m air temperature	51
4.2	Comparative evaluation of all simulations, precipitation amount	52
A.1	S1: D4a region, CQ plots, temperature	61
A.2	S1: D4a region, box-and-whisker plots, temperature	62
A.3	S1: D4a region, spatial and temporal Taylor diagrams, temperature	63
A.4	S1: D4a region, CQ plots, precipitation	64
A.5	S1: D4a region, box-and-whisker plots, precipitation	65
A.6	S1: D4a region, difference FSS plots, July 2007 precipitation	66
A.7	S1: D4a region, difference FSS plots, January 2008 precipitation	67
A.8	S1: D4a region, spatial and temporal Taylor diagrams, precipitation	68
A.9	S1: D4b region, CQ plots, temperature	69
A.10	S1: D4b region, box-and-whisker plots, temperature	70
A.11	S1: D4b region, spatial and temporal Taylor diagrams, temperature	71
A.12	S1: D4b region, CQ plots, precipitation	72
A.13	S1: D4b region, box-and-whisker plots, precipitation	73
A.14	S1: D4b region, FSS, precipitation	74
A.15	S1: D4b region, Spatial and temporal Taylor diagrams, precipitation	75
A.16	S2: Box-and-whisker plots, temperature and precipitation	76
A.17	S2: CQ plots, temperature and precipitation	77
A.18	S2: FSS plots, precipitation	77
A.19	S2: spatial Taylor diagram, comparison D3 with test regions, temperature	78
A.20	S2: temporal Taylor diagram, comparison D3 with test regions, temperature	78
A.21	S4: D4a region, box-and-whisker plots, temperature	79

List of Figures

A.22 S4: D4a region, CQ plots, temperature	80
A.23 S4: D4a region, spatial and temporal Taylor diagrams, temperature	81
A.24 S4: D4a region, box-and-whisker plots, precipitation	82
A.25 S4: D4a region, CQ plots, precipitation	83
A.26 S4: D4a region, difference FSS plots, precipitation	84
A.27 S4: D4a region, spatial and temporal Taylor diagrams, precipitation	85
A.28 S4: D4a region, box-and-whisker plots, global radiation	86
A.29 S4: D4a region, CQ plots, July 2007 global radiation	87
A.30 S4: D4a region, spatial and temporal Taylor diagram, global radiation . . .	88
A.31 S4: D4b region, box-and-whisker plots, temperature	89
A.32 S4: D4b region, CQ plots, temperature	90
A.33 S4: D4b region, spatial and temporal Taylor diagrams, temperature	91
A.34 S4: D4b region, box-and-whisker plots, precipitation	92
A.35 S4: D4b region, difference FSS plots, precipitation	93
A.36 S4: D4b region, CQ plots, precipitation	94
A.37 S4: D4b region, spatial and temporal Taylor diagrams, precipitation	95
A.38 S4: D4b region, box-and-whisker plots, global radiation	96
A.39 S4: D4b region, CQ plots, temperature	97
A.40 S4: D4b region, spatial and temporal Taylor diagrams, global radiation . .	98

List of Tables

2.1	Horizontal domain settings, default vertical levels	19
2.2a	COSMO-CLM S1 key settings	21
2.2b	MM5 S1 key settings	22
2.2c	WRF S1 key settings	22
2.3a	COSMO-CLM S2 key settings	23
2.3b	MM5 S2 key settings	23
2.4a	COSMO-CLM S4 key settings	24
2.4b	MM5 S4 key settings	25

Acronyms

Symbols

NHCM-1 Non-Hydrostatic Climate Modelling. [iii](#), [v](#), [14](#), [17](#), [19](#), [23](#), [26](#), [28](#), [50–52](#)

A

AOGCM coupled ocean-atmosphere general circulation model. [9](#)

Austro Control Österreichische Gesellschaft für Zivilluftfahrt mit beschränkter Haftung. [24](#)

C

CCLM short form for COSMO-CLM. [15](#)

COSMO Consortium on Small Scale Modelling. [vii](#), [CII](#), [15](#), [50](#), [57](#)

COSMO-CLM COSMO model in CLimate Mode. [vii](#), [CI](#), [10](#), [15](#), [17–21](#), [23](#), [24](#), [38–50](#), [53–58](#), [61](#), [64](#), [66](#), [67](#), [69](#), [72](#), [74](#), [77](#), [80](#), [83](#), [84](#), [87](#), [90](#), [93](#), [94](#), [97](#)

CQ conditional quantile. [XCIX](#), [C](#), [38–41](#), [43](#), [44](#), [46](#), [47](#), [55](#), [61](#), [64](#), [69](#), [72](#), [77](#), [80](#), [83](#), [87](#), [90](#), [94](#), [97](#)

CRCS Convection-Resolving Climate Simulations. [v](#), [59](#)

D

DWD German Weather Service [Deutscher Wetterdienst]. [vii](#), [21](#)

E

E-OBS observation dataset by the [ECA&D](#) project. [31](#)

ECA&D European Climate Assessment & Dataset. [CII](#)

ECMWF European Centre for Medium-Range Weather Forecasts. [vii](#), [9](#), [10](#), [16](#), [24](#), [28](#)

F

[CII](#)

FSS fractional skill score. **XCIX**, **C**, **37**, **42**, **43**, **45**, **48**, **66**, **67**, **74**, **77**, **84**, **93**

FWF Austrian Science Fund (Fonds zur Förderung der wissenschaftlichen Forschung).
iii, **v**, **vii**

G

GCM General Circulation Model. **9**, **10**

GFS Global Forecast System. **31**

H

HPC High Performance Computing. **10**

HZG Helmholtz-Zentrum Geesthacht. **vii**

I

IFS Integrated Forecasting System. **vii**, **XCIX**, **9**, **16**, **17**, **19**, **24**, **28–30**

INCA Integrated Nowcasting through Comprehensive Analysis. **vii**, **XCIX**, **23–30**, **34**,
39, **42**, **51**, **52**

J

JJA June–July–August. **28**

JSC Jülich Supercomputing Centre. **vii**

K

KIT Karlsruhe Institute of Technology. **vii**

L

LBC lateral boundary condition. **vii**, **16**, **21–25**, **55**

LocMIP Local Climate Model Intercomparison Project. **26**

M

MM5 Fifth-Generation Mesoscale Model. **CI**, **15–20**, **22**, **23**, **25**, **38–50**, **53–55**, **57**, **58**,
61, **64**, **66**, **67**, **69**, **72**, **74**, **77**, **80**, **83**, **84**, **87**, **90**, **93**, **94**, **97**

Acronyms

MSG Meteosat 2nd Generation. 25

N

NCEP National Centers for Environmental Prediction. 31

NWP Numerical Weather Prediction. 9, 16, 37

P

PBL planetary boundary layer. 13–15, 44, 50, 54

R

RCM Regional Climate Model. v, 9–15, 17, 18, 20–22, 25, 35–41, 44–50, 54, 55, 57–59, 61, 62, 64–67, 69, 70, 72, 73, 79, 80, 82, 83, 86, 87, 89, 90, 92, 94, 96, 97

S

SVAT soil vegetation atmosphere transfer. 14

T

TAWES Teilautomatische Wetterstation. 24, 27

TKE turbulent kinetic energy. 21, 23, 24

U

UG University of Graz. CIV

W

WEGC Wegener Center for Climate and Global Change [University of Graz]. vii

WRF Weather Research and Forecasting model. vii, CI, 15–20, 22, 38–42, 50, 54, 55, 57, 58, 61, 64, 66, 67, 69, 72

Z

ZAMG Zentralanstalt für Meteorologie und Geodynamik. vii, 23, 24, 26, 31

ZID, Uni Graz Center for IT services of the University of Graz [Zentraler Informatikdienst der Universität Graz]. vii

CIV

Bibliography

- Anthes, R. A. and T. T. Warner (1978). Development of hydrodynamic models suitable for air pollution and other mesometeorological studies. In: *Mon. Wea. Rev.* 106, pp. 1045–1078. See p. 16.
- Awan, N. K. et al. (2010). Parameterization induced error characteristics in regional climate models: An ensemble based analysis. In: *J. Climate*. submitted. See pp. 9, 17, 18.
- Bechtold, P. et al. (2008). Advances in simulating atmospheric variability with the ECMWF model: From synoptic to decadal time-scales. In: *Quart. J. Roy. Met. Soc.* 134 (634 2008), 1337–1351. DOI: [10.1002/qj.289](https://doi.org/10.1002/qj.289). See p. 16.
- Chen, F. and J. Dudhia (2001). Coupling an Advanced Land Surface-Hydrology Model with the Penn State-NCAR MM5 Modeling System. Part I: Model Implementation and Sensitivity. In: *Mon. Wea. Rev.* 129.4, pp. 569–585. See pp. 22, 23, 25.
- Christensen, J. H. et al. (2007). Evaluating the performance and utility of regional climate models: the PRUDENCE project. In: *Clim. Change* 81, pp. 1–6. DOI: [10.1007/s10584-006-9211-6](https://doi.org/10.1007/s10584-006-9211-6). See p. 9.
- Dudhia, J. (1989). Numerical study of convection observed during the winter monsoon experiment using a mesoscale two-dimensional model. In: *J. Atmos. Sci* 46, pp. 3077–3107. See pp. 22, 23, 25.
- (1993). A nonhydrostatic version of the Penn State/NCAR mesoscale model: Validation tests and simulation of an Atlantic cyclone and cold front. In: *Mon. Wea. Rev.* 121, pp. 1493–1513. See p. 16.
- Feldmann, H. et al. (2008). Evaluation of the precipitation for South-western Germany from high resolution simulations with regional climate models. In: *Meteorol. Z.* 17.4, pp. 455–465. DOI: [10.1127/0941-2948/2008/0295](https://doi.org/10.1127/0941-2948/2008/0295). See p. 16.
- Foerstner, J. and G. Doms (2006). *Runge-Kutta Time Integration and High-Order Spatial Discretization of Advection — A New Dynamical Core for the LMK*. COSMO Newsletter 4. Consortium for Small-Scale Modelling. See p. 21.

Bibliography

- Giorgi, F. and X. Bi (2000). A study of internal variability of a regional climate model.
In: *J. Geophys. Res.* 105.D24, pp. 29503–29521. See p. 17.
- Giorgi, F. and L. O. Mearns (1999).
Introduction to special section: Regional climate modeling revisited.
In: *J. Geophys. Res.* 104.D6, pp. 6335–6352. See p. 9.
- Gobiet, A. et al. (2010). *Integriertes Modellsystem Steiermark-Umwelt: Pilotprojekt Integrierte Wetter-Klima-Luftgüte-Land-Hydrologie Modellierung, IMOS-U v1.0 Final Report (FinRep)*. Tech. Rep.
University of Graz, Graz, Austria: Wegener Center for Climate and Global Change, p. 141. See pp. 27, 28.
- Grell, G. A. et al. (1995). *A Description of the Fifth-Generation Penn State/NCAR Mesoscale Model (MM5), NCAR/TN-398+STR*. Tech. rep.
Available at: <http://www.mmm.ucar.edu/mm5/mm5-home.html> (December 2010).
Boulder, USA: National Center for Atmospheric Research (NCAR).
See pp. 22, 23, 25.
- Haiden, T. et al. (2010). The Integrated Nowcasting through Comprehensive Analysis (INCA) system and its validation over the Eastern Alpine region.
In: *Wea. Forecasting* early online release. DOI: [10.1175/2010WAF2222451.1](https://doi.org/10.1175/2010WAF2222451.1).
See pp. 23–25, 27.
- Hewitt, C. D. (2005). The ENSEMBLES Project: Providing ensemble-based predictions of climate changes and their impacts. In: *EGGS Newsletter* 13, pp. 22–25. See p. 9.
- Hohenegger, C. et al. (2008). Towards climate simulations at cloud-resolving scales.
In: *Meteorol. Z.* 17.4 (Aug. 2008), pp. 383–394.
DOI: [10.1127/0941-2948/2008/0303](https://doi.org/10.1127/0941-2948/2008/0303). See p. 10.
- Hong, S. Y. et al. (2006).
A new vertical diffusion package with an explicit treatment of entrainment processes.
In: *Mon. Wea. Rev.* 134, pp. 2318–2341. See p. 22.
- Hong, S. and H. Pan (1996).
Nonlocal Boundary Layer Vertical Diffusion in a Medium-Range Forecast Model.
In: *Mon. Wea. Rev.* 124.10, pp. 2322–2339. See pp. 22, 23.
- Jaeger, E. et al. (2008). Analysis of ERA40-driven CLM simulations for Europe.
In: *Meteorol. Z.* 17.4. See p. 9.
- Janjic, Z. I. (1990). The step-mountain coordinate: Physical package.
In: *Mon. Wea. Rev.* 118.17, pp. 1429–1443. See p. 25.
- (1994). The step-mountain eta coordinate model: Further development of the convection, viscous sublayer, and turbulent closure schemes.
In: *Mon. Wea. Rev.* 122.5, pp. 927–945. See p. 25.

- Kain, J. S. (2003). The Kain-Fritsch convection parameterization: an update.
In: *J. Appl. Meteor.* 43, pp. 170–181. See pp. 21–25.
- Kain, J. S. and J. M. Fritsch (1993).
Convective parameterization for mesoscale models: the Kain-Fritsch scheme.
In: *Meteorol. Monogr.* 24, pp. 165–170. See pp. 21–25.
- Kalnay, E. et al. (1996). The NCEP&NCAR 40-Year Reanalysis Project.
In: *Bull. Am. Meteorol. Soc.* 77.3, pp. 437–471. See p. 9.
- Kirchengast, G. et al. (2008).
Pionierexperiment WegenerNet Klimastationsnetz: Ein neuartiges Messnetz in der Region Feldbach (Steiermark/Österreich) zur Beobachtung von Wetter und Klima mit sehr hoher Auflösung, (in German), Tech. Report, 23-2008. Tech. rep.
ISBN-13978-3-9502615-0-9. Graz, Austria: Wegener Center Verlag. See pp. 23, 26.
- Klemp, J. B. and R. B. Wilhelmson (1978).
Simulations of three-dimensional convective storm dynamics. In: *J. Atmos. Sci.* 35, pp. 1070–1096. See pp. 22, 23, 25.
- Knote, C. et al. (2010). Changes in weather extremes: Assessment of return values using high resolution climate simulations at convection-resolving scale.
In: *Meteorol. Z.* 19.1, pp. 11–23. DOI: [10.1127/0941-2948/2010/042](https://doi.org/10.1127/0941-2948/2010/042). See p. 10.
- Laprise, R. (2008). Regional Climate Modelling. In: *J. Comp. Phys.* 227, pp. 3641–3666. DOI: [doi:10.1016/j.jcp.2006.10.024](https://doi.org/10.1016/j.jcp.2006.10.024). See p. 9.
- Laprise, R. et al. (2008). Challenging some tenets of Regional Climate Modelling.
In: *Met. Atm. Phys.* 100, pp. 3–22. DOI: [doi:10.1007/s00703-008-0292-9](https://doi.org/10.1007/s00703-008-0292-9).
URL: <http://www.ingentaconnect.com/content/klu/703/2008/00000100/F0040001/00000292>. See p. 9.
- Lin, Y. et al. (1983). Bulk parameterization of the snow field in a cloud model.
In: *J. Clim. Appl. Meteor.* 22, pp. 1065–1092. See p. 25.
- Meissner, C. et al. (2009).
High resolution sensitivity studies with the regional climate model CCLM.
In: *Meteorol. Z.* 18.5, pp. 543–557. See p. 10.
- Mlawer, E. J. et al. (1997). Radiative transfer for inhomogeneous atmospheres: RRTM, a validated correlated-k model for the longwave. In: *J. Geophys. Res.* 102.D14, pp. 16663–16682. See pp. 22, 23, 25.
- Noda, A. T. et al. (2010). Importance of the subgrid-scale turbulent moist process: Cloud distribution in global cloud-resolving simulations. In: *Atmos. Res.* 96, pp. 208–217. DOI: [10.1016/j.atmosres.2009.05.007](https://doi.org/10.1016/j.atmosres.2009.05.007). See p. 10.
- Onogi, K. et al. (2007). The JRA-25 Reanalysis. In: *J. Meteor. Soc. Japan* 85, pp. 369–432. See p. 9.

Bibliography

- Pielke, Sr., R. A. (2002). *Mesoscale Meteorological Modeling*. 2nd edition. International Geophysics Series, Vol. 78. San Diego, California, USA: Academic Press. See p. 11.
- Prein, A. et al. (2010a). *NHCM-1: Non-hydrostatic climate modelling. Part I: Defining and Detecting Added Value in Cloud Resolving Climate Simulations*. WegCenter Report XX. WegCenter Verlag, Graz, Austria. Wegener Center for Climate and Global Change. See pp. 34, 36, 37.
- Prein, A. et al. (2010b). *NHCM-1: Non-hydrostatic climate modelling. Part III: Evaluation of the LocMIP simulations*. WegCenter Report YY. WegCenter Verlag, Graz, Austria. Wegener Center for Climate and Global Change. See p. 26.
- Reisner, J. et al. (1998). Explicit forecasting of supercooled liquid water in winter storms using the MM5 mesoscale model. In: *Quart. J. Roy. Met. Soc.* 124.B, pp. 1071–1107. See pp. 22, 23, 25.
- Ritter, B. and J. F. Geleyn (1992). A comprehensive radiation scheme for numerical weather prediction with potential applications in climate simulations. In: *Mon. Wea. Rev.* 120, pp. 303–325. See p. 21.
- Roberts, N. M. and H. W. Lean (2008). Scale-selective verification of rainfall accumulations from high-resolution forecasts of convective events. In: *Mon. Wea. Rev.* 136.1 (Jan. 2008), pp. 78–97. See p. 37.
- Rockel, B. and B. Geyer (2008). The performance of the regional climate model CLM in different climate regions, based on the example of precipitation. In: *Meteorol. Z.* 17.4, pp. 487–498. DOI: [10.1127/0941-2948/2008/0297](https://doi.org/10.1127/0941-2948/2008/0297). See p. 16.
- Rogers, E. et al. (2001). *Changes to NCEP meso ETA analysis and forecast system: increase in resolution, new cloud microphysics, modified precipitation assimilation, modified 3DVAR analysis*. NWS technical procedures bulletin. NOAA. See p. 22.
- Sato, T. et al. (2009). Diurnal Cycle of Precipitation in the Tropics Simulated in a Global Cloud-Resolving Model. In: *J. Climate* 22, pp. 4809–4826. DOI: [10.1175/2009JCLI2890.1](https://doi.org/10.1175/2009JCLI2890.1). See p. 10.
- Skamarock, W. C. et al. (2005). *A Description of the Advanced Research WRF Version 2*. NCAR Technical Note 468. Boulder: MesoscaleMicroscale Meteorology Division at NCAR. See p. 16.
- Skamarock, W. C. et al. (2007). *A Description of the Advanced Research WRF version 2*. Tech. rep. 468. Mesoscale and Microscale Meteorology Division at NCAR. See p. 22.

- Steiner, M. (2010). Integration of advanced land and soil data into the COSMO model in CLimate Mode. MA thesis. University of Graz. See p. 57.
- Stevenson, M. (2006).
Forecast verification: A practitioner's guide in atmospheric science.
In: *Int. J. Forecasting* 22.2, pp. 403–405. See p. 36.
- Suklitsch, M. et al. (2008). High Resolution Sensitivity Studies with the Regional Climate Model CCLM in the Alpine Region. In: *Meteorol. Z.* 17.4 (Aug. 2008), pp. 467–476. See pp. 30, 34.
- Suklitsch, M. et al. (2010). Error Characteristics of High Resolution Regional Climate Models over the Alpine Area. In: *Clim. Dyn.* revised. See pp. 9, 17, 18.
- Tao, W. and J. Simpson (1993).
Goddard Cumulus Ensemble Model. Part I: Model Description.
In: *Terrestrial, Atmospheric and Oceanic Sciences* 4, pp. 35–72. See p. 25.
- Tao, W. et al. (1989). Ice-water saturation adjustment. In: *Mon. Wea. Rev.* 117, pp. 231–235. See p. 25.
- Taylor, K. E. (2001).
Summarizing multiple aspects of model performance in a single diagram.
In: *J. Geophys. Res.* 106.D7, pp. 7183–7192. See p. 36.
- Tiedtke, M. (1989). A comprehensive mass flux scheme for cumulus parameterization in large-scale models. In: *Mon. Wea. Rev.* 117, pp. 1779–1800. See p. 21.
- Uppala, S. M. et al. (2005). The ERA-40 re-analysis. In: *Quart. J. Roy. Met. Soc.* 131, pp. 2961–3012. DOI: [10.1256/qj.04.176](https://doi.org/10.1256/qj.04.176). See p. 9.
- Wilks, D. S. (2005). *Statistical Methods in the Atmospheric Sciences, Volume 91, Second Edition (International Geophysics)*. 2nd ed. Academic Press.
ISBN: 0127519661.
URL: <http://www.amazon.com/exec/obidos/redirect?tag=citeulike07-20&path=ASIN/0127519661>. See p. 36.
- Zhong, Z. et al. (2007). Numerical experiments on the spin-up time for seasonal-scale regional climate modeling. In: *Acta Meteorol. Sin.* 21.4, pp. 409–419. See p. 17.
- Zängl, G. (2002).
An Improved Method for Computing Horizontal Diffusion in a Sigma-Coordinate Model and Its Application to Simulations over Mountainous Topography.
In: *Mon. Wea. Rev.* 130.5, pp. 1423–1432. See p. 25.

Abstract:

Regional Climate Models (RCMs) are widely used for case studies as well as regional climate projections. Their horizontal grid spacing is usually 10 km or larger. This is at the edge of the so-called 'cloud-resolving' or 'convection resolving' scale. Below that scale processes like deep convection start to get explicitly resolved, and hence it is believed that RCMs operated at horizontal resolutions of 3 km and below produce more accurate results.

The project NHCM-1, funded by the FWF under project ID P19619, was (amongst others) dedicated to find out whether or not there is an added value in Convection-Resolving Climate Simulations (CRCS), and how climate models should be improved to be successfully operated at such scales. Three different RCMs have been applied in various configurations in two regions and two periods. The two regions and periods differ strongly in their climatologic characteristics in order to allow to draw general conclusions from the results.

The results demonstrate that CRCS have comparable quality to conventional climate simulations and that they feature added value in some aspects, particularly regarding spatial patterns, biases related to specific temperatures or precipitation intensities, and partially also regarding overall biases. Model improvement options have been identified that could further enhance the quality of CRCS.

This demonstrates that the realisation of long-term CRCS is already in reach, but currently still at extremely high computational costs. Technical advances in the field of high performance computing are expected to allow long-term CRCS with about 3 km grid spacing at reasonable costs within the next few years.

Zum Inhalt:

Heutzutage sind regionale Klimamodelle (RCMs) weit verbreitet. Sie werden sowohl für Fallstudien als auch für regionale Klimaprojektionen verwendet. Im Allgemeinen liegt die dafür verwendete Gitterdistanz bei 10 km oder höher und damit nahe an der sogenannten „wolkenauflösenden Skala“. Bei höheren Auflösungen wird beispielsweise Konvektion teilweise explizit vom Modell erfasst. Daher glaubt man dass Simulationen mit einer Auflösung von 3 km oder weniger genauere Ergebnisse liefern.

Im Projekt NHCM-1 wurde unter anderem versucht herauszufinden ob diese Annahme gerechtfertigt ist, ob hoch aufgelöste Klimasimulationen - sogenannte „cloud resolving climate simulations“ (CRCS) - tatsächlich einen „added value“, einen „Mehrwert“, zeigen. Dafür wurden drei RCMs mit unterschiedlichen Einstellungen in zwei Testregionen und für zwei Testperioden, beide sehr unterschiedlich in ihren Klima-Charakteristika, betrieben. Auf diese Weise werden Potenzial und Probleme aktueller RCMs bei Auflösungen von 3 km und 1 km evaluiert, und es können allgemeine Schlüsse gezogen werden.

Die Ergebnisse zeigen dass die CRCS eine vergleichbare Qualität wie konventionelle Simulationen aufweisen, und dass in gewissen Teilaspekten tatsächlich ein Mehrwert vorhanden ist (vor allem hinsichtlich räumlicher Muster und Fehler bezüglich spezieller Niederschlags-Intensitäten). Weiters wurden Optionen zur Modellverbesserung identifiziert, die die Qualität der CRCS weiter steigern sollten.

Dadurch wird demonstriert, dass langfristige CRCS bereits in Reichweite sind, zur Zeit jedoch noch mit hohem Rechenaufwand verbunden sind. Aktuelle technische Weiterentwicklungen werden solche Simulationen voraussichtlich schon in wenigen Jahren ermöglichen.